TERAHERTZ WAVE SENSITIVE SUPERCONDUCTING BOLOMETRIC DETECTOR

A Thesis Submitted to
the Graduate School of Engineering and Sciences of
İzmir Institute of Technology
in Partial Fulfillment of the Requirements for the Degree of

MASTER OF SCIENCE

in Materials Science and Engineering

by
Tuğçe SEMERCİ

July 2015
İZMİR

We approve the thesis of **Tuğçe SEMERCİ**

Examining Committee Members:

_____

Prof. Dr. Lütfi ÖZYÜZER
Department of Physics, Izmir Institute of Technology

_____

Asst. Prof. Dr. Mehtap ÖZDEMİR KÖKLÜ
Department of Electrical-Electronics Engineering, Gediz University

_____

Prof. Dr. Birol ENGİN
Department of Physics, Dokuz Eylül University

_____

Assoc. Prof. Dr. Devrim PESEN OKVUR
Department of Molecular Biology and Genetic, Izmir Institute of Technology

_____

Asst. Prof. Dr. Enver TARHAN
Department of Physics, Izmir Institute of Technology

27 July 2015

_____

Prof. Dr. Lütfi ÖZYÜZER
Supervisor, Department of Physics
Izmir Institute of Technology

_____

Asst. Prof. Dr. Mehtap ÖZDEMİR KÖKLÜ
Co-Supervisor, Department of Electrical-
Electronics Engineering, Gediz University

_____

Prof. Dr. Mustafa M. DEMİR
Head of the Department of Materials
Science and Engineering

_____

Prof. Dr. Bilge KARAÇALI
Dean of the Graduated School of
Engineering and Sciences

ACKNOWLEDGEMENTS

I would like to express my appreciation and thanks to supervisor Prof. Dr. Lütfi ÖZYÜZER who gave me the opportunity to complete this thesis, for his instructive guidance, wisdom, inspiring suggestions and understanding, knowledge and experience about terahertz science and technology, took a crucial role during my master education. Additionally, I would like to say thanks to my co-advisor Asst. Prof. Dr. Mehtap ÖZDEMİR KÖKLÜ for understanding, guidance and support through this study.

This research was supported by Ministry of Science, Industry and Technology which is cooperated with ASELSAN under project number SANTEZ 1386.STZ.2012-1.

I thank to Enis Doyuran and Burak Işıktan from ASELSAN to give an ideas to provide improvement for this thesis.

I would also specially thank to colleagues from Izmir Institute of Technology and my group members.

I would like to thank especially Emre TARIM and Murat SAĞLAM for their friendship, support and understanding during my master education.

For their support, friendship and sincere love, I thank to my friends whom I called as “İzmir Tayfası”.

Last but not least, I would like to express immense appreciation and thanks my family for patience, endless love, understanding and support me any time. Without my family’s support and encouragement, it would not have been possible for me to achieve my educational goals.

ABSTRACT

TERAHERTZ WAVE SENSITIVE SUPERCONDUCTING BOLOMETRIC DETECTOR

Terahertz (THz) waves has varied properties than other part of the electromagnetic spectrum which between microwave and infrared and has 0.3-10 THz frequency range and 3-0.03 mm wavelength. There are many areas to utilize from THz radiation that defense industry particularly security part such as detecting of unknown materials, poison or explosive matters. Additionally, THz waves can pass through leather, fabric and paper despite of metal and water and there is no enough energy to ionize the atoms in THz radiation. That's why, THz radiation is not hazardous for human. Many detectors are developed to use these benefit of THz radiation. Bolometric detector is preferred between these detectors to detect the radiation above 1 THz frequency. $Bi_2Sr_2CaCu_2O_{8+\delta}$ (Bi2212) single crystal was used in literature for the first time to detect the THz waves with superconducting bolometers with our study. In this study, epoxy was used to transfer Bi2212 single crystal onto the sapphire substrate. Intended thickness was acquired by scotch tape via cleaved crystal mechanically. Edge of crystals were cut pyramid shape to provide each layer to contact with gold, crystal and silver epoxy. 150-200 nm crystals were shadowed by aluminum foil to deposit roughly 200 nm gold. Then clean room process was implemented to prepare our samples to electron beam lithography. Log-periodic antenna and four point contact structure was placed onto the crystals then UV light, developer and ion beam etching system were performed. Cryostat was designed and produced to measure electrical and bolometric measurements. Resistance-temperature in a-b axis gave the around 90 K as critical temperature. Bolometric measurement was done via superconducting transition region to decide the selected temperature to measure the change of resistance by sending signal from Stefan-Boltzmann Lamp in specific seconds. Change of resistance was observed from resistance-time measurement for bolometric measurement. Response time was calculated approaching 825 ms from the result of bolometric measurement. Our measurement set-up has limitation to read right data. Lock-in-amplifier may use to more accurate result.

ÖZET

TERAHERTZ DALGASI DUYARLI SÜPERİLETKEN BOLOMETRİK DEDEKTÖR

Terahertz (THz) dalgaları elektromanyetik spektrumun 0.3 ile 10 THz frekans aralığında ve 3 ile 0.03 mm dalga boyunda mikrodalga ve kızılötesi arasında kalan kısım olan terahertz radyasyonu elektromanyetik spektrumun sahip olduğu özelliklerden farklı özelliklere sahiptir. THz ışınımdan yararlanılan savunma sanayisi özellikle bilinmeyen, zararlı malzemelerin veya patlayıcıların tespiti gibi birçok alan vardır. Ayrıca, THz dalgaları deri, kumaş ve kâğıt gibi malzemelerden geçerken su ve metalden geçememektedir ve THz dalgası boyunca atomları iyonize etmek için yeterli enerjiye sahip olmadığından dolayı, THZ dalgaları canlı dokulara zarar vermemektedir. THz dalgasının bu faydalarından yararlanmak için birçok detektör üretilmiştir. Bolometrik dedektör 1 THz üzerindeki frekanslarda ışımayı algılamasından dolayı tercih edilmektedir. $Bi_2Sr_2CaCu_2O_{8+\delta}$ (Bi2212) tek kristali, bolometrik dedektör ile THz dalgalarını algılaması için literatür de ilk defa bu çalışmada kullanılmıştır. Bi2212 tek kristali epoksi yardımı ile safir alttaşa aktarılmıştır. Scotch bant ile mekanik olarak katmanlarına ayırarak 150-200 nm kalınlıkta kristaller elde edilmiştir. Kristallerin kenarları piramit şeklinde kesilerek, kristalin her yüzeyinin altın ile temas etmesi sağlanmıştır. Daha sonra, kristallerin gölgelendirmeleri yapılarak yaklaşık 200 nm altın kaplanmıştır. Temiz oda sürecinden sonra, Elektron Demeti Litografisi ile log-periyodik anten ve dört nokta kontak tasarımları yerleştirilmiş, birkaç işlemden sonra yongalar ölçüme hazır hala gelmiştir. Elektriksel ve bolometrik ölçümleri alabilmek için tasarlanan ve üretilen bolometrede alınan a-b ekseni direnç-sıcaklık ölçüm sonucunda yongalarımızın 90 K civarında kritik sıcaklık değerleri ölçülmüştür. Bolometrik ölçüm, belirlenmiş olan süperiletken geçiş bölgesinde bir sıcaklık belirleyerek bu sıcaklıktaki Stefan-Boltzmann lambası ile belirli saniye aralıklarında gönderilen sinyal ile dirençte oluşan değişime bakılarak yapılmıştır. Bolometrik ölçüm sonucundan yongalarımızın tepki süreleri hesaplanarak 825 ms'ye ulaşan değerler bulunmuştur. Ölçüm sistemimizde cihazların veri okuma hızına yetişememesinden dolayı, tepki süreleri asıl olduğundan daha yüksek okunmuştur.

To my family…

TABLE OF CONTENTS

LIST OF FIGURES

Figure **Page**

LIST OF TABLES

Table **Page**

CHAPTER 1

INTRODUCTION

1.1. Terahertz Radiation

The electromagnetic spectrum is described which comprise all recognized electromagnetic waves from gamma rays to radio waves. Basically, the spectrum is the occuring that the physical facts are arranged sequentially and electromagnetic beam is the emergent the energy types from atoms in various ways. Additionally, radiation is described that the energy spread from waves or photons and these spreading beams are called as electromagnetic radiation. In electromagnetic spectrum, wavelengths of electromagnetic radiation can be changed from electrical to cosmic waves due to this reason that between low and high wave frequencies are showed the diversity in electromagnetic spectrum. According to frequency and wavelength range, gamma rays has the highest energy and frequency. On the contrary, microwave and radio waves have longer wavelength and lower energy than other radiations in electromagnetic spectrum.

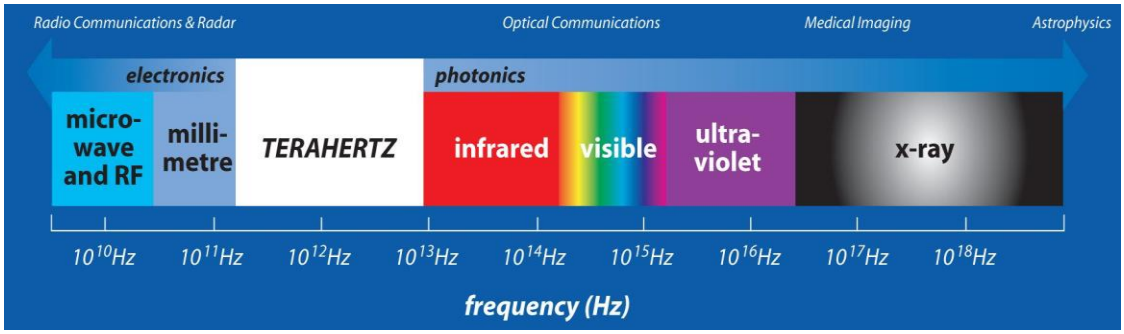

Figure 1.1. The electromagnetic spectrum

There is newly developed spectral region in spite of occupying wide range in electromagnetic spectrum which is called Terahertz radiation. This Terahertz (THz) region is between microwaves and far infrared region by having frequency ranging from 0.1 to 10 THz. Furthermore, these frequencies refer from 3 mm to 0.03 mm for wavelength range as round about dimension of paper thickness. THz radiation get

started with 3 mm and continue to shorter wavelengths. THz radiation has been the most working subject between the researching areas for specific reasons recently. THz radiation has non-ionizing, invisible to naked eye and non-destructive property as radio waves and microwaves contrary to X-rays but like infrared and microwave radiation. Because of ionizing process of X-rays by having enough energy to ionize the atom via removal an electron, it damage the living tissue. On the contrary, THz radiation has non-ionizing and having low energy property, people cannot damaged like cancer by T-rays unlike X-rays. Kawase's study has showed that T-rays do not influence on human body adversely (Kawase 2004). Another property of THz radiation is that it absorbed by metals and water (Ferguson, et al. 2002) but it can penetrate through some materials such as fabric, leather and paper via penetration depth is less than microwave radiation range. But there is a limitation about penetration by passing clouds, fog, metal and liquid water (Kohler, et al. 2003). These properties are used to many significant applications by having the rich band of frequencies in the electromagnetic spectrum. THz radiation matches the molecules in chemical and biological materials by detect the explosive materials in frequency range. These materials has own THz absorption range fingerprints to characterize THz modes by supply spectroscopic knowledge (Fischer, et al. 2005). Explosive materials and biological weapons can be detected by the existing of THz radiation (Mueller, 2006). Spectroscopic property of THz radiation is useful for medicament sector by descrying the exact matters of drugs. There are many other application areas of THz radiation which will be explained in next section.

1.2. Applications of Terahertz Radiation

By virtue of the fact that THz region has wide range between microwaves and infrared in electromagnetic spectrum, remarkable application of THz radiation is existed. THz technology grow quickly due to its extensive region. This growing provide imaging and spectroscopy development in THz range. Imaging technology obtain security, bio-medical imaging and quality assessment. In addition, spectroscopy technology supply chemical analysis, biological spectroscopy and environmental sensing.

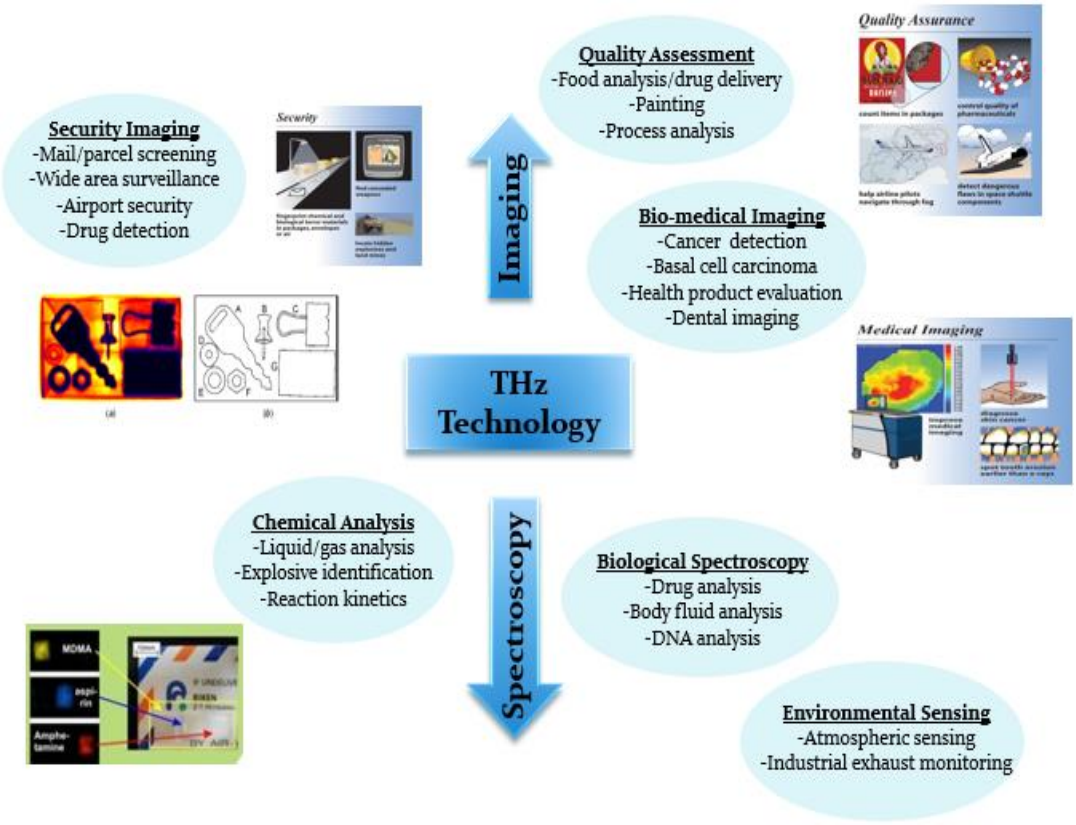

Figure 1.2. Application areas of THz radiation

Terahertz spectroscopy's applications can be arranged from detecting defects in tablet coating as medical industry, chemistry, astronomy, product or material inspection to detecting of cancer. As a pharmaceutical industry, there is a coating layer outside of tablet which is using for mixture of active substances as a powder or condensed powder. It is important to have uniform and purity surface by coating because of developing the efficiency of product. In pharmaceutical industry, THz image is used to get best result for implementing 3D analysis for tablets with coating layer. Additionally, THz image method is useful technique for specify the thickness of coating for tablets because of being semitransparent to THz frequencies and cannot strew them and rom each coating layer THz radiation is reflected to the detector. Incident THz pulses can penetrate on coating tablet surface by different coating tablet layers. It is verified that THz spectroscopy is an available method to separate between distinctive forms of the tablets (Fitzgerald, et al. 2005). In pharmaceutical industry, detection of impurities in production as a tablet is significant factor. If the result of tablets fall through, whole work will be disappointment. That's why, THz radiation can take information from

chemical and physical properties which make possible to identify the structures and performance speciality of the tablets such as purity, stability and decomposition. It is important to detect the defects in coating tablet by THz radiation because of the fact that if product get in touch with water, it may influence the performance of product (Pawar, et al. 2013).

THz spectroscopy supply quickly identification and crystallization of coating tablets which may show different properties. It can be detected discrepancy between samples and realize crystalline states in coating tablets as well. This method based on vibrations between chemical kinds by sensitivity of THz radiation. It may also determine discrepancy forms of hydrate which has the most finding essential matter is lactose in tablets. There are three shapes of hydrate lactose in terahertz spectrum which are α monohydrate, α anhydrate and β anhydrate to make an analysis as crystalline forms and lattice structures of materials which is showing in Figure 1.3.

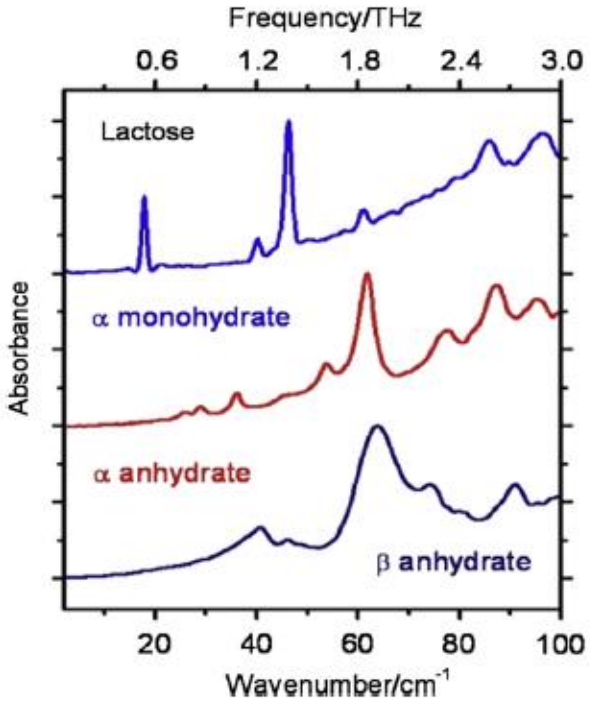

Figure 1.3. Terahertz spectroscopy to diversify hydrate forms
(Source: Pawar, et al. 2013)

Many materials have special peak in THz electromagnetic spectrum as a fingerprints. This makes able to discover the spectral identification with THz imaging. THz peaks are characterized by transmitted and reflected THz radiation that include vibration modes which obtain spectroscopic knowledge about materials (Fischer, et al. 2005). By this way, THz radiation information may be influence to examine the explosive which are chemical and biological materials such as sarin, soman for nerve agents and RDX, TNT which are used to make a bomb. Figure 1.4 and 1.5 show the explosive materials has specific peaks at different THz frequencies to detect explosive materials in a closed package. THz technology is an influence method to examine explosive materials as mentioned and studied before (Arnone et al., 1999).

THz imaging technology can be used in security, medical imaging and quality assessment. It is used as mail/parcel screening, wide area surveillance, airport security and drug detection in security imaging. Medical imagining can be used for cancer detection, base cell cancer, health product assessment and dental imaging. THz imaging is used for food analysis or drug delivery and also process analysis as quality assessment. As mentioned, THz radiation is used in surveillance to security scanning to discover the hidden materials in closed package. Dangerous hidden metallic or non-metallic such as ceramic and plastic materials are detected by THz radiation. THz rays cannot penetrate skin due to the water content in contrast clothes. This makes the possible to use THz rays in security purpose (Pawar, et al. 2013).

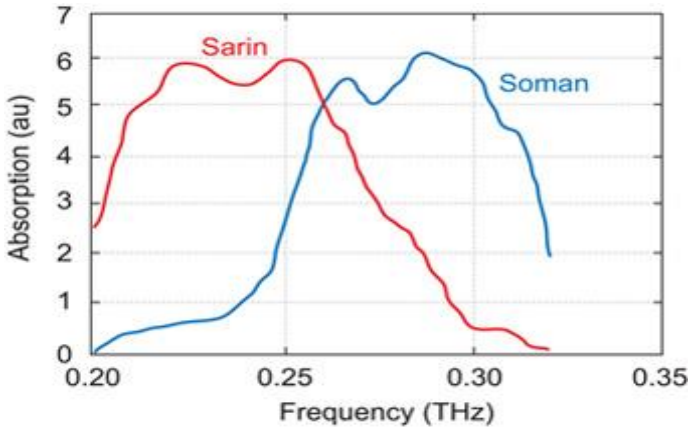

Figure 1.4. Terahertz spectroscopy of sarin and soman nerve agents
(Source: Hight-Walker, et al. 1997)

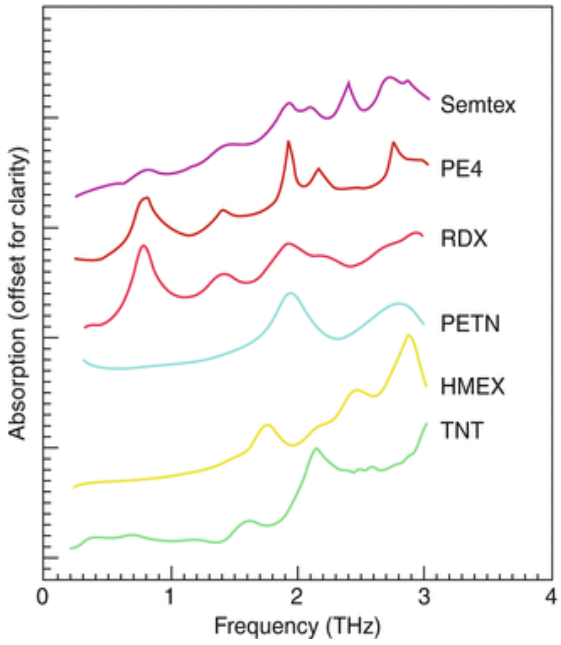

Figure 1.5. Terahertz spectroscopy of explosive materials
(Source: Kemp et al., 2003)

THz radiation is not harmful for the tissues and DNA because it has a relatively low photon energy by contrast with X-rays. By having specific frequency terahertz radiation in materials, THz can pass by benefit of having water ingredients via reflection is occurred. This makes THz radiation as a safe and painless method for imaging or detection (Pawar, et al. 2013).

THz rays are so suitable for communication because of having broad bandwidth to supply the large transmission data however there is limitation about penetration through fog and cloud and earth's atmosphere is a powerful absorber for THz rays contrary to infrared radiation as some define absorption bands (Su, et al. 2012). Addition, there is a possibility for high bandwidth to wireless and satellite communication (Tonouchi and Saijo, 2003).

Unfortunately, there are some difficulty for communication by THz radiation cause from powerful atmosphere absorptions and small power sources. Fox's study explained that this method may use for over altitudes which water vapor lead to absorption for telecommunication from aircraft to satellite or from satellite to satellite (Fox 2002).

1.3. Terahertz Sources

There are an increasing and developing areas which are the applications of terahertz radiation in recent years because of used efficient strong terahertz sources. Four major advance contribute to develop of THz sources. Firstly, microwave and millimeter waves devices enter through THz gap. In the second place, free electron lasers and backward wave oscillator (BWO) contribute to THz range. As a third addition part for THZ range is optical THz generation and lastly Quantum Cascade Laser (QCL) has recently contributed to THz range. These major and variety of THz sources can be seen in Figure 1.6.

To begin with, solid state electronic sources have limitation about low frequency at high THz waves. Emission of solid state electronic sources is tunable until to 1.5 THz. Gunn diodes, IMPATT diodes (Impact Avalanche Transit Time) and TUNNETT diodes (Tunnel Injection Transit Time) are example for solid state electronic sources at high frequency. Gunn and IMPATT diodes reach 400-500 GHz as oscillating frequencies on the other hand, TUNNETT diode (GaAs) generate 10 mW at 202 GHz. Uni-travelling carrier photodiode (UTC-PD) were produced with difference between two wavelengths light from two distinct wavelength laser diode. Ito and colleagues succeed in output power with 20 nW and 10 μm at 100 GHz and 1 THz, respectively by using laser diode which was operating at 1.55 μm (Ito et al., 2005) Resonant tunneling diode (RTD) has form of quantum well in structure with double barrier that semiconductor device. RTD can work at high frequencies which InGaAs/AlAs has frequency of 915 GHz at low output of few ten of nW. RTD was used to show successfully over 1 THz range, recently. High Electron Mobility Transistor (HEMT) is reported as solid state electronic device by Northrop Grumman. AlGaN/GaN HEMT was reported THz generation at 0.75 and 2.1 THz in 2010 (Fatimy et al., 2010) There is a multiplier as an example for solid state electronics which has output power is lower than input that cause obstacle in THz range. Recently, solid state electronic sources are used for wireless communication, astronomy at THz range.

Secondly, free electron lasers and backward wave oscillator (BWO) utilize to THz range. They create continuous wave or pulsed THz waves. But they have disadvantage as cost and large size with regard to other THz sources. Working principle of electron lasers and BWO is same each other. BWOs need cryogenic cooling but size and weight

of them is not big and heavy because of reason, they have wider applications areas than electron lasers.

As a third part, optical THz emission contribute to THz sources. The most widespread optical THz sources are continuous waves THz sources which 0.9-3 THz range versus 1-30 mW output power. Also, photomixing is used to produce continuous wave in THz radiation via using lasers. Optical rectification occurs in short laser pulsed interaction as an ultrafast laser for THz range.

Lastly, Quantum Cascade Laser (QCL) is challenging source for THz generation. QCL was suggested in 1971 but this idea was developed and demonstrated in 1994 (Faist et al., 1994). It was started with frequency of nearly 70 THz, after some search, 4.4 THz range was acquired (Köhler et al., 2002). Kohler and collages reported the first working QCL in 2002 (Köhler et al., 2002). This QCL conveys 2 mW power with 50 K at 4.4 THz range. By decreasing the output power with increasing temperature was observed in this QCL and result in zero output power at room temperature. Recently, 1.59 THz frequency was reported for QCL and 1.39 THz lasing frequency when apply the magnetic field was succeed (Scalari et al., 2006). After reported some QCL, operating up to temperature of 186 K, QCL showed by Kumar and collages in 2009 (Kumar et al., 2009). Recent studies for QCL have focused to decrease the lasing frequency and increase operating temperature, frequency range.

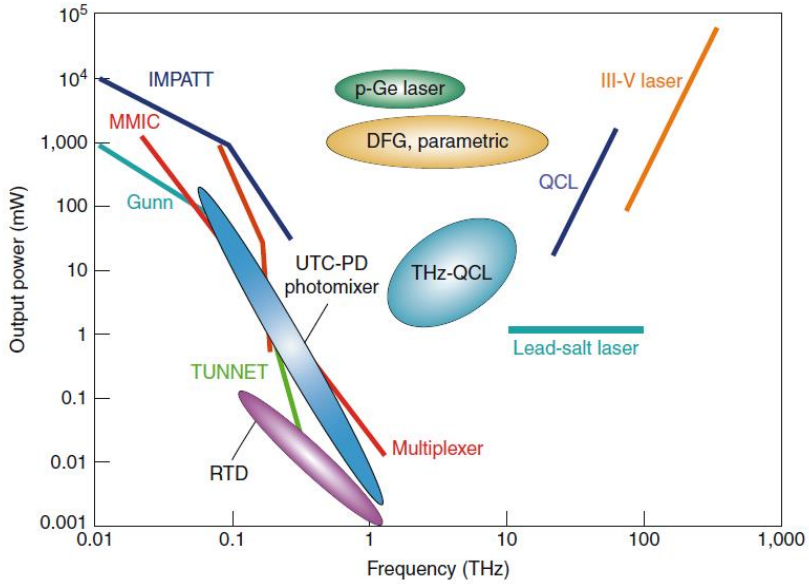

Figure 1.6. Terahertz emission power (mW) as a function of frequency (THz) (Source: Tonouchi 2007)

1.4. Superconductivity

Backgrounds of superconductivity will mention at this section. Scientists concentrate to superconductivity after discovering by Onnes and its diverse applications. After intensive studies, scientists get over many challenges about superconductivity. By developing potential of superconductors, various applications are created by cooperation between theoretical and experimental scientists.

Improving by discovering the new superconductors and their timelines, fundamental properties as zero resistivity and perfect diamagnetism, Type I and II Superconductors and high, low temperature superconductors will mention at this section. BSCCO high temperature superconductor will mention as last section for superconductivity.

1.5. History of Superconductivity

Working about superconductivity was started in 1908 with liquefy the helium by Dutch physicist H. Kamerling Onnes. Additionally, behaviors of electrical resistivity of metals at low temperature was firstly studied by Onnes. The results of these working by Onnes from Leiden University, it was discovered to drop the resistivity of mercury at 4.2 K temperature very small resistance almost zero in 1911 which is shown in Figure 1.7. He received The Nobel prize in physics for investigation of properties of low temperature materials which are led and production of liquid helium in 1933.

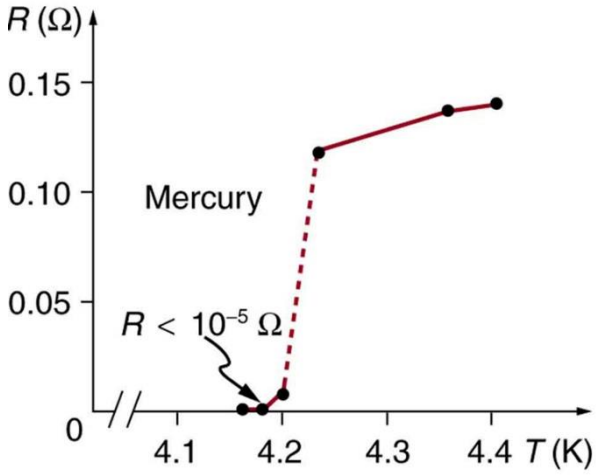

Figure 1.7. Superconductivity property of mercury
(Source: Onnes, College Physics 2012)

Besides, superconductors surpass to normal state with effect of high applied magnetic field and it was discovered the superconductors' magnetic properties. After discovered of superconductivity, intensive studies were started through superconductors. As the result of these studies, it was discovered to indicate superconducting properties of lead with 7.2 K in 1913 by Onnes, niobium with 9.2 K in 1930 by Chapnik. After 25 years discovered the superconductivity, Walter Meissner and Robert Ochsenfeld discovered the expelling the magnetic field from interior of the superconductors in 1933 (Meissner et al., 1933). Due to discovering this decisive property of superconductors lead to new applications for magnetic region.

Niobium nitride (NbN) was discovered the new superconductor material with 16 K critical temperature in 1941. Vanadium silicide (V_3Si) showed superconductivity at 17.5 K in 1953.

John Bardeen, Leon Cooper and John Schrieffer asserted the BCS theory about understanding superconductivity at nearly zero Kelvin in 1957. BCS theory describe the superconductors about absolute zero. Cooper realized the atomic lattice vibrations responsible to associate the electrons. These vibrations cause to electrons to pair and pass inside the lattice without any collision. These pair electrons are called as Cooper pairs. But at later years by discovering the high temperature superconductors, BCS theory was becoming insufficient to explain the principle on it.

First wire from niobium titanium (NbTi) was produced from superconductors in 1962 at Westinghouse.

Brain D. Josephson at Cambridge University suggest that it is possible to pass current through compacted metallic layer between two superconducting layer in 1962. This suggestion theoretically anticipated quantum tunneling of Cooper pair through the few nanometers insulator layer. This was proved in a short time and cause to electronic application area for superconductors.

Alex Müller and Georg Bednorz discovered the brittle ceramic with critical temperature is highest until 1986. They showed the lantanium, barium and copper oxide ceramics has 30 K critical temperature as superconductors in 1986 as a breakthrough discovery until that time. In real, scientist know that ceramics do not conduct the electricity well but after discovering the cuprates, it was realized the breakthrough development about ceramics and superconductors. That's why, high temperature superconductors in cuprates encouraged to superconductivity. After short time, they had a Nobel Prize for superconductor copper oxides-cuprates.

It was discovered that yttrium has higher critical temperature 92 K instead of using lantanium in1987. Thus, exceeding of temperature liquid nitrogen 77 K was succeed with yttrium. Superconductor works with liquid nitrogen instead of liquid helium lead to extend the application areas. That's why, this discovery is important to show critical temperature above liquid nitrogen for superconductors. Anderson suppose the form of superconductivity in cuprate about pairing at the same year.

Davydov offered the theory about electron-phonon coupling in 1990. It relates to electron or hole pairs that chain in CuO_2 superconducting plane cause to deformation.

$Hg_{0.8}Ti_{0.2}Ba_2Ca_2Cu_3O_{8.33}$ ceramic was discovered with 138 K critical temperature in 1995. This material has the highest critical temperature under normal pressure until that time.

Alloy of gold-indium was noticed that they are both superconductor and magnet in 1997. Scientists discovered magnesium diboride (MgB_2) with not too high critical temperature 39 K but after discovery, some enhancements were applied to MgB_2 to use in application areas.

Until 2005, many high temperature superconductors were discovered and evolve the application of superconductivity. In recent times, iron based superconducting material was realized with almost 50 K critical temperature. If scientists succeed in increasing the critical temperature, this superconductor may be candidate to use in applications.

1.6. Fundamental Properties of Superconductors

Resistance passes current through conductor to apply the voltage and as a result of this passed current heats the conductor. The more resistance is big, the more big applying voltage is needed and missing energy is occurred. But in some conductors, if we cool the material under the specific temperature depending on the type of material, electrons which carry the current cannot to turn energy to heat and then material's resistance drops to zero. If material is cooled below the critical temperature, phonon effect disappears and electrons moves easily in structure without any contact with lattice. By this time, there will be decrease about material's resistance to drop zero below critical temperature which is called zero resistivity property. These materials pass the current with infinite resistance without crossing any resistance when material is cooled below critical temperature. Zero resistivity contribute to notice the properties of metals during critical temperature. This transition which passing from metal to superconductor at critical temperature is like evaporation or melting process in other materials however there will be no change at other properties of superconductor materials except only one part of electrons pass different quantum state.

This superconducting transition mechanism is related to chemically Bi, Ti and Hg cuprate which are indicated superconducting properties. If we compare the sharpness of transition region for high and low temperature superconductors, low temperature superconductors indicate high sharp than single phase high temperature superconductors as 1K width.

If we look the metals, there will be loss of energy during passing current on the conductor in contrast to superconductors. Electrical heater spread the heat from causing electrical resistance. This phenomena occurs by outer electrons passing through another energy level as copper, aluminum and other similar metals. Electrons starts to move and collide with defects or contamination in lattice structure. When electrons collide with this obstacle randomly, they loss energies to release heat energy. Electrical resistivity of metals decreases steadily then get through the constant resistivity value.

Electrons behavior is different inside of the superconductor in contrast of conductors. Electrons can move without any collide with contamination or defects by not losing the current or energies. It is occupy to scientist that why electrons cannot collide any contamination or defects during moving the electrons. Lattice vibrations are

increased by heating the superconducting material also conduction electrons and vibrations are decreased by cooling it. Many suggestions like lattice vibrations were propound to understand zero or very tiny resistance change during moving of the electrons until Heike Kammerling Onnes was explained in 1911. When cooling the superconducting until critical temperature (T_c), resistance of superconductor reach the unmeasurable value which very tiny as zero which was called as zero resistivity was discovered by Onnes.

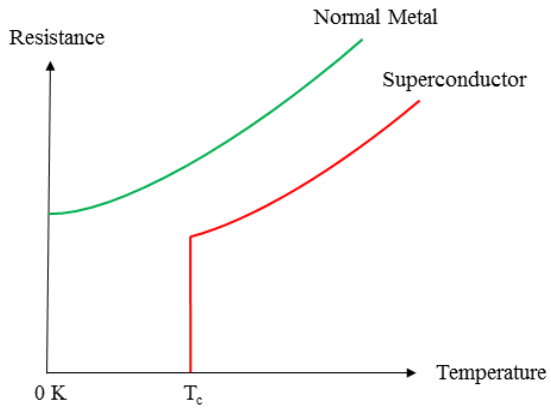

Figure 1.8. Temperature dependence of resistance with normal metal and superconductor

Superconductors show distinctive electrical and magnetic properties. Superconductor not only show zero resistivity, but also perfect diamagnetism which is known as Meissner Effect. This effect was discovered by Meissner and Ochsenfeld in 1933 (Meissner et al., 1933). When superconductor is cooled below the critical temperature as have zero resistivity, they expel magnetic field from their interior due to Maxwell's equations. These are not allowed to enter the magnetic field through the superconductors inside.

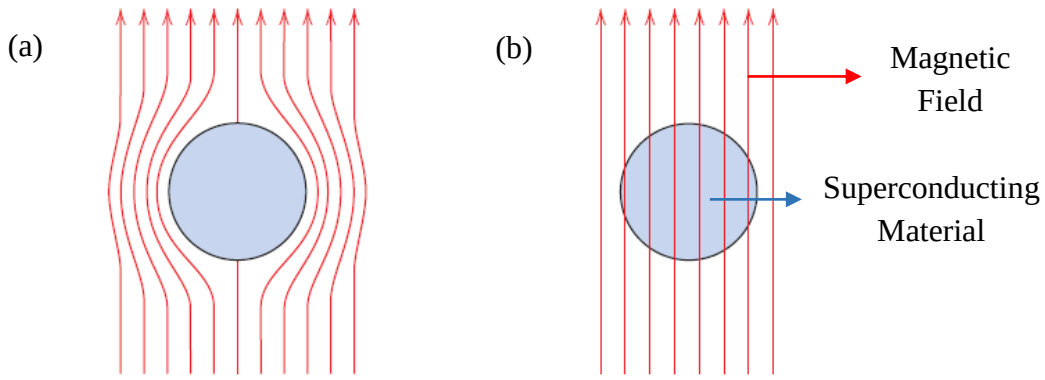

Figure 1.9. Figuration of Meissner Effect a) Superconductor repels the magnetic field from interior b) Superconductor becomes conductive when magnetic field penetrate inside.

If we look detail to Meissner Effect, it will be easier to understand the effect of magnetic field on superconductor. Figure 1.10 explain the behavior of perfect conductor and conductor in magnetic field. Figure 1.10 (a) shows the conductor is cooled below critical temperature which represent zero resistivity. The magnetic field in conductor depends on some parameters such as size of field pre-cooled below critical temperature. Figure 1.10 (b) shows results of Meissner effect on superconductor materials. When magnetic field is applied to superconductor material below critical temperature, field is expelled from interior of it. To explain the Meissner effect, perfect conductor is not enough. There is a limitation about critical current value and it is possible to pass from superconductor state to normal state if applied magnetic field surpass certain field. In superconductors, if magnetic exist inside the material before becoming the perfect conductor, magnetic field will stay inside the superconductor.

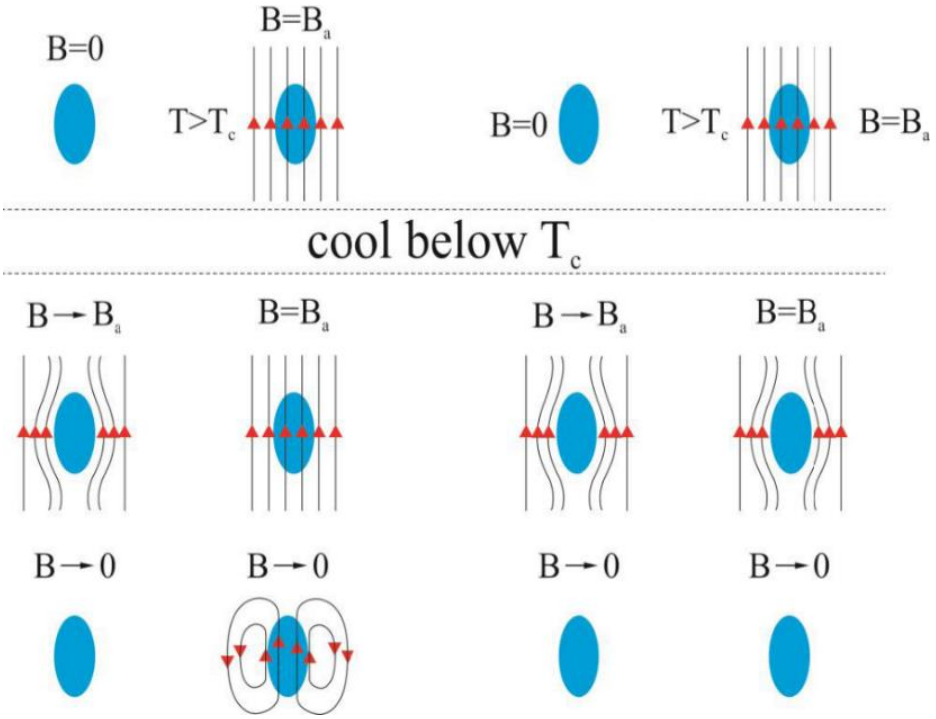

(a) Perfect Conductor (b) Superconductor

Figure 1.10. Meissner Effect
(Source: Meissner Effect of Superconductivity, 2002)

If we look the difference between impure and pure superconductors, it is obviously seen the diversity at the superconducting transition region. Transition temperature or sharpness of this region is changed by depending on pure or impure superconductors. If material is pure, it shows superconducting transition region is sharp. This sharpness can be observed when superconductor is exactly cooled. If material has some impurities, transition region is shown broadened.

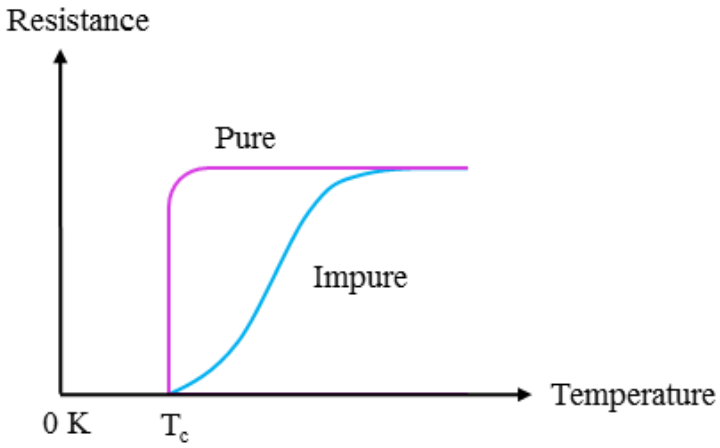

Figure 1.11. Transition temperature for pure and impure superconductors

1.7. Type I and Type II Superconductors

Superconductors are divided two group as Type I and II according to behavior of exposing the magnetic field to normal or superconducting state in 19th century. There are no difference between Type I and II about superconducting mechanism. Soft superconductors belong to Type I and they entail the cooler temperature to behave as superconductors. Pure metals can be example for Type I superconductors. Type II superconductors known as hard that discovered by W. de Haas and J. Voogd in 1930. Metallic compounds and some alloys belong to Type II superconductors. Both of them has similar superconducting-normal transition properties however, effect of Meissner is different. Meissner effect based on that magnetic field cannot penetrate though the superconducting material during below critical temperature.

Magnetic field exclusion originate surface current with induction in Type I superconductors. This type superconductors repel the applied magnetic field nevertheless magnetic field penetrate through material at the critical magnetic field value (H_c) and material translate the normal state. Similarly, until critical magnetic field value, Type I superconductors' magnetism increase linearly in negative direction, however, there will be a sharp decrease at H_c and it goes to very small value, even almost zero.

As mentioned above, Type I superconductors has sharp normal-superconductor transition region and are not functional for superconductor magnet due to small H_c. Pure metals show Type I on the contrary transition metals.

Type II superconductors behave like Type I properties, until H_{c1} critical magnetic value that they repel the magnetic field until H_{c1} and magnetism in negative direction which means Meissner effect. If applied magnetic field value is over than H_{c1}, magnetic field diffuse to the superconductors by penetrating one part. In that situation, material continue the superconducting property however, when material reach the magnetic field value H_{c2}, magnetic field entirely penetrate through the superconductor and it lose the superconductivity property. Type I superconductors have low H_{c1}, on the contrary Type II superconductors have high H_{c2} magnetic field value. Between area H_{c1} and H_{c2} is called as mixture of normal and superconducting state. In that situation, magnetic fields penetrate through material as flux lines and tubes. These flux lines that girded superconducting areas with small cylindrical normal region is called vortex. When the magnetic field increases, the number of vortex increases and with this increment the vortex combine together after that the material pass normal state. In mixture situation, the material is formed like superconductor-normal-superconductor-normal and the intensity of magnetic field spreads completely in normal regions but in superconductor region it decreases until the definite depth (λ). There is no difference between normal and superconductor regions in terms of chemical and crystallographic. Flux lines are parallel to the applied magnetic field in direction of main axis and the magnetic field causes current around the vortex. As a result, this current separates the normal region from the superconductor region. This flux is not actually transition flux but it is screening flux for first Type superconductor which causes ideal diamagnetism. The flux which is around the vortex causes that each vortex behaves like magnets and so, when there is a flux on Type II superconductor, it effects Lorentz force and the vortex will move on because of this effect. This movement of the vortex induce parallel electric field which uses the energy from circuit and leads to the resistant effect.

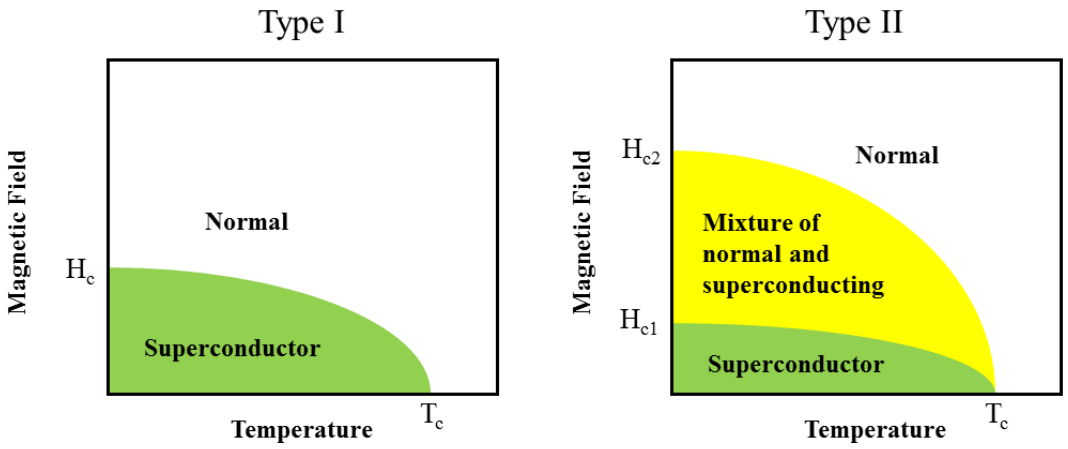

Figure 1.12. Type I and II Superconductors

Another most important different between Type I and II superconductor is that difference of independent ways of electrons in normal situation. Because the amplitude of average independent ways, used for the types of superconductor, determines the length of penetration and coherence. For Type I superconductors, the length of coherence is bigger than the length of penetration, so it causes an increment of positive gap of surface energy at transition between superconductor and normal region. In Type II superconductor, it is exactly opposite from the Type I superconductor, which is that the length of penetration is bigger than the length of coherence, so it causes vortex and an increment of negative gap of surface energy at transition between superconductor and normal region. Because of that Type II superconductors has high critical magnetic field, they are used for magnet production and also it is very important in technological application fields.

1.8. High Temperature Superconductors

J. George Bednorz and Karl Alex Müller discovered crucial case in superconductivity research area at Zurich IBM Research Center in 1936. They found the new superconductor with composition of lanthanum, barium, copper and oxygen by critical temperature 35 K (Bednorz et al., 1986). By starting the discovery of the high temperature of superconductors that are called also Type II superconductors. After that, it was found $La_{2x}Ba_xCuO_4$ with x=0.2 superconducting phase. Scientist studied to increase the critical temperature for barium, that's why it was succeed by using

strontium instead of barium with 36 K. After this improvement, scientist continued to work on lanthanum structure and got the critical temperature 52 K at high pressure (Chu et al., 1987). Later this considerable studies, scientist from Alabama and Houston University found the new material has yttrium, copper, barium and oxygen with specific phase ($YBa_2Cu_3O_7$) and observed the transition temperature around 92 K (Wu et al., 1987). This discovery is the turning point of superconductors because of that it has critical temperature above the temperature of liquid nitrogen (77 K). That's why, it was possible to use easy obtainable cooler and reduce the cryogenic costs by using liquid nitrogen instead of liquid helium (4 K). Superconductors which has critical temperature below and above liquid nitrogen can be seen in Figure 1.13. After this crucial discovery, scientists focused detail to superconductivity and they found bismuth, strontium, calcium, copper and oxide composition Bi-Sr-Ca-Cu-O as two phased $Bi_2Sr_2CaCu_2O_{8+\delta}$ (Bi2212) with critical temperature 95 K, $Bi_2Sr_2Ca_2Cu_2O_{10+\delta}$ (Bi2223) transition temperature 110 K in 1988 (Maeda et al., 1988). After discovery of BSCCO, scientists reported the $Tl_2Ba_2Ca_2Cu_2O_\delta$ (Tl2223) with critical temperature 125K (Hazen et al., 1988) and then Hg-Ba-Ca-Cu-O compounds $HgBa_2Ca_2Cu_3O_{8+\delta}$ (Hg1223) with critical temperature 135 K (Schilling et al., 1993). After some studies about Hg1223 superconductor, scientists attained the higher critical temperature as 166 K (Gao et al., 1994).

As can be understand above, high T_c superconductors have nearly copper oxide component. Until that time, investigating compounds has perovskite lattice structure. After discovering copper based superconductors, MgB_2 material was discovered with critical temperature 39 K in 2001. 5 years later in 2006 LaOFeP was discovered but it has low critical temperature that's why, this superconductor was not use very much in technological applications (Kamihara et al., 2006). Scientist searched the doped LaOFeP to increase the critical temperature for this reason LaOFeP doped with Fe and got 43 K as critical temperature (Takahashi et al., 2008).

After discovering the high and low temperature superconductors, high temperature superconductors known as possess Cu-O plane regardless of high critical temperature value and low temperature superconductors called known as not have Cu-O plane. By the starting to discover high temperature superconductors, critical value was nearly 30 K but now Hg based superconductors have 166 K critical temperature. It was explored that there is a relation between number of copper oxide layer and critical temperature of superconductor. Repeating of copper oxide layers as periodical increase

the critical temperature of material. Because of this investigation, scientist expects to increase the critical temperature nearly 200 K. High temperature superconductors have anisotropic property unlike low temperature superconductors. Anisotropic property caused from layered structure of superconductors.

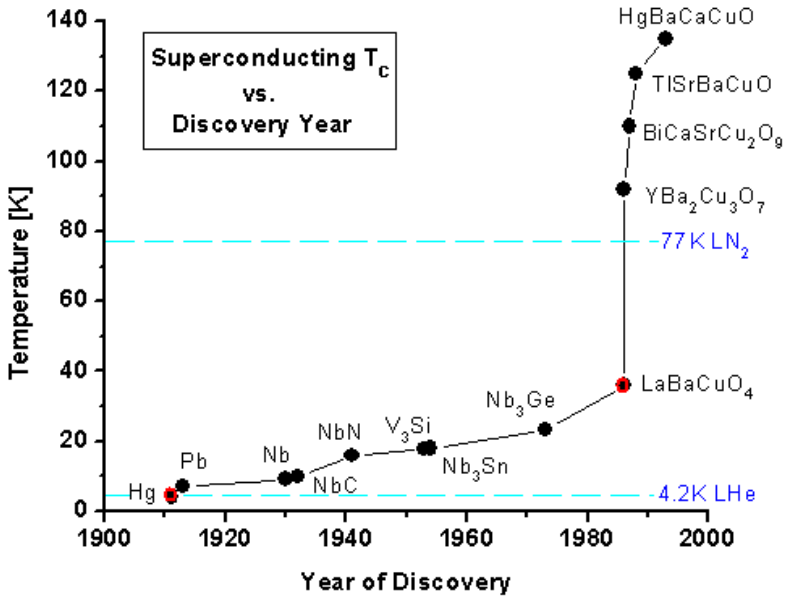

Figure 1.13. Discovery of the superconducting materials in the last century (Source: Hoffman Laboratory, 2010)

1.9. Properties of BSCCO Single Crystal

Bi-Sr-Ca-Cu-O (BSCCO) was discovered by scientist group of Maeda in 1988 (Maeda et al., 1988) $Bi_2Sr_2Ca_{n-1}Cu_nO_{2n+4+\delta}$ (BSCCO) has three different phases by n means the number of unit cell of the copper oxide layer with n=1 $Bi_2Sr_2CuO_{6+\delta}$ (Bi2201) (Yurgens 2000) and $T_c \leq 20$ K, for n=2 $Bi_2Sr_2CaCu_2O_{8+\delta}$ (Bi2212) and $T_c \approx 95$ K and for n=3 $Bi_2Sr_2Ca_2Cu_3O_{10+\delta}$ (Bi2223) and T_c=110 K. In this type superconductor, unit cells have Bi-O with Sr-O, Cu-O and Ca-O layers. Sr-O and Bi-O layers do not show the superconducting property on the contrary C-O layers. If compare the chemical bond, Bi-O has the weakest bond with compare the Cu-O that's why, any deformation or crack occurs in that layer. BSCCO is high temperature superconductor that's why, it has anisotropic property due to layered structure so it can be separated easily without any damage. Additionally, properties of BSCCO depends on some parameters such as compositions, annealing temperature, preparation method of superconductors and so on.

As mentioned above, BSCCO has 3 phases. To begin with, n=1 phase $Bi_2Sr_2CuO_{6+\delta}$ (Bi2201) has Cu and O atoms with square pyramid structure by both side of it, have Sr-O layers. Distance between BiO_3 and SrO_2 is 2.9 Å, Bi-O and BiO_2 is 2.0 Å. These distances are available both above and bottom of the structure. Unit cell of Bi2201 generally refers to a=b≈5.4 Å and c≈24.4 but a, b values can be changed from 3.9 to 5.4 Å, depends on structure of superconductor (Mei et al., 1988).

Continue with n=2 phase $Bi_2Sr_2CaCu_2O_{8+\delta}$ (Bi2212) has only Ca-O layer between Cu-O layer than Bi2201 as difference. In this phase, Sr-Cu-Sr order is destroyed via Cu-O layer which is occurred between two Sr-O_2 layers. Additionally, Ca-O layer is inserted between two Cu-O layers. Thus, Sr-Cu-Ca-Cu-Sr order is occurred in Bi2212 phase. Unit cell, lattice parameter refers to a=b≈5.37 Å and c≈30.8 Å. According to this layered model, C-O double layers has 3 Å, Sr-O and Bi layers has 12 Å with intrinsic Josephson Junction 15 Å thickness. Each copper atom has four oxygen with separated 1.9 Å thickness in CuO_2 plane. Critical temperature of Bi2212 phase is changed with the number of CuO_2 layer. Increasing the number of copper oxide layer, critical temperature of BSCCO is increased.

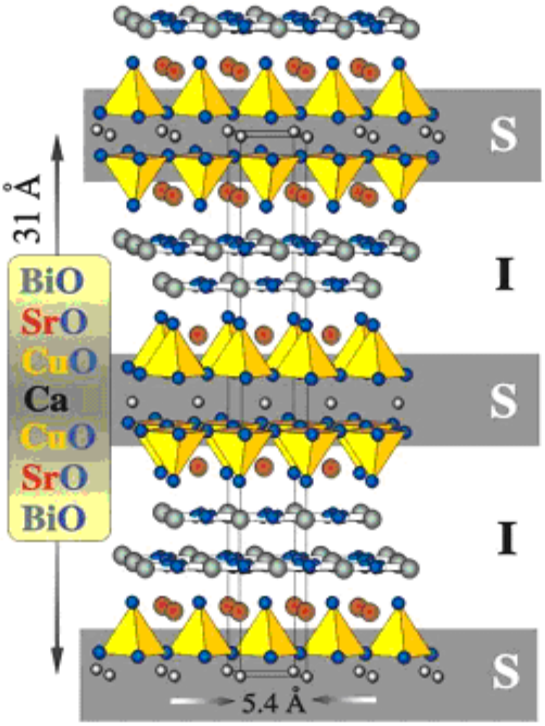

Figure 1.14 The crystal structure of Bi2212
(Source: Yurgens et al., 1996a)

Bi2212 phase has easy cleaved property because of layered structure. These layers can be overdoped or underdoped by adding or removing oxygen from Bi2212. This property alter the electrical property of crystal. By increasing the doped, critical value of Bi2212 is increased, too.

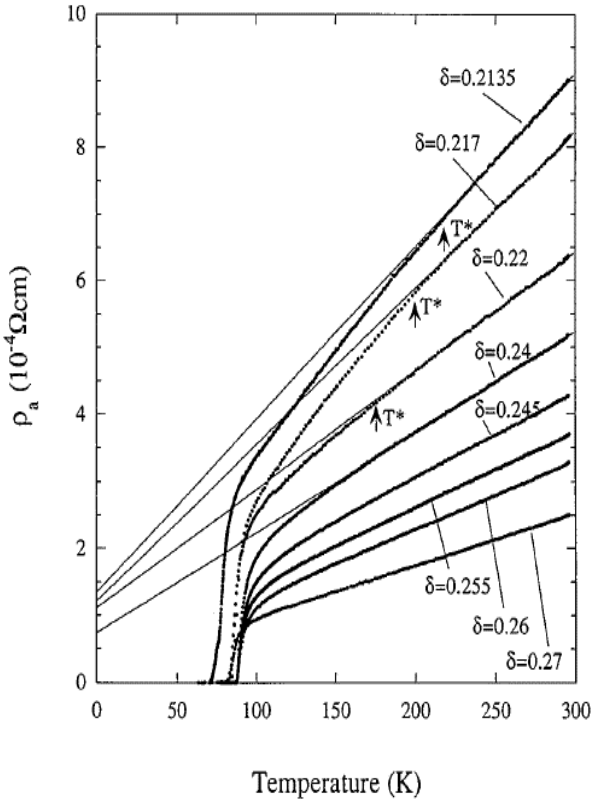

Figure 1.15 In a-plane resistivity of Bi2212 single crystal versus temperature with different oxygen doped δ (Source: Watanabe et al., 1997)

There is a research about doped or underdoped level of Bi2212 that has 90 transition temperature. Figure 1.15 shows the a-plane resistivity verses temperature measurement with distinct oxygen levels. This graph refers that while oxygen level increasing critical temperature of superconductor is increased, too. By developing critical temperature, superconductor has doped property but decreasing the critical temperature, it has underdoped property. Watanabe et al. showed that optimally doped superconductor has δ= 0.24-0.25 oxygen level with decreasing oxygen level below 0.22, it become underdoped with almost 77 K critical temperature (Watanabe et al., 1997). Last phase, n=3 $Bi_2Sr_2Ca_2Cu_3O_{10+\delta}$ (Bi2223) has same number and order Bi-O and Sr-O layers but Cu-O and Ca-O are intervened in this layer and Sr-Cu-Ca-Cu-Ca-Cu-Sr order is occurred. Unit cell refers to a=b≈5.4 Å and c≈37.1 Å. Bi2223 phase has small a of Bi2212 phase that affect intrinsic property of Bi2223.

CHAPTER 2

TERAHERTZ DETECTORS

Terahertz detectors (THz detectors) act crucial role in distinct areas for instance, material identification for security (explosive, biological materials and drugs), material imaging, communication and cancer detection for human activities. THz detectors are also used for astrophysics because THz waves have nearly half of luminosity of the universe and nearly all photons spread for the Big Bang (Blain et al., 2002).

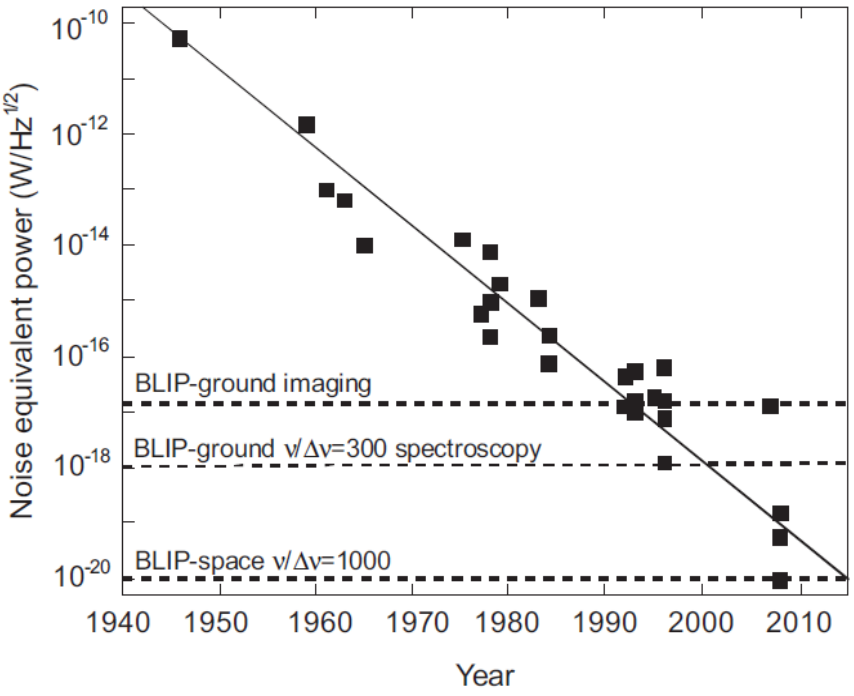

Figure 2.1. Improving of NEP for bolometers in half a century
(Source: Sizov et al., 2010, Benfrod, Transition Edge Bolometer for CMB Polatimetry)

Recently, many detector have been produced and developed which based on different principle and used for distinct application areas but the common important point between these developed detectors is the increasing of the detectivity, sensitivity and decreasing of Noise Equivalent Power (NEP) (parameters to determine the performance of detector). Development of NEP for bolometers (kind of detector) is

enchanting which NEP has been diminished by a factor 10^{11} in 70 years can been seen in Figure 2.1.

Detectors can be divided two group according to broadband and narrowband detections. First, direct detectors (incoherent detection systems) permit only amplitude of signal, based on thermal absorption principle. While, indirect detectors (coherent detection systems) use for narrowband detections that permit both signal amplitude and its phase. Direct detectors are room temperature detector which has big response time (nearly 10^{-2}-10^{-3} s). They have NEP 10^{-10}-10^{-9} W/Hz$^{1/2}$ for uncooled direct detectors but it was reported that is possible to get smaller NEP as 10^{-13}-10^{-17} W/Hz$^{1/2}$ and response time 10^{-6}-10^{-8} s for semiconductor detectors which operates at liquid helium temperature (Sizov et al., 2010).Actually, higher detectivity and sensitivity of detectors have to cool until nearly mK temperatures to get smaller response time from detector. Golay cells, pyroelectric detectors, bolometers can be an example for direct detectors. Indirect detectors, recently have been used for spectroscopic researches based on fast laser principle. Schottky barrier diode (SBD), Superconductor-insulator-superconductor junction (SIS), superconductor and semiconductor hot electron bolometer (HEB) are detectors for example of indirect type. Photomixing, heterodyne detection is also kind of indirect detectors. Electro-optic sampling and photoconductive switching are called as pulsed type detectors whereas photomixing and heterodyne detection are known as continuous wave (CW) detectors. Additionally, Schottky diodes can be used as mixers. Unit of NEP is W/Hz$^{1/2}$ for direct detectors whereas W/Hz is unit for indirect detectors. Many studies still publish W/Hz$^{1/2}$ as a unit for indirect detector that's why, in this thesis W/Hz$^{1/2}$ is used for this type detector as unit. If we compare direct and indirect detectors, indirect detectors provide higher spectral resolution then direct detector and direct detectors have wider spectral range that's why, they prefer to image. Direct detectors are used for application which detectivity is more effective for results than spectral properties. Direct detectors have higher sensitivity because of low temperature bolometers and response time of detector can be stated by changing of power of signal.

Terahertz detectors can be divided two group according to their operating temperature as room temperature and cryogenic detectors but cryogenic detectors has lower NEP than room temperature detectors because of cryogenic effect and have higher detectivity and sensitivity.

Table 2.1. Comparison of THz detection technologies
(Source: Pala et al., 2012)

Detector Type	NEP ($W/Hz^{1/2}$)	Responsivity (V/W)	Response Time (s)	Operating Temperature (K)
Bolometers	10^{-16}-10^{-13}	10^{5}-10^{7}	10^{-3}-10^{-2}	≤ 4.2
Hot Electron Micro Bolometers	10^{-19}-10^{-17}	10^{9}	10^{-8}	≤ 0.3
Golay Cells	10^{-10}	10^{5}	10^{-2}	300
Pyroelectric Detectors	10^{-10}	10^{5}	10^{-2}	240-350
Schottky Diode	10^{-12}	10^{3}	10^{-12}	10-420

2.1. Room Temperature Detectors

Room temperature detectors are Golay cell, Pyroelectric detector, Schottky diode have NEP nearly 10^{-9} – 10^{-12} $W/Hz^{½}$ which is higher than cryogenic detectors. Golay cell and pyroelectric detector based on gas pressure, ferroelectric material parameter, respectively. These incoherent detectors based on thermal sensor principle. Temperature difference at absorber is defined by thermometer via incoming radiation to heat sink. These detectors operate at room temperature that's why, they do not need to cryogenic cooling it provides to reduce the cryogenic cost.

2.1.1. Golay Cells

First Golay Cell is discovered by M. J. E. Golay in 1947. Golay Cell has operating temperature as 4-40 C˚ (room temperatures).Scientist have worked on developing the Golay Cells detectivity or sensitivity (Karpowicz et al., 2005, Hargreaves et al., 2007). Golay Cells based on volume change in pneumatic chamber by effects. The working principle of it, first, there is transmitting window to pass THz waves into the absorbing film. Secondly, incoming THz radiation is absorbed by absorbing film. By this effect, absorbing energy occurs and heats the inert gas in

pneumatic chamber. This change of temperature cause to pressure on chamber. Expansion of gas, flexible mirror is moved. Finally, light reflected off membrane that is determined by photodetector and then signal on the photodetector is changed by the effect of motion of the membrane. This working principle of Golay Cell can be seen as schematic presentation in Figure 2.2.

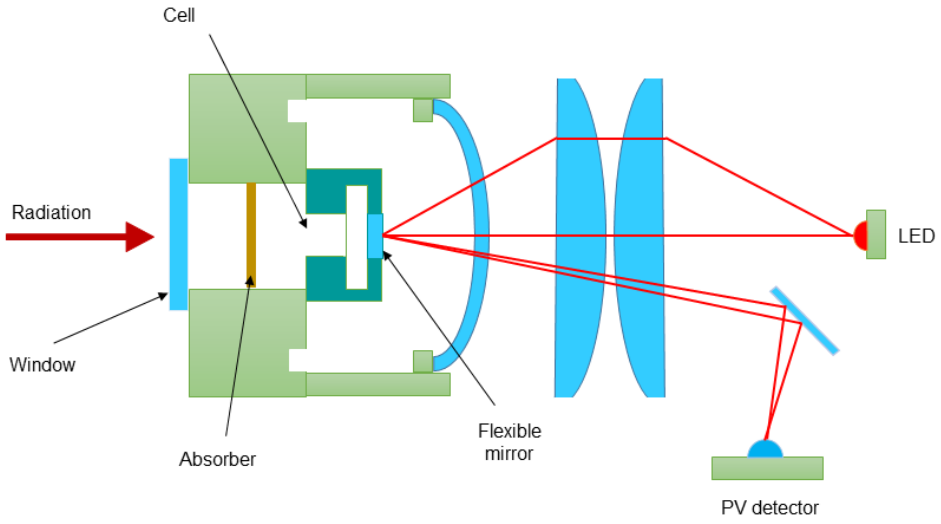

Figure 2.2. Schematic diagram of Golay Cell

Golay Cell has response time 10-25 ms, NEP 1.2 x 10^{-10} W/$Hz^{1/2}$ and detectivity 7 x 10^{9} cm.$Hz^{1/2}$/W. It is higher detectivity and sensitivity, lower response time and NEP than other room temperature detectors. High efficiency can be provided from Golay Cell but it has some disadvantages that used membrane may be very fragile and they are large and cost is higher than other room temperature detectors.

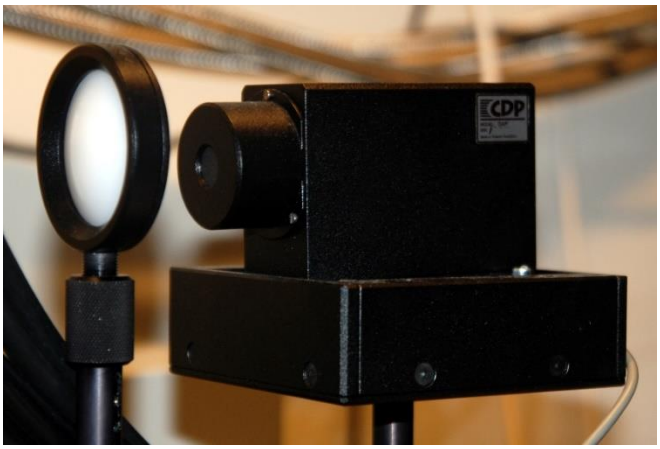

Figure 2.3. Golay cell as a THz detector
(Source: Golay Cell, 2010)

2.1.2. Pyroelectric Detectors

Pyroelectric detectors operates at room temperatures and they based on creating of temperature on polarization. In general, change of polarization is concerned with change of charge considering time and passed current. In detail, working principle of Pyroelectric detector is start with coming of THz radiation through absorber and then radiation is absorbed by absorber. Metallic absorber have been usually used for THz detectors. Mostly, this pyroelectric rest on detector's temperature that's why, made up of heat energy is transferred by heat conduction. Additionally, this effect only depend on heat and sensitive to AC signals. This transferred occurs through pyroelectric sensor and then sensor's temperature is changed. For this reason, free charges are created on both side of the pyroelectric sensor.

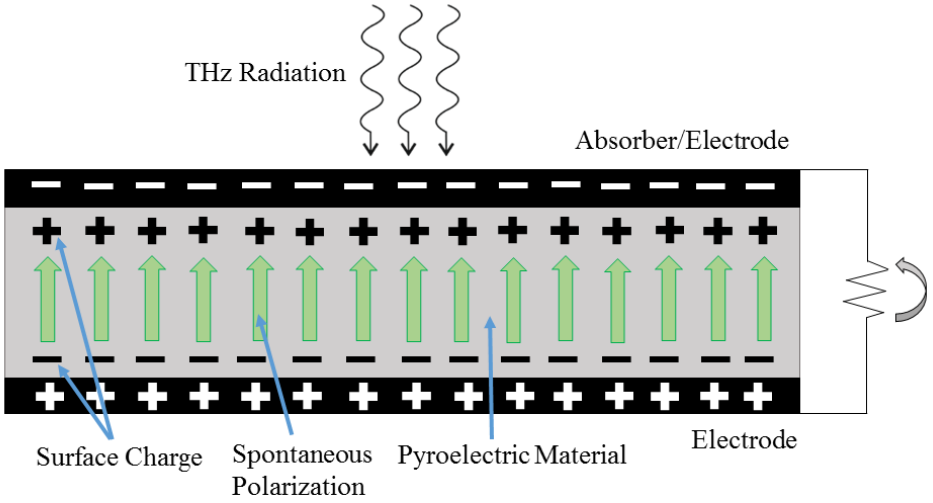

Figure 2.4 Schematic diagram of Pyroelectric Detector

Pyroelectric detectors can be made many materials such as Triglycine Sulfate (TGS), Deuterated Triglycine Sulfate (DTGS), Lithium Tantalate ($LiTaO_3$), Lithium Niobate ($LiNbO_3$). It has small area than Golay Cell, can give faster thermal response time depending on area of pyroelectric sensor. It has response time nearly 500 ms, NEP 3 x 10^{-9}-10^{-10} W/$Hz^{1/2}$ and detectivity 6 x 10^8 cm.$Hz^{1/2}$/W. Actually, it is possible to get better response time for pyroelectric detector than other room temperature detectors, but there is a limitation which noise of the preamplifier.

Figure 2.5. THz detector with pyroelectric sensor
(Source: Product of Gentec Electro-Optics (Gentec-EO), 2015)

2.1.3. Schottky Diodes

Schottky diodes consist of semiconductor materials which operates with fine results in THz range. It does not need low temperature to operate, but it might have noise exceed of the limits. It is possible to increase the efficiency from detector by getting smaller diode area. This cause to increase the frequency of operation and resistance of series. There exist many material to use for Schottky diode but GaAs is the most used as a semiconductor because of the fact that it has equilibrium between mobility and bandgap in GaAs.

First GaAs Schottky diode was improved via using photolithography by Young and Irvin in 1965 (Young et al., 1965).

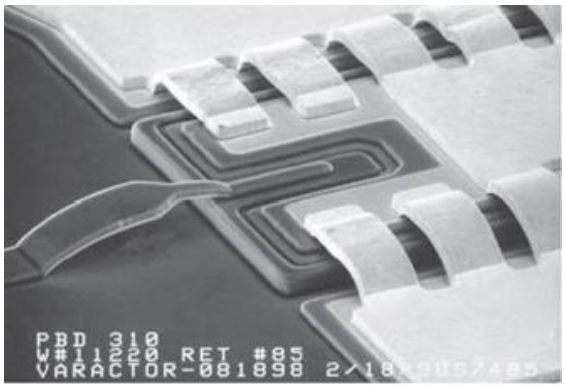

Figure 2.6. Bridge Schottky Diode
(Source: Mehdi et al., 2006, Sizov et al., 2010)

Figure 2.6 belongs to planer GaAs Schottky diode chip to show the bridge of Schottky diode by Mehdi and collages in 2006 (Mehdi et al., 2006). Lately, searchers work terahertz range by obtained result as 1-2 THz gap.

Schottky diodes has NEP as 10^{-10}-10^{-12} W/Hz$^{1/2}$. NEP value can be changed by depending on spectral band that operates. It means that it is possible to decrease NEP by increases frequency of diode. Efficiency of diode can better by providing higher switching speed for diode.

2.2. Cryogenic Detectors

Bolometers can be given as a type for cryogenic detectors, has NEP nearly 10^{-12} – 10^{-14} W/Hz^{½} which is smaller than room temperature detector. They need to cryogenic cooling, but they provide higher detectivity, sensitivity and smaller response time than room temperature detectors as an advantage. There are many bolometers which semiconductor, SIS (Superconductor Insulator Superconductor), Superconducting Hot Electron Bolometer and Transition Edge Sensor. In this thesis, Superconducting Hot Electron Bolometer and Transition Edge Sensor will be explained because our detector based on these bolometer's principles.

2.2.1. Bolometers

Bolometer means beam of light in Greek and first bolometer was invented by S. P. Langley in 1878 (Langley et al., 1881). It was discovered to measure the spectrum of sun in the 19th century. First bolometer's principle is that there was a two platinum strips which one of them was covered by carbon lampblack and other one was used to expose to sun light and was heated by light. It caused to change on resistivity which measure by two strip with Wheatstone bridge (Langley 1898).

Bolometer is a detector of heat or power, based on resistance mechanism. Although many years have passed from invented of bolometer since 19th century, main component of bolometer is not changed too much. It is a thermal detector to measure the change of resistance which is response to incoming THz radiation. Bolometer consists of absorber, heat sink, thermal coupling to connect absorber and heat sink. These component of the bolometer is shown in Figure 2.7.

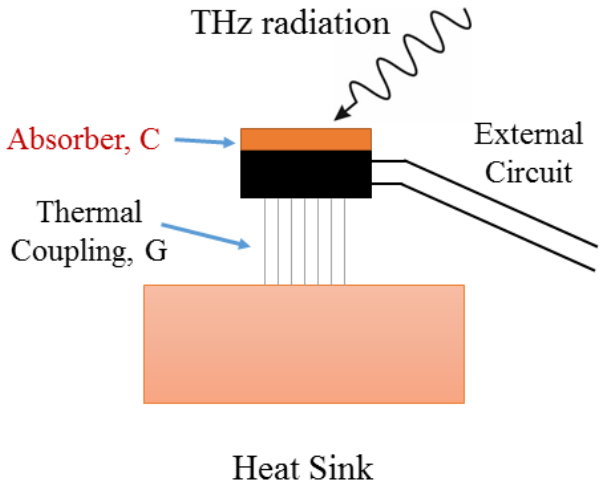

Figure 2.7. Schematic diagram of Bolometer

The working principle of bolometer is that incoming THz radiation absorbed by absorber and absorbed radiation turn into heat. This heat is transferred through heat sink (thermal reservoir) by heat capacity C_{th} and thermal conductance G_{th}. Two elementary parameter effects the bolometer which are heat capacity to characterize the bolometer and thermal conductance of the heat sink. It depend on that when absorber power is, larger heat capacity will be larger by proportional. This change of temperature cause to determine the amount of incoming radiation onto bolometer. If incoming THz radiation power P which is detected by detector, temperature (T_b) of the absorber is increased by the ratio of $\frac{dT_B}{dt} = \frac{P}{C_{th}}$ by having $\tau = \frac{C_{th}}{G_{th}}$ response time (time constant) (τ). When incoming radiation is ceased, it backs to normal state by response time value. To provide fast response time from bolometer, small heat capacity and high thermal conductance are needed. To determine the noise level of bolometer, Noise Equivalent Power (NEP) which is the amount of incident power required to produce a signal which is above noise level of the detector. To get smaller NEP, incoming radiation power should be higher than noise of the bolometer. Responsivity is the other parameter which determinate the output signal of the detector because of the incoming radiation by detector. Additionally, small heat capacity is the most important parameter to get best result from bolometer as detectivity, sensitivity. Bolometer's NEP roughly 10^{-16}-10^{-13} W/Hz$^{1/2}$, responsivity 10^{5}-10^{7} V/W and response time 10^{-3}-10^{-2} s at cryogenic temperatures.

It is crucial to choose the right material as absorber to bolometer to get higher detectivity and sensitivity from detector. By right chosen, absorber can absorb higher from incoming radiation to provide better efficiency for bolometer. There is also parameter Temperature Coefficient of Resistance (TCR) $= \frac{1}{R} \frac{dR}{dT}$ to choose the right material of detector. Value of TCR depend on material metal or semiconductor. If there is a metal, TCR is equal to positive value which means resistance is proportional with temperature (resistance increase with temperature). Semiconductors like germanium, silicon, carbon show negative value for TCR with decreasing resistance during increasing temperature of detector. Slope of the resistance versus temperature measurement and resistance should be high and small, respectively.

2.2.1.1. Superconducting Hot Electron Bolometers

Hot electron Bolometer (HEB) arise from two metal layer which are connected each other by micro bridge. This type bolometer has hot electrons for superconductors, but hot electrons expression was first identified to define the electrons inside semiconductor in 1967 (Conwell 1967). After expression of hot electron, combination with bolometer was first discovered as low temperature with InSb material (Kinch et al., 1963, Phillips et al., 1973). First hot electrons and hot electron discovered with semiconductors, but superconducting hot electron bolometers have higher speed and detectivity. HEB working principle is occurred that small change of resistance comprised from the incoming radiation through bridge at the near superconducting transition region. Because of not own absorber, HEB's response times are smaller which means higher speed than other bolometers. Incoming radiation is absorbed directly by electrons inside of the superconductors. Energy is transferred by phonons after that, electrons take the energies to share with another electrons and is caused to change of the temperature by increasing. HEB based on two principle which are phonon-cooled and diffusion-cooled according to their changing of electron's energies and phonon's heating.

Idea of phonon-cooled hot electron bolometer was firstly propounded by Gershenzon in 1990 (Gerchenzon et al., 1990). In this mechanism, hot electrons are transferred by energy through phonons and incremental energy travel through substrate. To get efficiency from this mechanism, electron interaction time should be smaller than

transferring time of hot electron's energy through phonons. Secondly, thickness of superconducting film should be thin like nanometers to provide efficiency to HEB. That's why, area between superconductor film and substrate is important parameter for detectivity of HEB in this mechanism. Finally, if thermal conductivity of substrate is high and fine contact with below cold finger, efficiency from phonon will be higher and then speed of response will better. These parameters affect the detectivity, sensitivity of HEB.

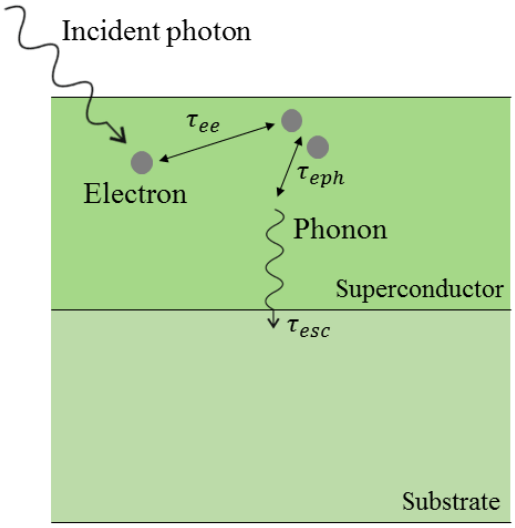

Figure 2.8. Schematic diagram of phonon-cooled HEB

Idea of diffusion-cooled hot electron bolometer was firstly propounded by Prober in 1993 (Prober 1993). In this mechanism, there is an antenna structure with planar, bow-tie, spiral and log-periodic designs. There are pads-normal metals which depend on number of design to make a measurement from arms of antenna structure. Middle of the structure comprise from superconducting material and then hot electrons escape from superconductor through normal metals by diffusion. Hot electrons are escaped from microbridge of superconductor that's why, length of microbridge is important parameter to detectivity. Length of microbridge should be small as soon as possible with supreme $L_{max} = 2(D_e\tau_{ee})^{1/2}$, τ_{ee} is electron-electron interaction time and D_e is electron diffusion. That's why, between normal metal and superconductor area is important parameter for diffusion-cooled HEB. (Sizov et al., 2010).

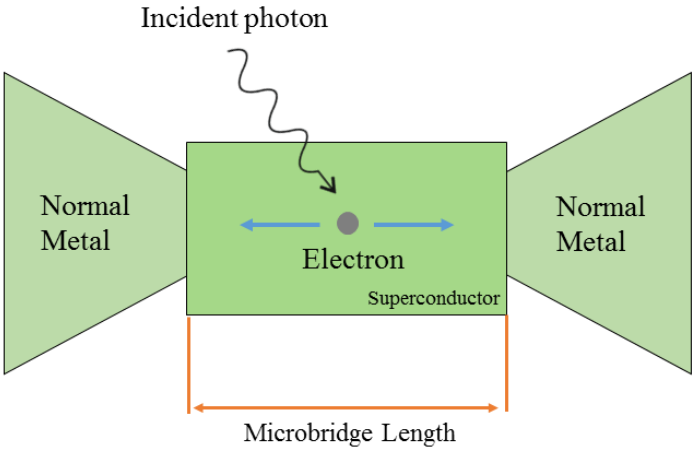

Figure 2.9. Schematic diagram of diffusion-cooled HEB

In literature, there are many HEB from superconducting material except Bi2212 single crystal, as far as we know. In this thesis, detector's chip was produced and developed from Bi2212. Other superconducting material's not Bi2212 response times and NEP will be given to compare and opinion about our bolometric detector's performance. Firstly, it is obviously known as superconducting bolometer has smaller response time than other detectors. Nb and NbN superconducting thin film is usually used for bolometric detector with own smaller response time and NEP values. Time constant for Nb bolometer 25 μs at 190 mK have been represented. Gershenson and colleagues produced bolometer from Nb has NEP $3x10^{-13}$-W/$Hz^{1/2}$ by have operating temperature 4 K in 1989 (Gershenson et al., 1989). Bolometer from NbN superconducting film has smaller response time than Nb films (Karasik et al., 1999). Ultrathin 3 nm NbN film bolometer, 30 ps response time was acquired in 2000. (IIin et al., 2000). Hammar and colleagues used YBCO thin film for bolometer and got response time nearly nanoseconds. Also, they showed that responsivity is decreased when increasing the antenna structure area which 1.5 μm x 1.5 μm area has nearly 180 V/W and 4 μm x 1μm area has 100 V/W as responsivity (Hammar et al., 2011).

2.2.1.2. Transition Edge Sensors

Superconducting transition region is important for Transition Edge Sensors because of working principle. Its principle is similar to Hot Electron Bolometers. There is absorber in TES that's why, HEB's response times are faster than TES, and incoming radiation is absorbed directly through superconductor. Phonons take a role in TES to transferred absorbed radiation. In TES, superconducting transition region is chosen because maximum change of resistance via resistance occurs in transition region.

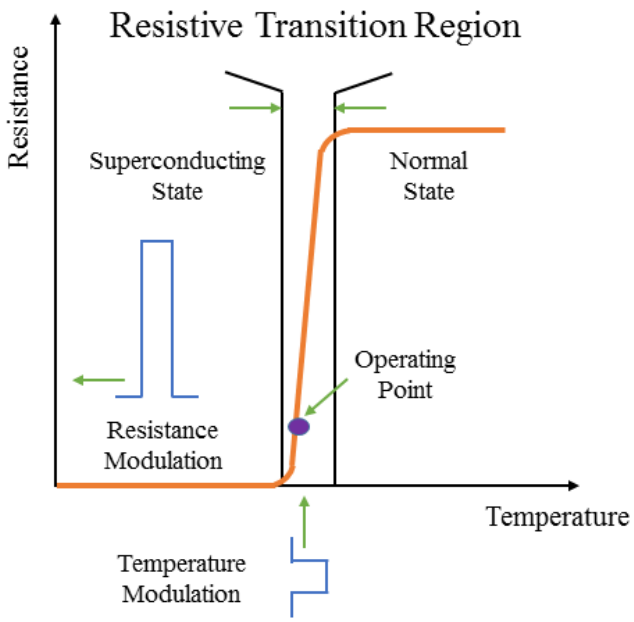

Figure 2.10 Operating region of superconductor transition edge sensor

THz radiation strike through chip and this radiation cause to change of temperature inside chip that's why, resistance of chip is changed, also. When sending signal from source, this radiation increase the temperature and lead to change of resistance inside superconducting transition region. In TES, operating temperature is chosen within transition region. Standing in the operating temperature to send and paused signal and observed the change of resistance by the effect of increasing and decreasing temperature of chip.

2.3. Antenna Structures

Antenna structures have been successfully applied to place as supply the electromagnetic waves on falling them onto micro bridge by comprehending THz wave (Cibella, et al. 2009; Du Hamel, et al. 1957). There are antenna structures to increase the detectivity of bolometer and absorb the THz radiation in literature (Moftakharzadeh, et al. 2008).

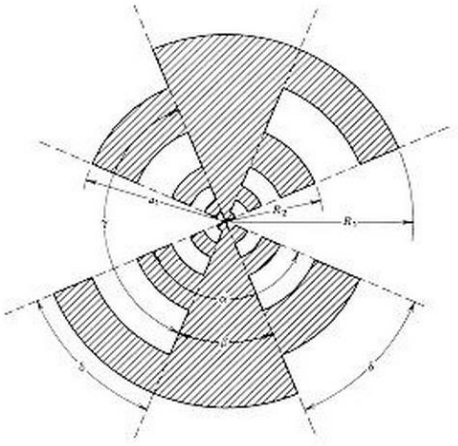

Figure 2.11. Log-periodic planer antenna structure
(Source: Warren, et al. 1981)

These basic antenna structures are dipole (Fumeaux et al., 2000), bowtie (Kocakarin and Yegin, 2013), patch (Codreanu, et al. 1999), spiral (Dattoma, et al. 2011), log-periodic (Gonzalez and Boreman, 2005). Log periodic antennas was designed by DuHamel and Isbell (Du Hamel, et al. 1957; Saijo, et al. 2001). It has designed as logarithmic repeating factors in the way of antenna size and space from the center point. Log periodic factors should be continued to outside, inside and center point as an infinitive but these factors which occur antenna structure is ceased in both side as take account of bandwidth.

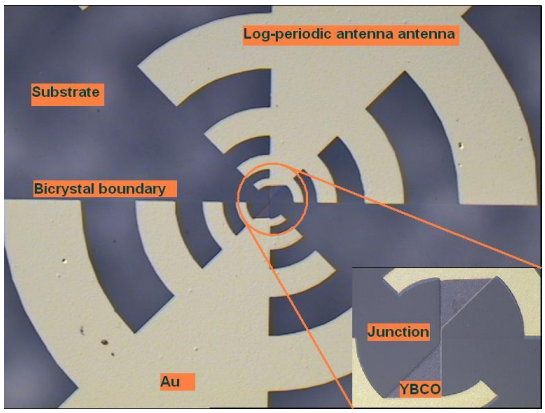

Figure 2.12. Log periodic antenna patterned on YBCO
(Source: National Physical Laboratory 2011)

The central angle of the log periodic antenna is 45°. In design, there is a relation between inner and outer semi diameter r_n/R_n=0.49 and R_{n-1}/R_n=0. (Tonouchi and Saijo, 2003). Log periodic design has maximum and minimum semi diameters are 700 and 82 µm. Additionally, it has 30 µm strip line at the center of the structure and describe as the geometric ratio of the antenna design,

$$x = \frac{rn}{\mathrm{Rn+1}} \tag{2.1}$$

The width of the antenna is calculated by describing the τ as geometric rate of the operation rates (Saijo, et al. 2001),

$$\tau = \frac{Rn}{\mathrm{Rn+1}} \tag{2.2}$$

If two frequency f_1 and f_2 are one period by $f_2 > f_1$, geometric ratio is described as,

$$\tau = \frac{f1}{f2} \tag{2.3}$$

Log periodic antennas are polarized as a linear instead of circular on contrary to other antennas structures.

$$\ln = \frac{\pi}{2}\frac{Rn+rn}{2} \tag{2.4}$$

$$\lambda m = \lambda 0/\sqrt{\varepsilon} m \quad (2.5)$$

$$\varepsilon_m = 1+\varepsilon_r/2 \quad (2.6)$$

Arc distance is equal to (ln)$\lambda m/2$ when antenna is in resonance which is described as λ_0 is the wavelength of the free space and ε_r is the dielectric constant of the substrate.

2.4. Motivation

High temperature superconductors have higher energy gap than low temperature superconductors. HTS detectors are candidate to fill THz gap by providing enough strong source. That's why, high temperature superconductors give great response at the frequency of the THz range. Energy gap is wide from 15 to 40 meV for Bi2212 which refer to wide THz gap (Ozyuzer, et al. 2007; Ozyuzer, et al. 2009). Hence, Bi2212 is important for our study because of possess broad THz energy gap. Doping of Bi2212 superconductor can be determined by adding or removed oxygen with Cu-O planes. This parameter affect a-b axis resistance-temperature measurement with critical temperature of Bi2212.

In this experimental part, epoxy and scotch was used to transfer Bi2212 single crystal onto substrate and decrease the thickness of Bi2212, respectively. After shadow, coated with gold, clean room process, pattern antenna structura by electron-beam lithography and ion-beam etching process was applied, respectively. This procedure will detail explain in Chapter 3. After produce the chip, a-b axis resistance-temperature measurements was done to determine the critical temperature of Bi2212. After that, bolometric measurement was done and response times of chips was calculated from change of resistivity in bolometric measurement. Results of electrical, bolometric measurement and response time will detail express in Chapter 4.

Eventually, there are many studies about detector from superconducting materials such as Nb, YBCO however, as far as we know, utilizing from Bi2212 single crystal for detector is the first study in literature.

CHAPTER 3

EXPERIMENTAL

3.1. Growth of Bi2212 Single Crystals

There is a difficulty to acquire the pure and smooth surface as bulk high temperature superconducting material (Michishita, et al. 1996). That's why, there are lots method to produce high quality the Bi2212 single crystal. In these methods, sintering is the chosen and easy technique to produce the bulk superconductor material in contrast to melting process. Crystals are growth three kinds which are solid, liquid (melt) and vapour growth (Pamplin 1980). Growth from melt is occurred by process involving from liquid to solid phase transition. This category has Bridgman, Czohralski, Zone melting techniques depending on thermal characteristics. Zone melting process has some advantages in contrast to other growth methods. Firstly, it is possible to control the impurity of samples and reduce the contamination of the melting by crucible. Additionally, less heater power is used and more uniform surface is obtained. There are some limitations that contamination from crucible and thermal, volume expansion which can solved by float zone technique.

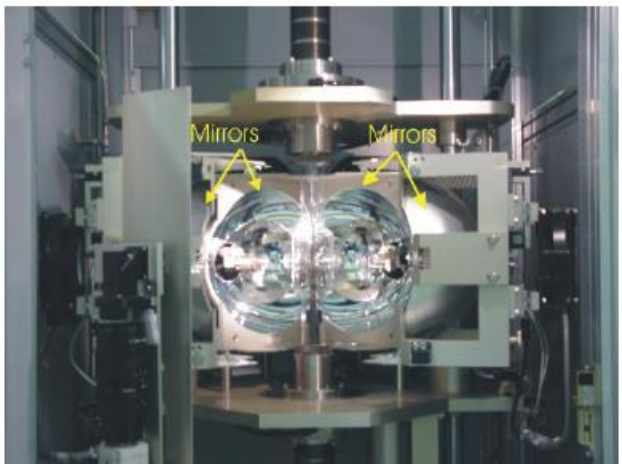

Figure 3.1. Optical image of float zone technique
(Source: Material Science Center, University of Groningen, 2015)

There is a one method to produce the quality bulk HTSs which is called travelling solvent floating zone method (Takekawa, et al. 1988).

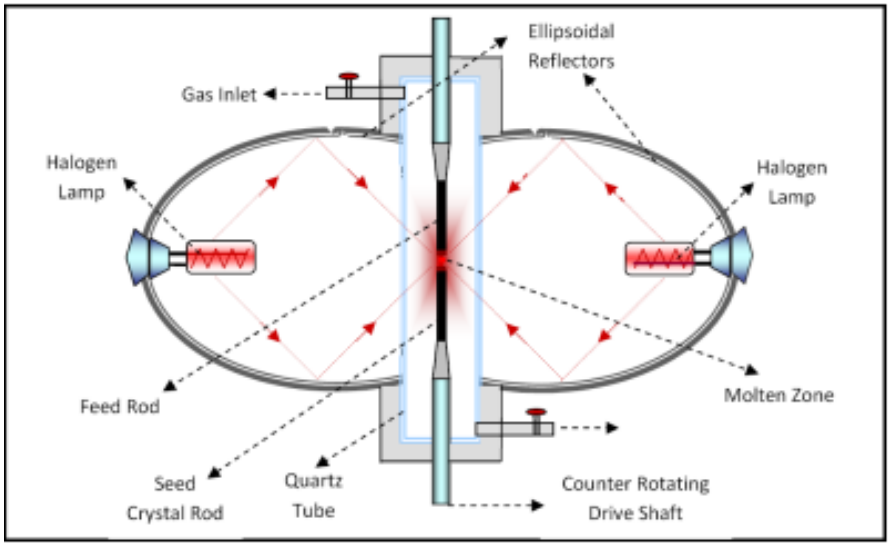

Figure 3.2. Double ellipsoid image furnaces
(Source: Simsek 2008)

Traveling solvent floating zone method was developed by Pfann for germanium and has been well discussed in several books (Pfann 1952). There are feed and seed rots at the end and begin in this one. These rods are protect the molten zone from surface tension between them. Also, rods are rotated to supply the homogen surface during the growth. In this process, it is first task is to mix and calcine the material then isostatic pressure is applied to them by sintering to a rod. There is occurred the pre melting of the sintered rod. In growth process, O_2 gas is used to supply the oxygen to the grown evaporated material. It is crucial element to hold constant the melting point as O_2 pressure (Michishita et al. 1996). Finally, continue with the molten zone is formed by heat which is focused by mirrors and then crystal is growth by travelling of the molten zone. In our study, we used Bi2212 crystal grown by traveling solvent floating zone method.

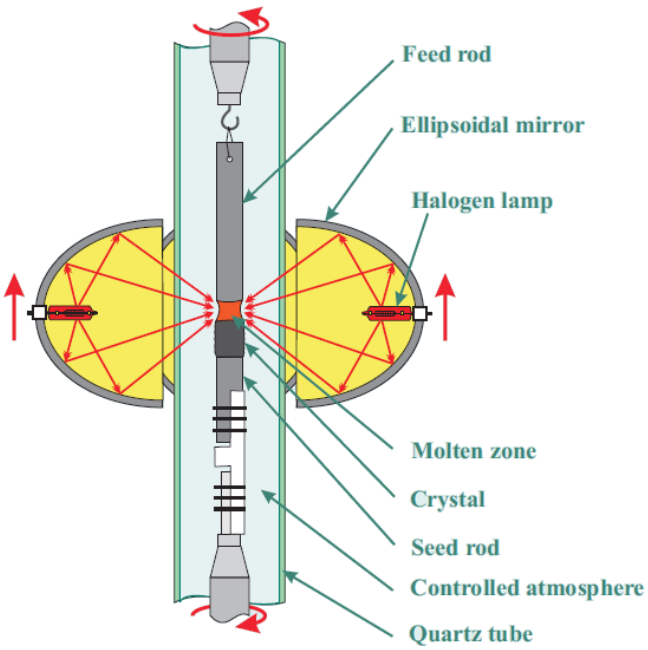

Figure 3.3. Principle of float zone technique
(Source: Victor Jones, 2001)

3.2. Superconducting Bolometric Detector Fabrication

To fabricate the quality superconducting bolometric detector, many steps are completed which are preparing the thinner Bi2212 crystal, thermal evaporation, clean room process, electron beam lithography and ion beam etching. These process will be explained in the next parts.

3.2.1. Preparing of Bi2212 Single Crystal

In literature, there are studies about the transfer of Bi2212 single crystal onto the substrate with different adhesive. It was studied successfully that THz source is occurred by Bi2212 single crystal transferred with silver epoxy (Turkoglu, et al. 2012; Turkoglu, et al. 2012; Koseoglu, et al. 2011). Additionally, there are other adhesive to transfer Bi2212 single crystal successfully such as polyimide, non-photosensitive polyimide PIX (Yamada, et al. 2007; You, et al. 2005; Wang, et al. 2001; Yamaki, et al. 2011; Yamaki et al. 2011). In our study, two component fast dry epoxy is used to transfer Bi2212 single crystal onto sapphire substrate.

Before Bi2212 single crystal transfer onto the sapphire substrate, two component of fast dry epoxy should be stirred homogeny because of providing evenly the conductivity. As a substrate, sapphire is chosen because of perfect thermal conductors. Mixed epoxy is putted onto 6x6 mm^2 sapphire substrate and then 0.5 mm^2 or 1 mm^2 Bi2212 single crystal is placed onto epoxy. Samples are waited in air condition to dry and cut their edges as pyramids form to coat every Bi2212 single layer with gold. By cutting the pyramid, it is advance to provide to get in touch with each layer via gold wire during contact and deposition gold. After this step, crystal surface should be smooth and thinner. That's why, Bi2212 single crystals are cleaved by scotch tape until get intented thickness. In this step, crystals are separated by layers carefully (Yamaki, et al. 2011; Yamaki, et al. 2011; Yamaki et al. 2011). This cleaved process is occurred between the weakest layer which is BiO layer in Bi2212 single crystal (Yamaki, et al. 2011; Yamaki, et al. 2011).

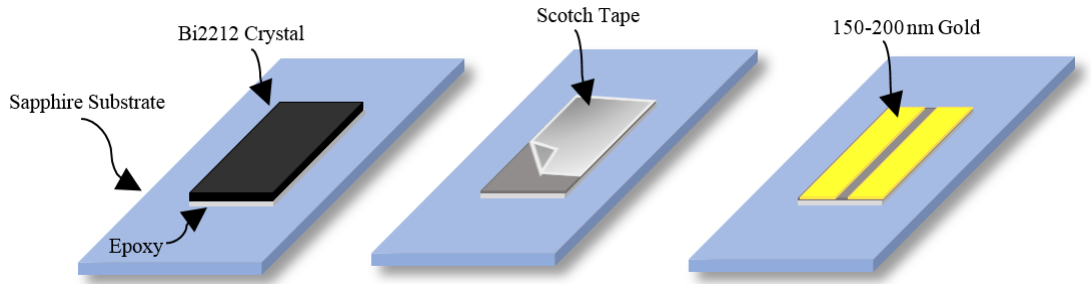

Figure 3.4. Steps of fabrication for Bi2212 with transferred, cleaved and deposited

By this cleaved process, different thickness and layers can be obtained successfully. Before the cleaved the thickness of the Bi2212 single crystal is roughly 700 nm and after the cleaved the thickness is decreased to 200 nm. The thickness of the crystals can be obtained from profilometer which based on quantify of roughness or result of I-V measurement. In I-V measurement, each layer refers to one line in graph and layers has thickness as 1.5 nm. Thickness of Bi2212 single crystal is calculated from multiply number of the lines with 1.5 nm. According to thickness of the Bi2212 single crystal, superconductivity property of the crystal is changed (Yamaki, et al. 2011). After cleaved process, Bi2212 single crystal is shadowed with mask which makes the bridge for the antenna structure before the thermal evaporation. There are two option to shadow the crystal which are 25 µm gold wire and aluminum foil. This is applied to prevent our samples from contact resistance by taking 4 point 4 probe contact

because when taking 2 point 4 probe or 2 point 2 probe contact, there will be a contact resistance.

3.2.2. Thermal Evaporation

To prevent the Bi2212 surface from possible deterioration and take electrical contact easily in the following process, gold layer is sputtered onto the immediately cleaved BSCCO single crystal. As a deposition system, thermal evaporation system has some advantages that it is possible to coat thin film as a purity by simple and cheap with less substrate surface damage. That's why, this method is chosen to deposit as a protect layer for transferred and cleaved Bi2212 single crystal easily.

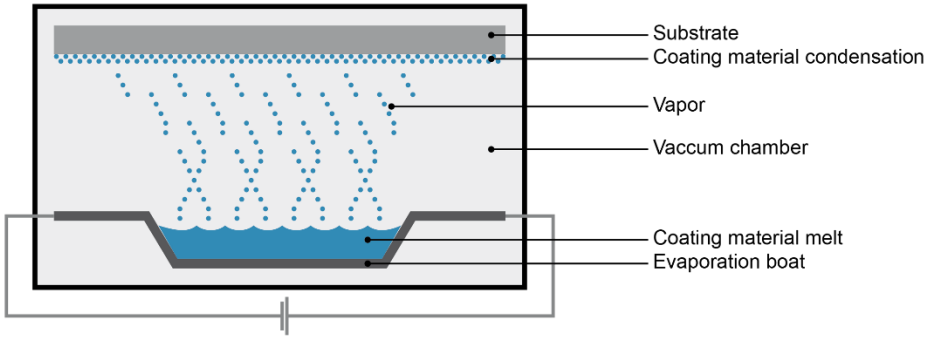

Figure 3.5. Principle of thermal evaporation
(Source: Plansee Group, 2015)

The principle of thermal evaporation can be seen in Figure 3.5. This method, material is evaporated by applying the high current on filament boat and continue with the condensation to the substrate surface. It is important to choose the right boat to have high quality deposition. There are some boat's materials such as tungsten, molybdenum and tantalum. Tungsten has the highest melting point between molybdenum and tantalum. Additionally, it resistant to corrosion during deposition any contact with molten deposition material. Tantalum is evaporated more slowly than molybdenum which is more stable to deposition. In our system, tungsten is used as a base material for a boat. In this technique, material which in tungsten boat should be heated to melt them. For this reason, tungsten boat is heated by carrying out the large current which is enough to evaporate the material in tungsten boat. Roughly 100 A current is used for deposition thin film onto the substrate. The temperature of the tungsten boat can be

changed by changing the thickness of the boat. Thickness of the thin film is changed by the effect of pressure, power and distance from source to substrate and there is a shutter in system to provide to determine thickness of the thin film and control the coming contamination from boat which do not want. In our measurement, 150-200 nm gold is deposited to fabricated and cleaved Bi2212 single crystal. There is a quartz crystal is supplied to determine the thickness of the thin film and rate of the coating. To get the fine morphology vacuum should be in low pressure with 10^{-6} Torr as in our thermal evaporation system. With this low pressure, evaporated particles move to the directly substrate surface providing by high quality morphology.

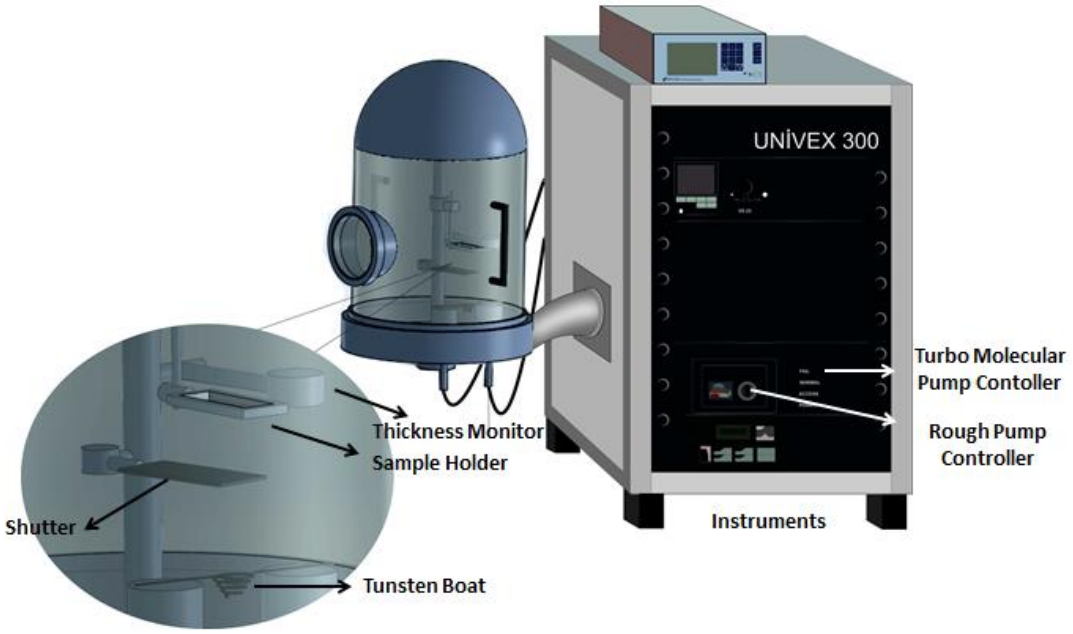

Figure 3.6. Schematic image of our thermal evaporation system

3.2.3. Clean Room Process

After deposition of gold layer, sample is prepared to electron beam lithography to pattern antenna structure by not any damage to the crystal surface. In clean room, Bi2212 single crystals are coated with spin coater. It takes 88 second with 3000 rpm to coat the samples surface with photoresist. We used AZ5214 type photoresist (PR), its thickness is roughly 2 μm with this type PR. After that, samples are soft baked using oven with 30 minutes at 90℃ to drive off the excess solvent of the PR and make harder

the PR for pattering the antenna structure. Then, these samples are now ready to electron beam lithography for log-periodic antenna and 4 point design.

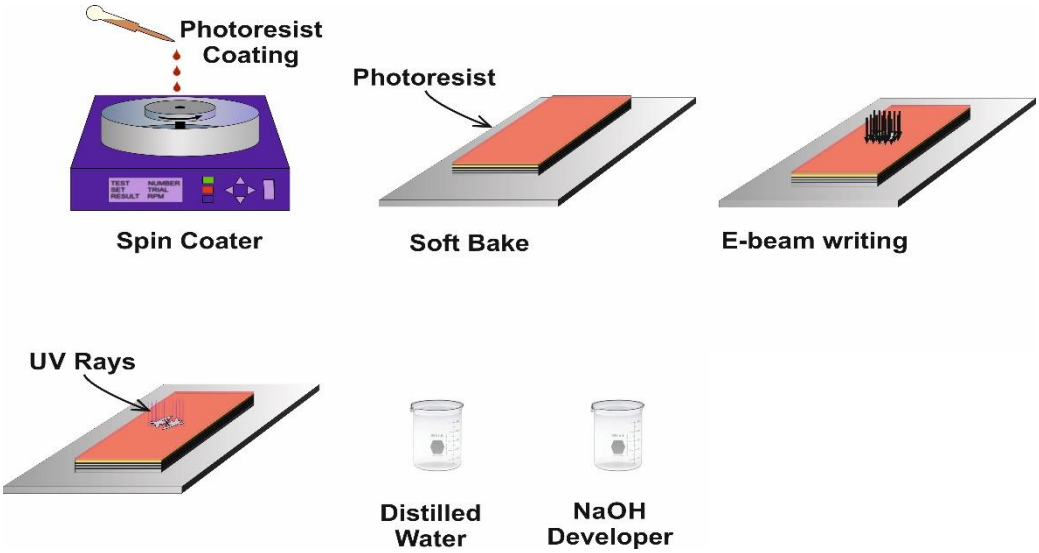

Figure 3.7. Schematic representation of clean room and e-beam lithography process

Electron beam lithography will be explained in next part. After electron beam lithography, clean room process is continued with exposing the samples to UV light for 7 seconds and developed in NaOH (sodium hydroxide) solution for 25 second to lift off the parts which electrons are not collided. After developed, sample is checked under the microscope and if necessary, sample is developed for a few second.

3.2.4. Electron-Beam Lithography

Electron beam lithography is an efficient method to pattern structure on sample than photolithography because of having maskless method and as a scale roughly 10 nm. It is possible to make speciality under the diffraction limit of light because of having short wavelength of the electrons. Additionally, it provides to work kinds of materials and high resolution. On the other hand, it has some deficit like expensive, complicated parts of system and slow exposure time than photolithography. It involved high vacuum because of charged electrons during exposure.

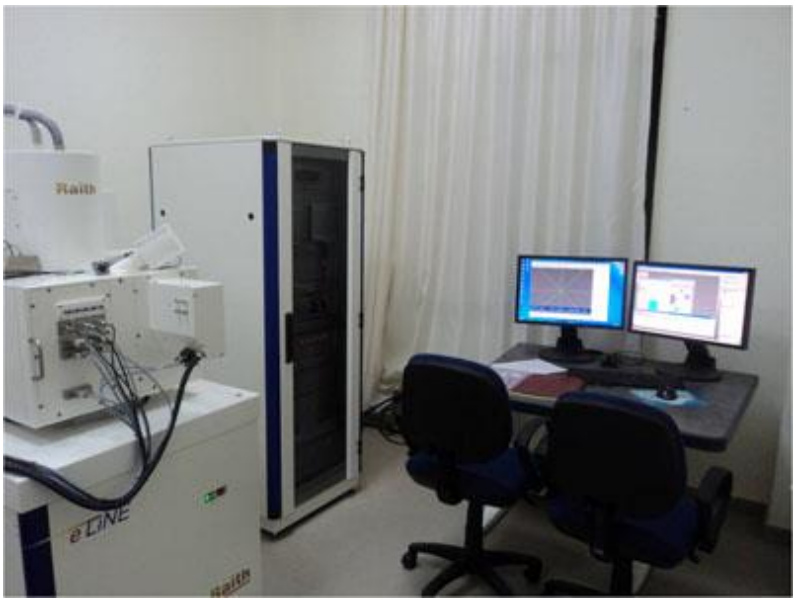

Figure 3.8. Picture of our electron beam lithography system

Before electron beam lithography, substrate is coated with photoresist which is changed under electrons beam as happening chemical. After that, exposure can be started to pattern the antenna structure on samples.

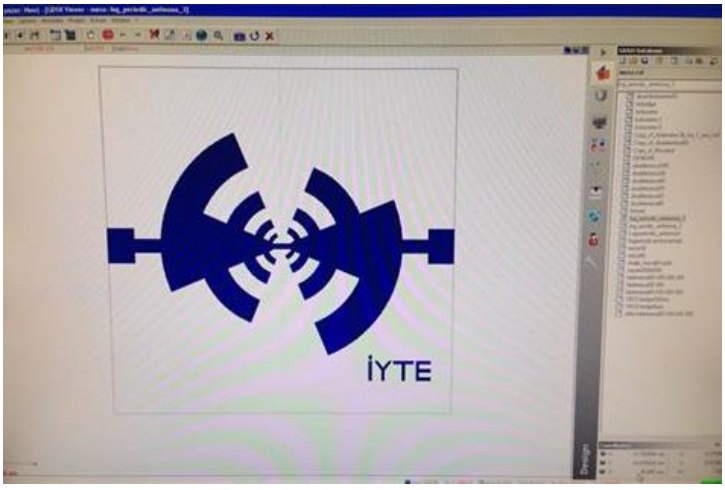

Figure 3.9. Log-periodic antenna structure by e-line program

For fabrication by e-beam lithography, we designed log periodic antenna and 4 point structures by e-line program. There are only two contact area which can cause to contact resistance for log-periodic antenna. That's why, we designed 4 point structures to provide less or no contact resistance during measurement.

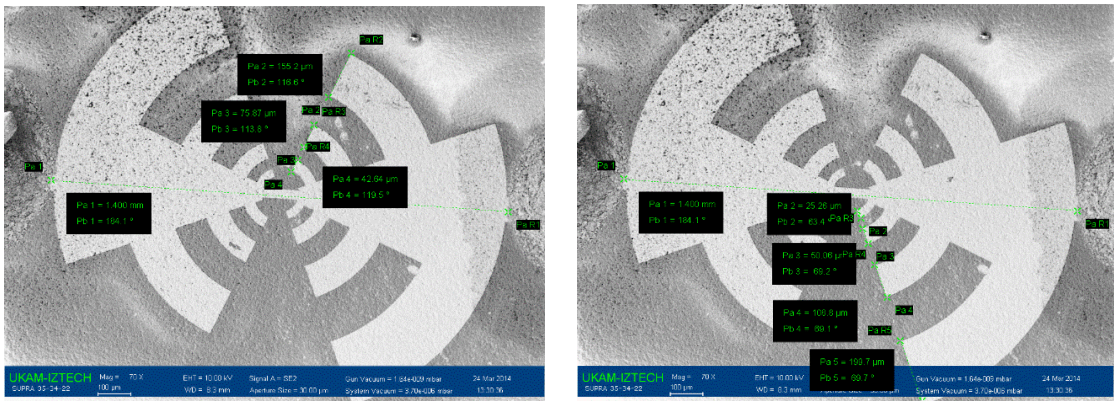

Figure 3.10. Design of log periodic antenna with dimensions

Figure 3.10 shows log-periodic antenna structure which is designed with e-line program. Each line has a degree as 45° with the center of the design. It is possible to see in SEM images the relation between inner and outer semi diameter r_n/R_n=0.49 and R_{n-1}/R_n=0.7. Additionally, it has 700 and 82 µm as maximum and minimum semi diameters and it has 30 µm strip line which are in depth explained Section 2.3.4.

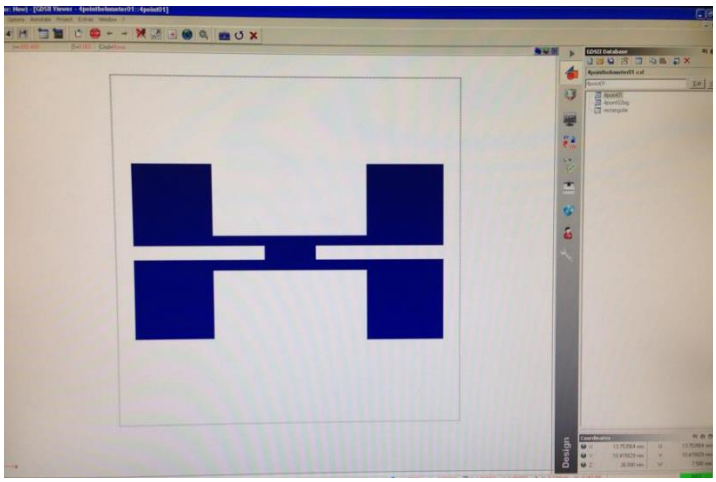

Figure 3.11. 4 point structure is designed by e-line program

Figure 3.11 provides us to take 4 point contact for our chips without any contact resistance. It has totally 900 µm length and 225x225 μm^2 contact areas. Bridges between arms has 150 µm width and 100 µm length. We designed the distance between contact areas as 40 µm to make easy to take a contact. In this design, shadow crystal should be in the middle of the bridge. That's why, we can change the length of the design about arms and bridge's distance with respect to crystals size. Distance between contact areas is 450 µm in Figure 3.11. This design is suitable for length which is

smaller than 450 µm as a bridge length. It is possible to change the design's length considering variety of the crystal.

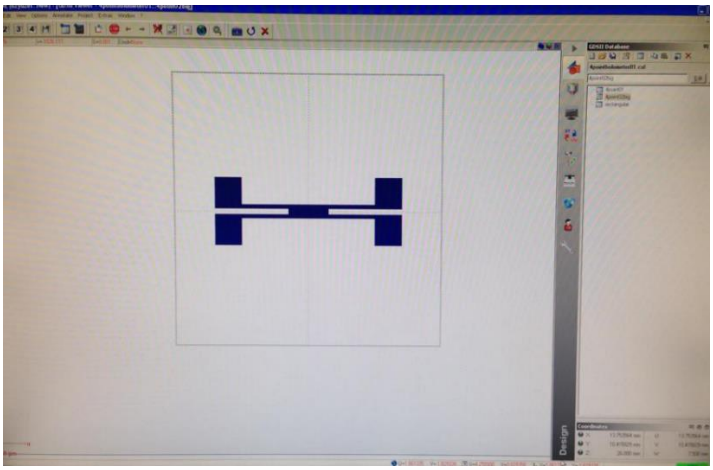

Figure 3.12. 4 point structure is designed with different length by e-line program

Design in Figure 3.12, bridge's distance is 300 µm and length of the design is 1400 µm. We designed contact areas' length as 200 µm, the distance between two contact areas is 1000 µm. Above the 1000 µm as a bridge distance is not able to our studies. For this reason, this design is suitable for length which is smaller than 1000 µm as a bridge length.

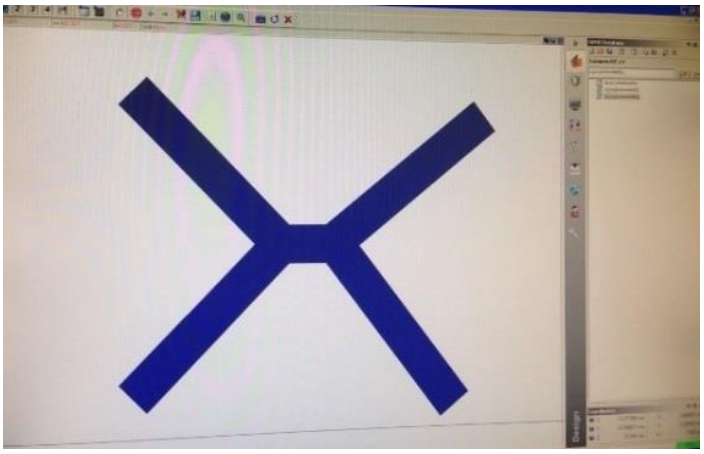

Figure 3.13. 4 point structure is designed by e-line program

Other design for 4 point structure is shown in Figure 3.13. This design has 100 μm as an arm distance and 300 μm length and 100 μm width. It is possible to take a contact with arms in this design instead of contact areas.

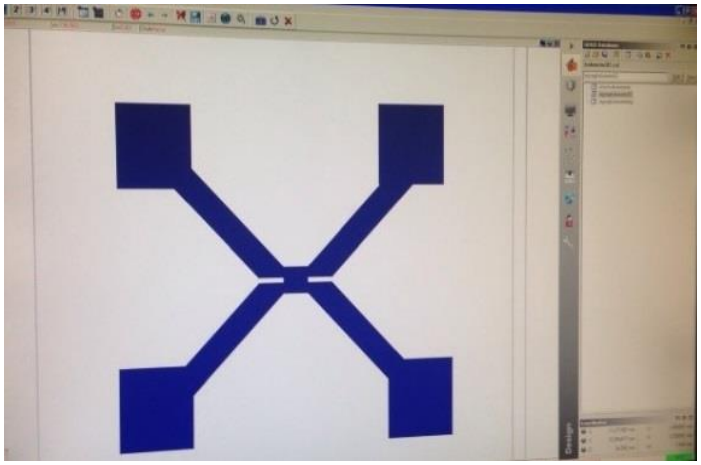

Figure 3.14. 4 point structure (bridge is changed) is designed by e-line program

In Figure 3.14, there are contact areas and smaller bridge than previous design. It is design as a smaller bridge because of providing the same area to pass current and voltage at the same time. There are 100 μm bridge length and the distance between them is 20 μm. It has same length with 4 point structure as 300 μm length and 100 μm width in this design. Additionally, Figure 3.14 has contact areas 300x300 μm^2 to provide take contact easily.

3.2.5. Ion Beam Etching

There are many techniques to pattern the fabricated antenna structure as micro fabrication such as wet, anisotropic wet and plasma etching. Isotropy and anisotropy depend on removed the materials from the surface uniformly all or one direction. Wet etching refers to chemical or liquid etching and plasma etching refers to dry, gas or physical dry etching. The basic difference between wet and plasma etching is time of etching which is slower in plasma etching. Ion beam etching is used in our experiment setup.

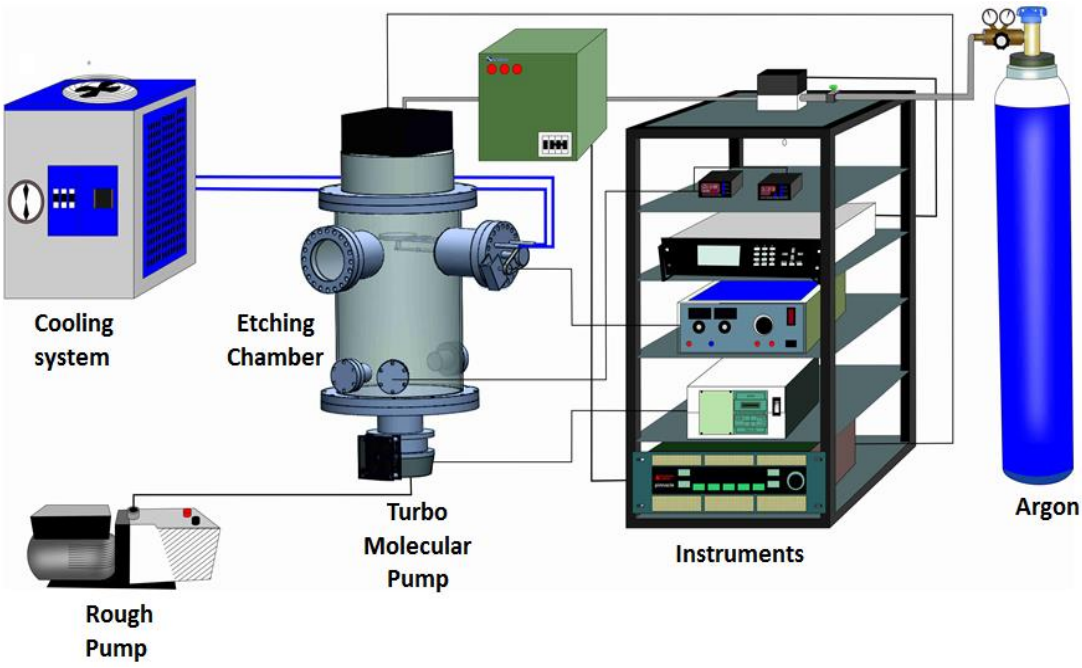

Figure 3.15. Schematic image of out ion beam etching system

In this system, before starting the etching, system is pumped with turbo mechanical pump until 10^{-6} Torr because it is need to low pressure to increase the free ion beams in system. To generate the plasma with Argon gases, it should be sent from mass flow controller as 30 sccm Ar. By the way, our samples are placed to the sample holder with 67.5^{o} and start to etch with unprotected layer with photoresist. Etching time is changed with the crystals thickness. We etched our samples by rotating at 60 minutes in a 2 part according to thickness of crystals. Then, antenna structure is appeared by etching area of non- exposure part of chip.

3.3. Bolometric Cryostat for THz Radiation

We designed cryostat for electrical and bolometric measurements of our chip in THz range. Cryostat have chamber as 250 mm height and 200 mm diameter by having THz window and vacuum input. Inside of the chamber, there is liquid nitrogen chamber which has 3 liters to cool our chip up to 77 K. It has 153 mm diameter and 150 mm height. After that, firstly THz wave collector is placed to the surface of the liquid nitrogen chamber to focus incident THz waves to the chip.

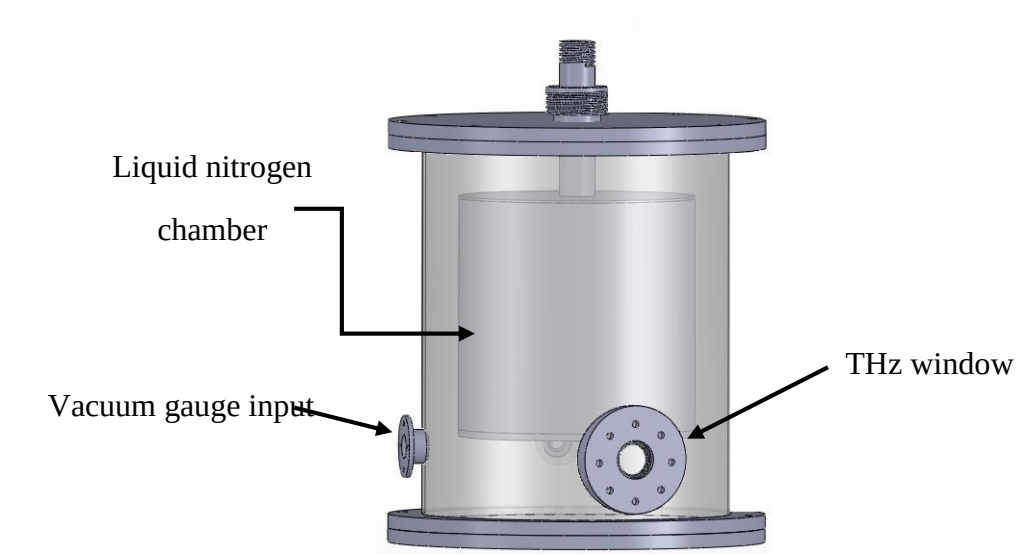

Figure 3.16. The schematic of designed THz cryostat

Sample holder is placed to the surface of the liquid nitrogen surface to hold other materials. To measure the temperature of the chip Lake Shore Thermal Sensor is placed to the sample holder. It has 83.7 Ω at room temperature and 300 Ω at the liquid nitrogen which can be seen in Figure 3.17.

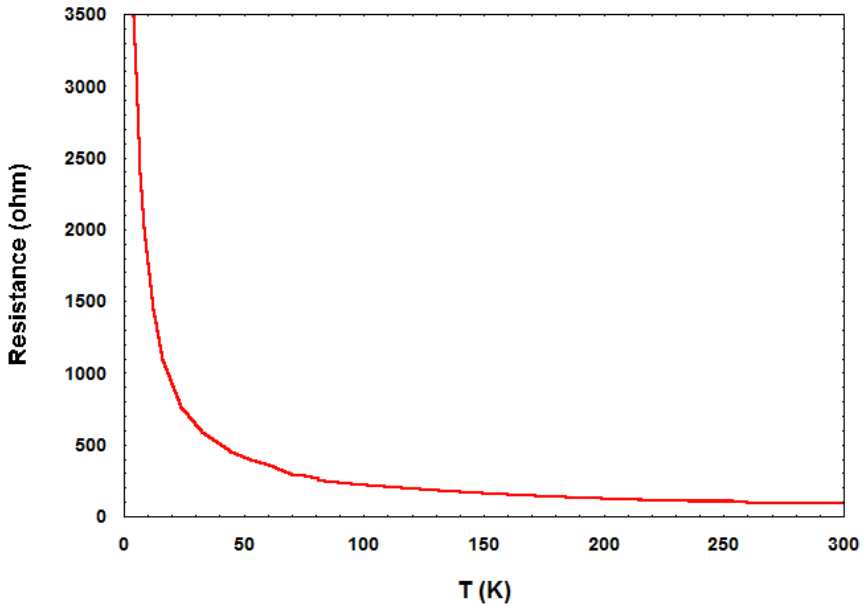

Figure 3.17. Resistance vs Temperature of Thermal Sensor

It is placed the heater which has initial resistance 120 Ω on sample holder to hold the sample's temperature at the superconducting transition region. After that,

electrical connection is done between temperature controller, sample, heater, temperature sensor and cryostat.

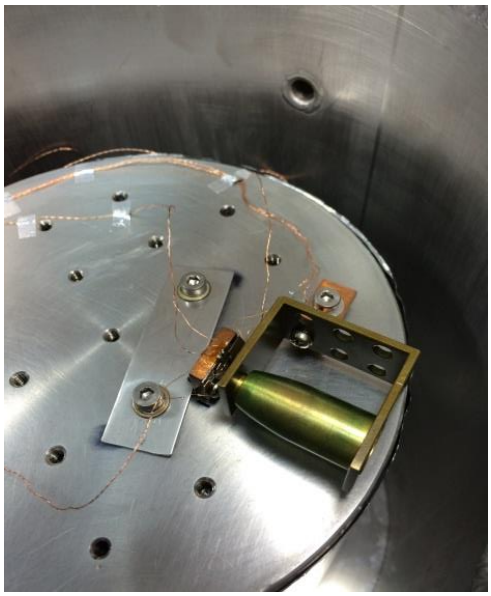

Figure 3.18. Image of the inside cryostat

After placed the materials inside the cryostat, liquid nitrogen chamber is surrounded with 15 μm metalize film 4 times to hold liquid nitrogen inside the chamber longer.

Figure 3.19. Liquid nitrogen chamber surrounding with metalize film

Before the metalize film, cryostat hold liquid nitrogen inside 22 hour when system is working. After metalize film, this time is improved to 30 hour to hold the temperature of liquid nitrogen as seen in Figure 3.20.

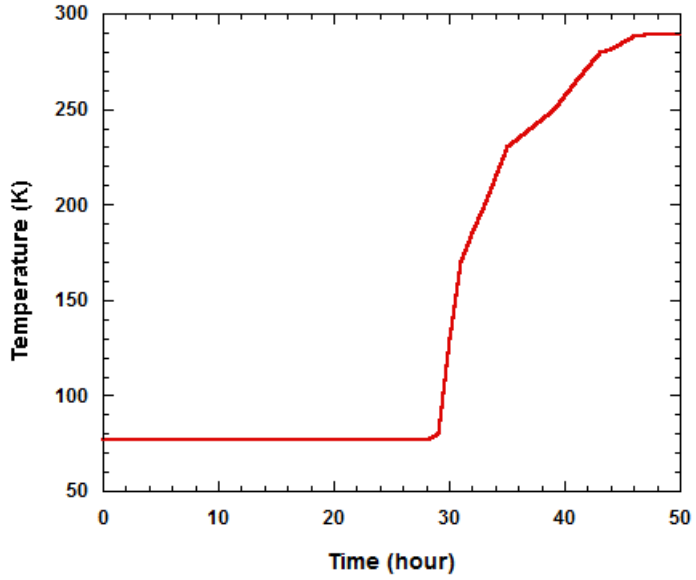

Figure 3.20. Time of hold liquid nitrogen inside the chamber

On the other hand, speed of the vaporization of the liquid nitrogen is 0.085 liter/hour during system is not working. After testing of the storage of the liquid nitrogen chamber, Agilent Technologies vacuum gauge is placed to the cryostat to control the vacuum values of the chamber.

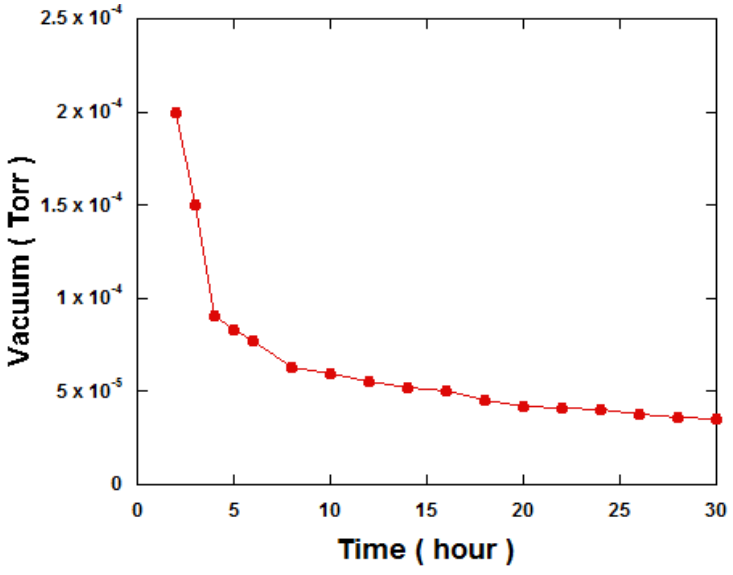

Figure 3.21. Vacuum change during addition of the liquid nitrogen

As can be seen from Figure 3.21, vacuum value is decreased from $2x10^{-4}$ to $4.8x10^{-5}$ Torr when adding liquid nitrogen into the cryostat during its working.

3.4. Characterization Measurements

After designed and production of THz cryostat, firstly electrical characterization setup is placed to the cryostat and then to calculate the response time of the cryostat bolometric measurement setup is prepared which is detail explained in next section.

3.4.1. Electrical Measurement

For electrical measurement, incoming 10 pin from electrical connection is divided 3 parts which are 4 of them connect chip as 2 current and 2 voltage wire, 2 of them connect with heater and remain of them connect with thermal sensor. Other sides of these wires are connect with current source, nanovoltmeter and temperature controller. Wires which are inside of the chamber are fixed with the aluminum tape on the surface of the chamber. Electrical measurement was done with 10 μA current and refers to voltage by finding the resistance via Labview program which is shown in Figure 3.23.

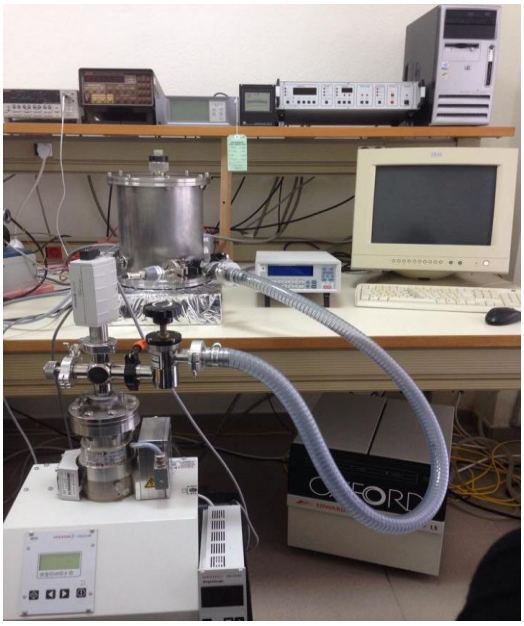

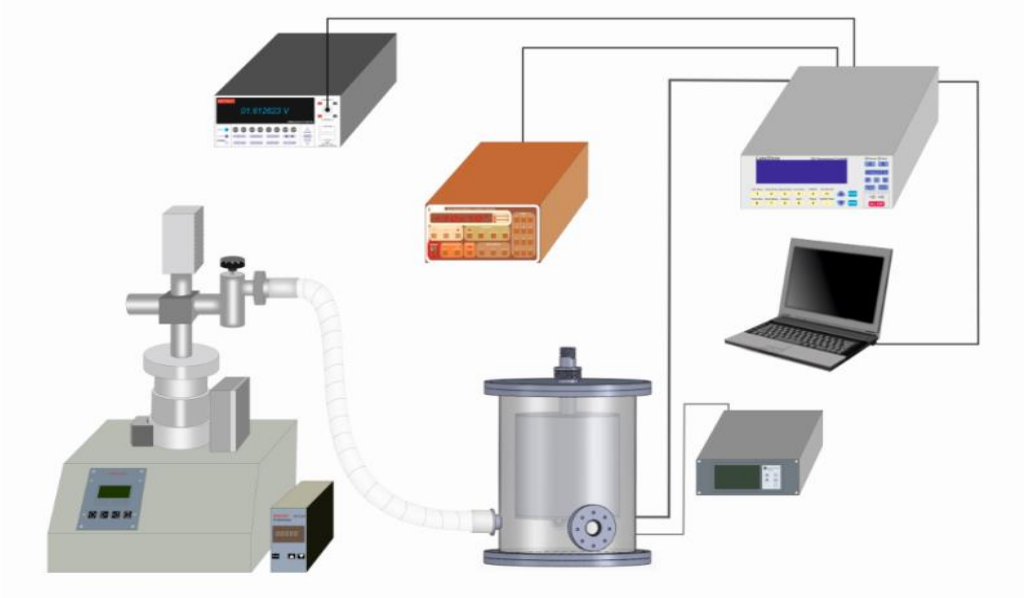

Figure 3.22. Electrical measurement setup of THz cryostat

By measuring the resistance – temperature, it is determined the superconducting transition region and critical temperature of each chip. In this region, it is crucial important to designate the correct temperature for bolometric measurement.

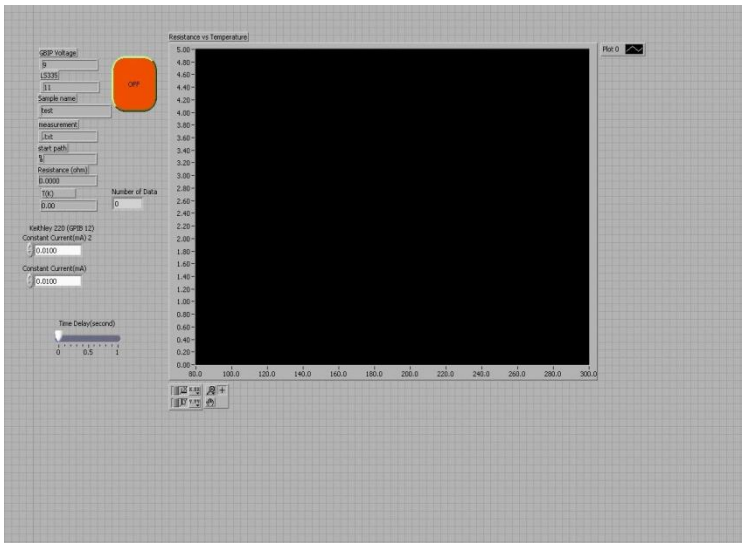

Figure 3.23. Labview of resistance – temperature measurement for THz cryostat

3.4.2. Bolometric Measurement

It is crucial to see the exponential decreasing until the critic temperature in result of electrical measurement. However, this transition region may be shown change in transition region with respect to thickness of the crystal. In our measurement, it is important to see this superconducting transition region as quite abrupt. In this region, we select the temperature approximate middle of the region which occurs the bolometric measurement. Figure 3.24 (a) shows the bolometric measurement setup with this superconducting transition region knowledge. It can be seen from Figure 3.24 (b), FTIR measurement was taken between 0.2-1.6 THz range for PE THz window to provide passing signal through the chip.

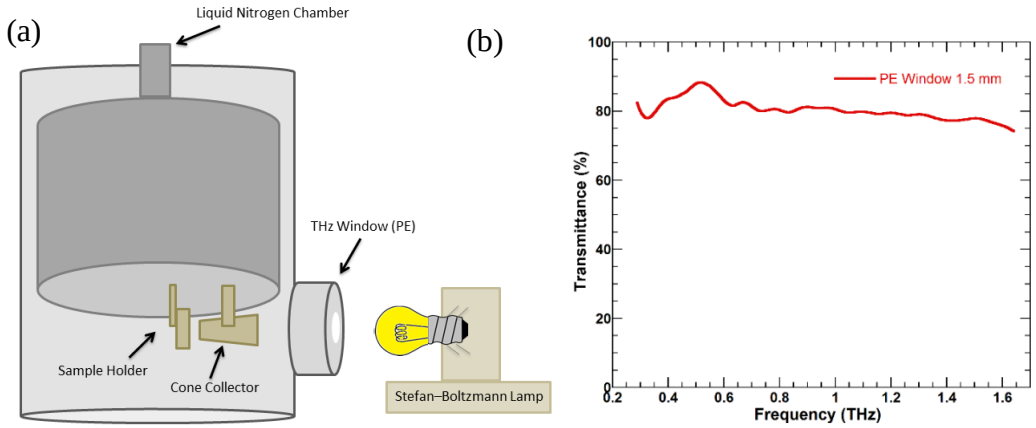

Figure 3.24 a) Bolometric measurement setup for cryostat b) Transmittance of THz window

First, chip was placed to the sample holder by making the wires connection, system was taken in vacuum, when it reached 10^{-5} Torr, liquid nitrogen was added from liquid nitrogen chamber. In this system, after taking the electrical measurement, bolometric measurement was starts with respect to selected temperature in superconducting region. For bolometric measurement, chip's temperature is hold the selected temperature by using the heater. Each temperature refers to specific resistance. It is possible to see the reference resistance when making the bolometric measurement to check.

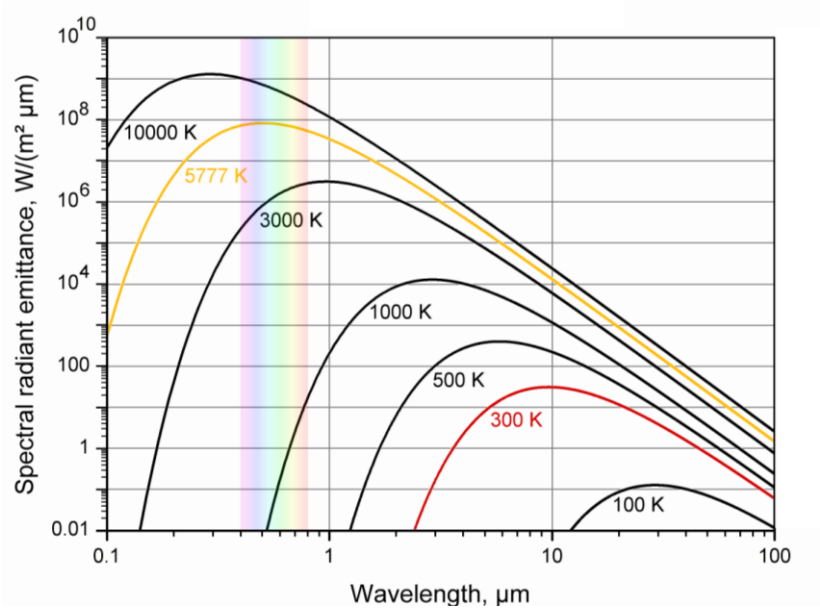

Figure 3.25 Spectrum of Stefan Boltzmann Lamp

When stable of temperate at the selected temperature, 5 cm distance from THz window Stefan Boltzmann Lamp signal was sent at certain times. These signals was focused onto the chip by wave collector. By this way, there was occurred the change of resistance give us the working principle of bolometer. Figure 3.25 shows the spectrum of Stephan Boltzmann with increasing the intensity decreasing the wavelength at 3000 K, roughly 100 μm refers to THz waves. There are change of resistance value during sending signal from Stefan Boltzmann Lamp. These variation of resistance is occurred because of focusing the signal onto the chip. After bolometric measurement, response time was calculated from resistance-time graphs as a result of bolometric measurement. (Danilchenko et al., 2004; Semenov et al., 2009; Hammar et al., 2011; Thoma et al., 2012). Response time is calculated which is shown in Figure 3.26 initial resistance point accept as reference point which is almost zero. Response time is the elapse time 1/e of the moment of qiving up the sending the signal

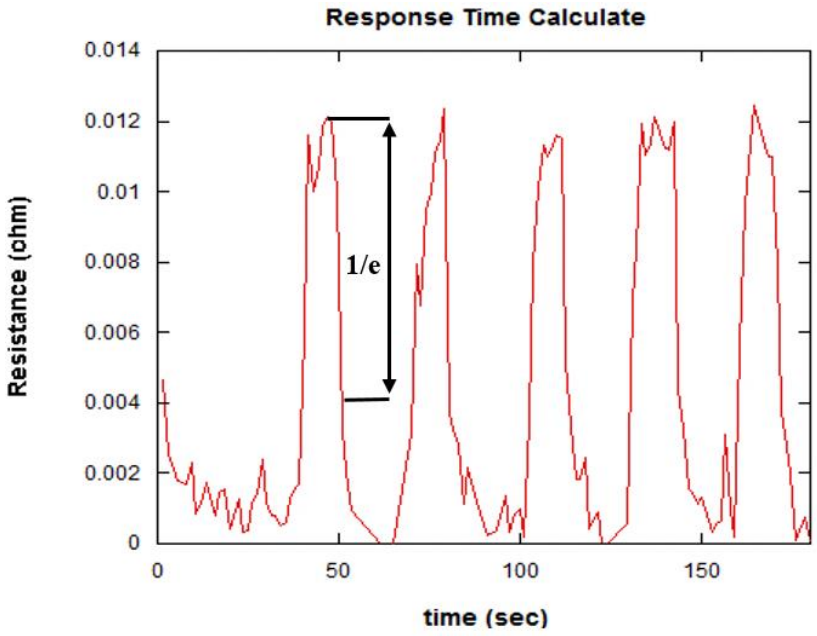

Figure 3.26. Response time calculation

CHAPTER 4

RESULTS AND DISCUSSIONS

In this section, I will explain the structural characterization of Bi2212 single crystals and chips. Then, a-b axis electrical results of chips continue with the bolometric results and response time of each measurement in our designed cryostat.

4.1. SEM and Optical Microscope Images

Surface properties of Bi2212 single crystals are crucial because it effects our electrical and bolometric measurement adversely by sensitivity of bolometer. Any contamination should not be on the surface Bi2212 single crystal, that's why, optic microscope is efficient equipment for checking crystal's surface any time.

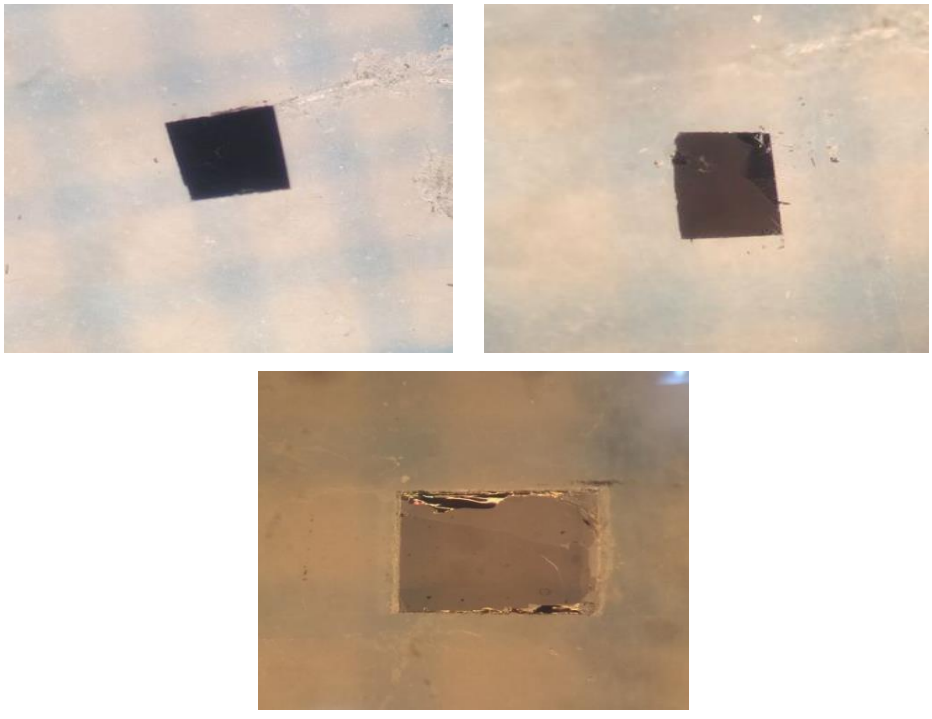

Figure 4.1. Optic microscope images of cleaved Bi2212 crystals

By cleaving, it is possible to get any thickness of crystal. These images show the smooth and clear surface for crystals. In Figure 4.1, crystal's thickness of showing optic microscope images are roughly 1 μm, 800 and 200 nm. These thickness can be measured by profilometer or I-V characterization method. Profilometer gives instantly the result as a thickness however, result of I-V measurement each line refer to 1.5 nm. Lines refers to each layer of the BSCCO single crystal. Thickness from I-V result is found by crossing the 1.5 nm with the number of line in I-V graph. As you can see from optic microscope images, thickness of the crystals are changed by effect of the cleaving process with scotch tape. It is understand from images smooth, fresh and clear surface can be acquired successfully.

To determine the amount of the epoxy to take correct measurement. It should be as much as possible little. If epoxy is too much for our chip, crystal can be cracked on the surface during electrical measurement. In Figure 4.2 shows SEM images as the result of using much epoxy during transfer of Bi2212 single crystal to sapphire. This problem can be solved by using less epoxy to transfer crystal and get it more convincing electrical and bolometric measurement results.

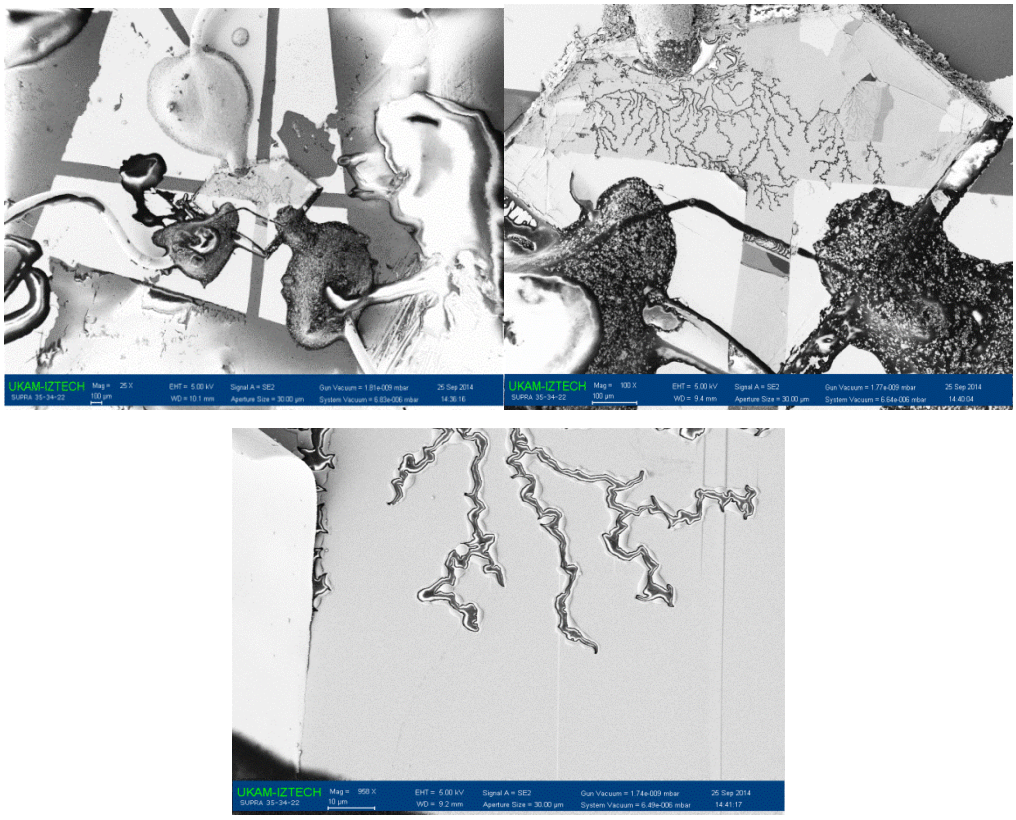

Figure 4.2. SEM images of cracking on Bi2212 single crystal's surface

Before electrical measurement of antenna structure, Bi2212 single crystals' analyzes were done by taking 4 point contact not with antenna for a chip. That's reason, after crystals are cleaved, they shadow with aluminum foil with 2 point 4 probe or 4 point 4 probe. Crystals which are transferred to the sapphire substrate has 0.5 mm^2 and 1 mm^2 areas. In Figure 4.3, crystal has roughly 200 nm thickness. It first shadowed with aluminum foil and coated with 200 nm gold then with silver epoxy are taken of contacts for electrical measurement. To take contact, silver epoxy is used due to perfect thermal conductor and low electrical resistance.

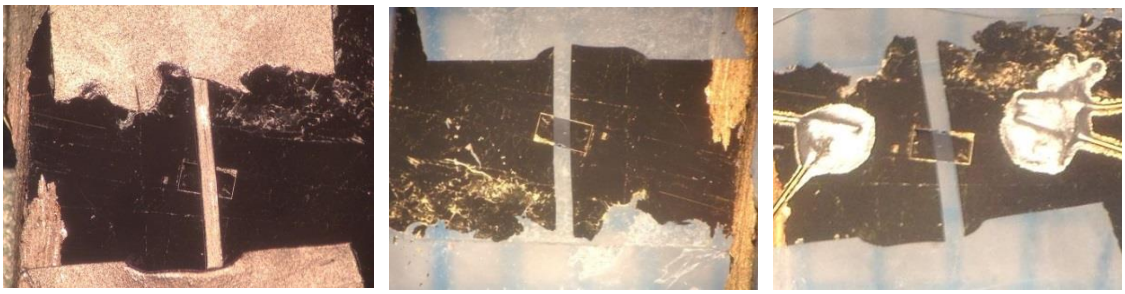

Figure 4.3. Optic microscope images of 2 point 4 probe contact

To get better electrical results, Bi2212 single crystals contacts are taken as 4 point 4 probe. Because, 2 point 4 probe contact may have some contact resistance to affect our result adversely. That's why, 4 point 4 probe method was chosen to characterize our samples to get better electrical measurement. In Figure 4.4, it can be seen the cleaved smooth crystal surface with gold wire contact which is ready for taking electrical measurement. Additionally, it can be seen on the optic microscope images that any photoresist is remained after etching depending on the time of etching.

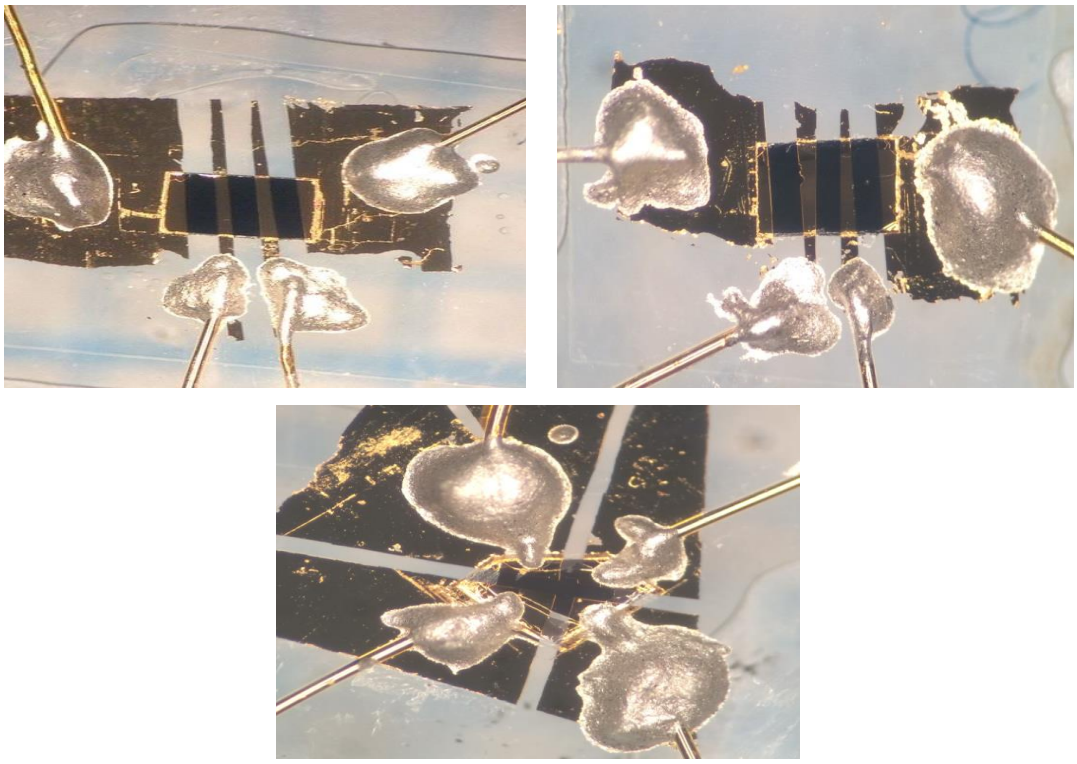

Figure 4.4. Optic microscope images of 4 point 4 probe contact

Antenna structure was patterned the crystal surface for bolometric measurement. That's why, before antenna, transferred and cleaved crystals firstly were shadowed. These crystals can be seen in Figure 4.5 which two of them has roughly 1 μm and bottom of them has roughly 150 nm as a thickness. They have smooth surface due to cleaved process without any contamination.

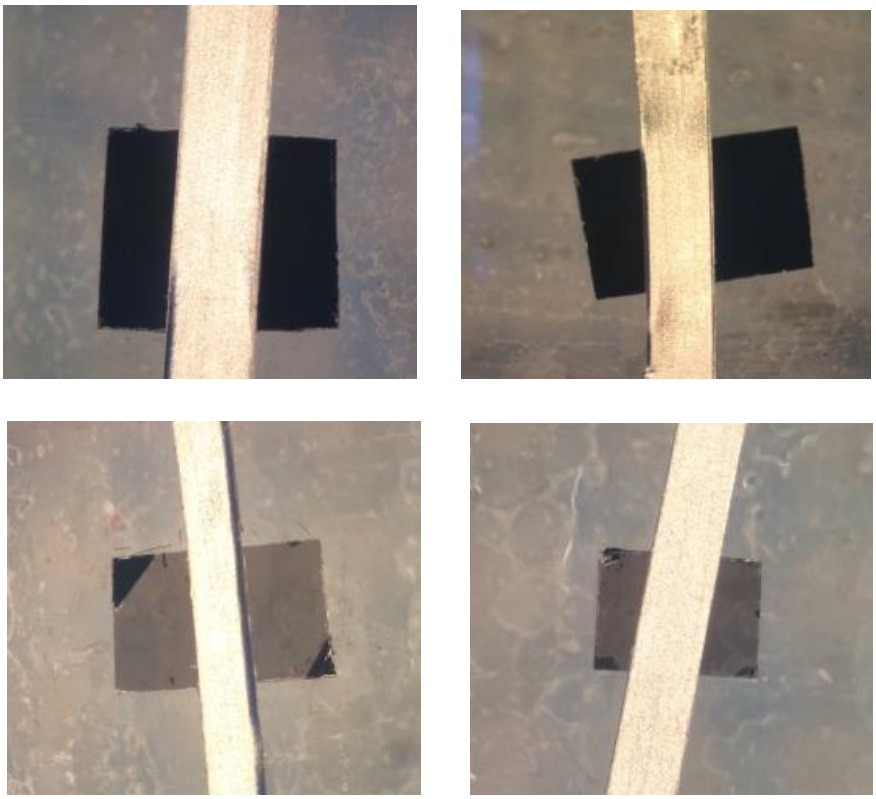

Figure 4.5 Optic microscope images of shadowed cleaved Bi2212 single crystals

It can be see the clear deposition from optic microscope images in Figure 4.6. Black areas belong to gold deposition roughly 200 nm and bright lines belong to aluminum foil to shadow. After deposition, the surface of the coated layer and crystals are controlled by optic microscope to check any contamination stay or not. There are not seen any contamination on the surface however some lines can be seen in the dark areas that belong to trace of scotch tape. These traces do not affect our electrical and bolometric measurements. Each step of process it is possible to check the surface of chip by optic microscope as you can see from images.

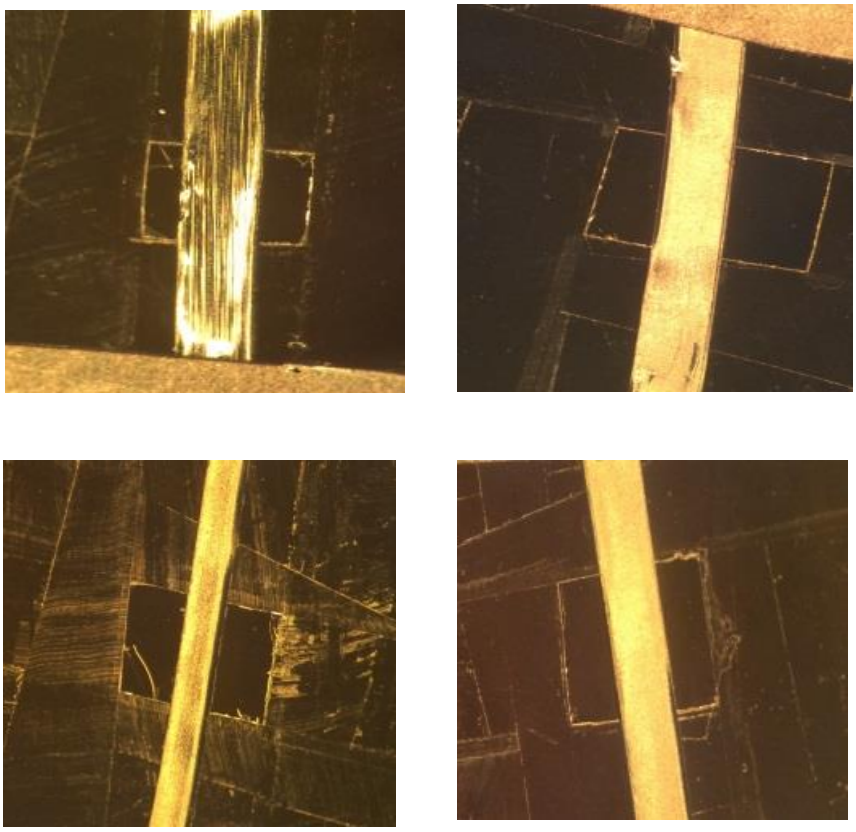

Figure 4.6. Optic microscope images of deposited with gold Bi2212 single crystals

Figure 4.7 shows the optic microscope images of chips with different antenna structures by gold wire and silver epoxy for contact. Gold areas belong to planned antenna structure as can be seen in optic microscope images. Structures were successfully patterned onto the Bi2212 single crystal without any deformation. Epoxy under the crystal which is seen as transparent, clear and homogeneous property from optic microscope images. Any distortion on the antenna structures are not seen in images. This is crucial step to continue for measurement without any failure.

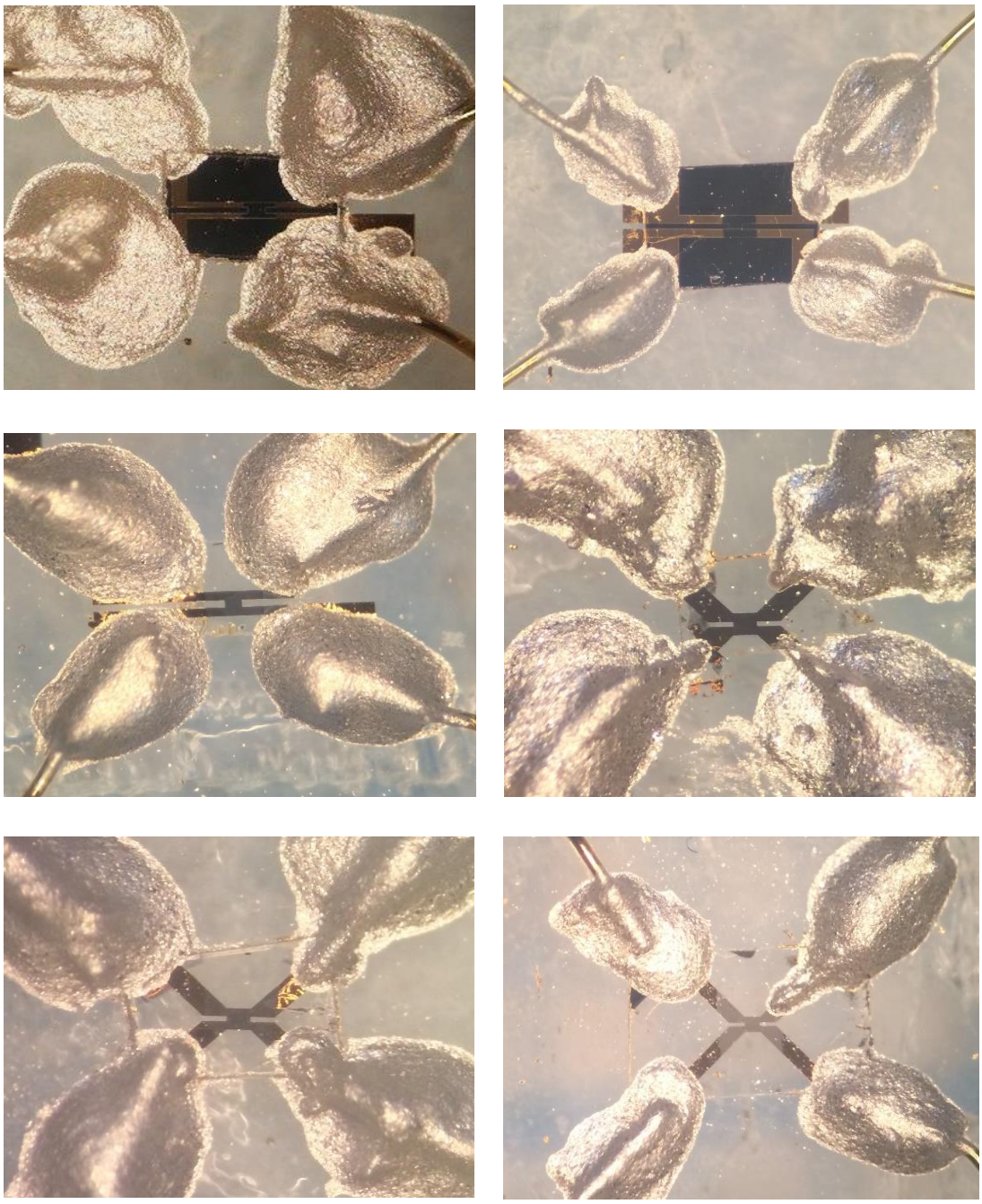

Figure 4.7. Optic microscope images of patterned antenna structures by e-beam lithography on Bi2212 single crystals

Log periodic antenna structure was patterned on Bi2212 single crystal o shown in Figure 4.8 and Figure 4.9. It can be seen that crystal surfaces are clear and antenna structure is placed the right place which is the middle of the crystal. Antenna structures are exposed right and smooth without any deformation.

Figure 4.8. SEM image of log-periodic antenna by e-beam lithography on Bi2212 single crystal

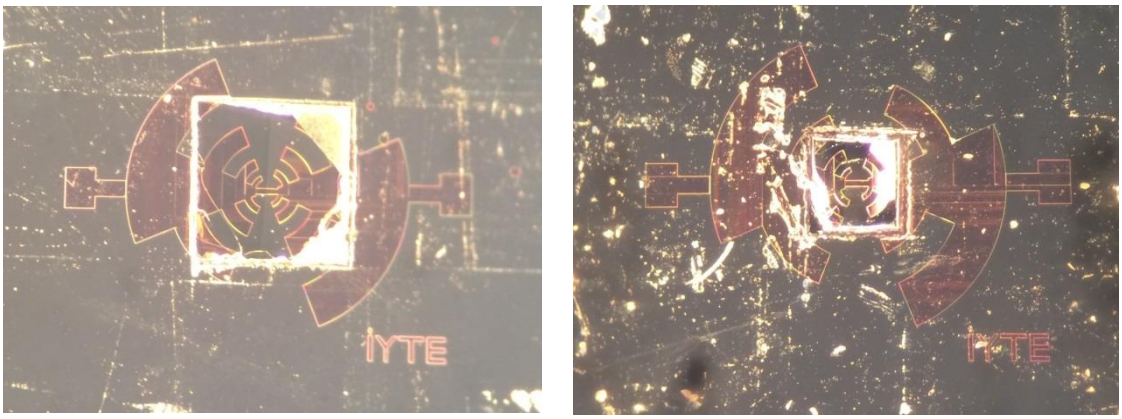

Figure 4.9. Optic microscope images of log-periodic antenna by e-beam lithography on Bi2212 single crystal before etching

4.2. Electrical Results

After fabricated antenna structure our sample, chips are taken a-b axis resistance measurements was taken. I will give result of electrical measurement in the next section.

4.2.1. Temperature Dependence of a-b axis Resistance Measurement

Temperature dependence of a-b axis measurement was taken in our designed cryostat with 10 μA current and cooled by liquid nitrogen. As a result of electrical measurement, superconducting transition region is decreased sharply and exponentially. Each chip has sharp and critical temperature as T_c (onset). For bolometric measurement, superconducting transition region is important how much abrupt. They have different critical temperature because of depending on thickness of cleaved Bi2212 single

crystals. resistance of the chip is changed by the effect of the thickness of the crystal (You, et al. 2006). When increasing the thickness of crystal, its room temperature (R_{300K}) and critical temperature resistance (R_{Tc}) is decreased. These chips' thickness which are shown are changed between 200 nm to 1µm. R_{Tc}/ R_{300K} value is determinate the under or over doped of the Bi2212 single crystal. Additionally, contact resistance did not seen in our samples as you can see from resistance vs temperature graphs. If contact resistance is below 3 Ω, it count as there is no contact resistance problem (Watanabe, et al. 1997). If assume optimum doped Bi2212 single crystals, resistivity admit as $5x10^{-4}$ Ω cm in a-b axis electrical measurement (Watanabe, et al. 1997). By knowing this resistivity, it is possible to calculate resistance of chip via thickness and size of crystals for each sample.

The Figure 4.10 shows the electrical behavior of YT29 sample. It has critical temperature (T_c) 90 K, room temperature resistance (R_{300K}) 1.6 Ω, critical temperature resistance (R_{Tc}) 1.1 Ω, R_{Tc}/ R_{300K} value is 0.69.

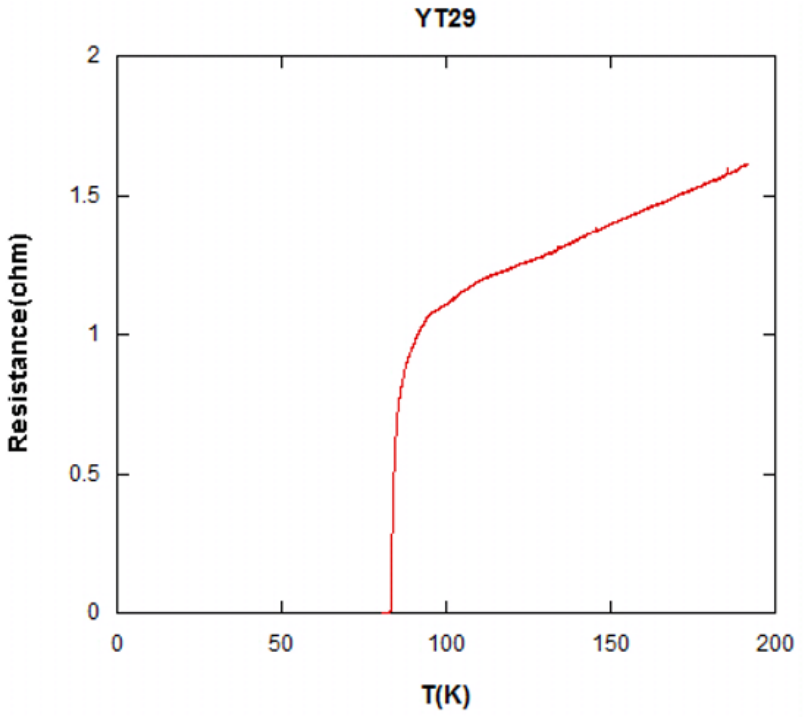

Figure 4.10. Resistance-Temperature behavior of YT29

The Figure 4.11 shows the electrical behavior of YT32 sample. It has critical temperature (T_c) 89 K, room temperature resistance (R_{300K}) 0.54 Ω, critical temperature resistance (R_{Tc}) 0.26 Ω, R_{Tc}/ R_{300K} value is 0.48.

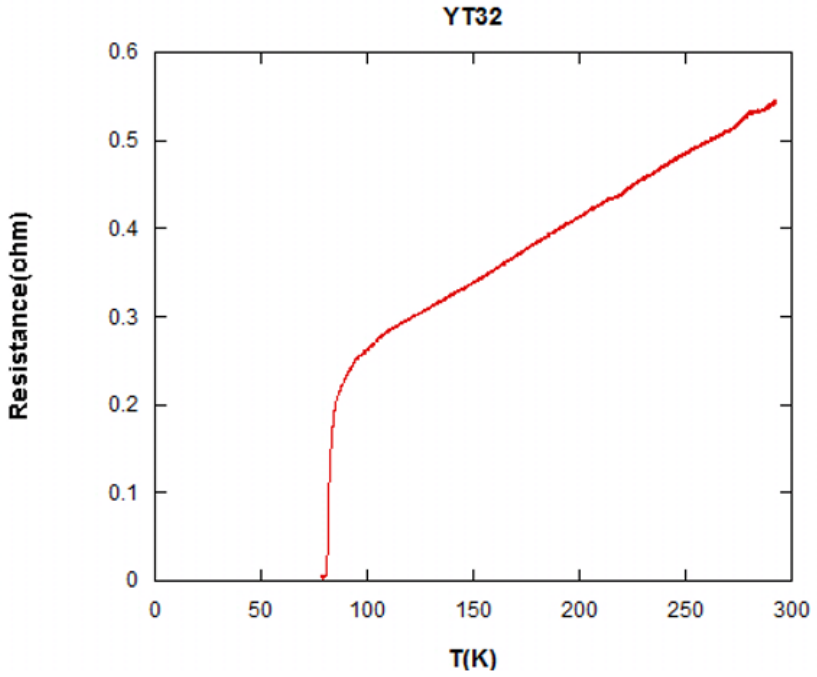

Figure 4.11 Resistance-Temperature behavior of YT32

The Figure 4.12 shows the electrical behavior of YT36 sample. It has critical temperature (T_c) 87 K, room temperature resistance (R_{300K}) 0.81 Ω, critical temperature resistance (R_{Tc}) 0.44 Ω, R_{Tc}/ R_{300K} value is 0.54.

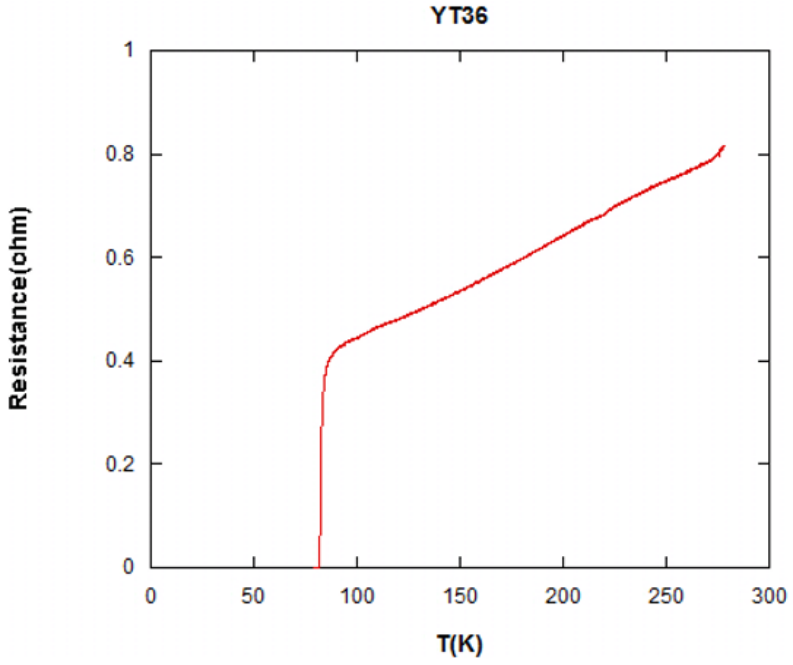

Figure 4.12 Resistance-Temperature behavior of YT36

The Figure 4.13 shows the electrical behavior of YT37 sample. It has critical temperature (T_c) 90 K, room temperature resistance (R_{300K}) 5.4 Ω, critical temperature resistance (R_{Tc}) 2.1 Ω, R_{Tc}/ R_{300K} value is 0.38.

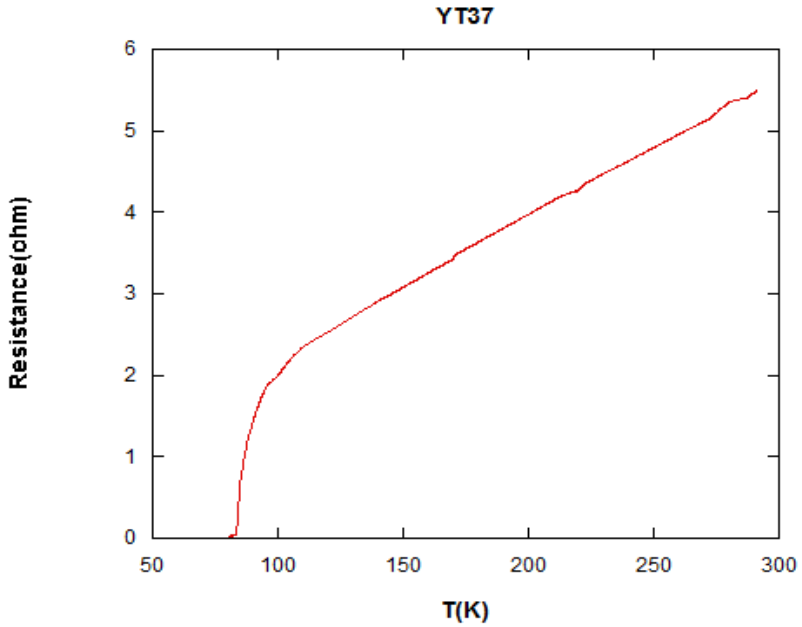

Figure 4.13 Resistance-Temperature behavior of YT37

The Figure 4.14 shows the electrical behavior of YT38 sample. It has critical temperature (T_c) 89 K, room temperature resistance (R_{300K}) 1.12 Ω, critical temperature resistance (R_{Tc}) 0.57 Ω, R_{Tc}/ R_{300K} value is 0.51.

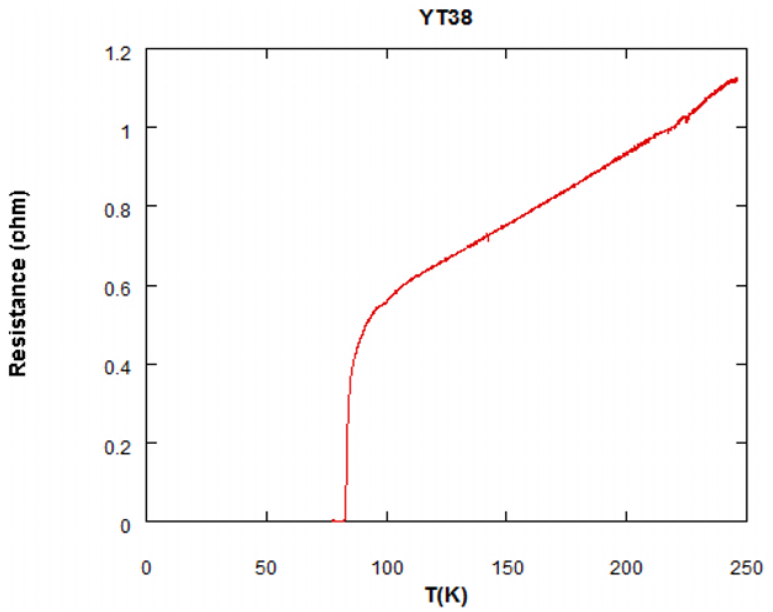

Figure 4.14 Resistance-Temperature behavior of YT38

The Figure 4.15 shows the electrical behavior of YT44 sample. It has critical temperature (T_c) 88 K, room temperature resistance (R_{300K}) 0.27 Ω, critical temperature resistance (R_{Tc}) 0.18 Ω, R_{Tc}/ R_{300K} value is 0.67.

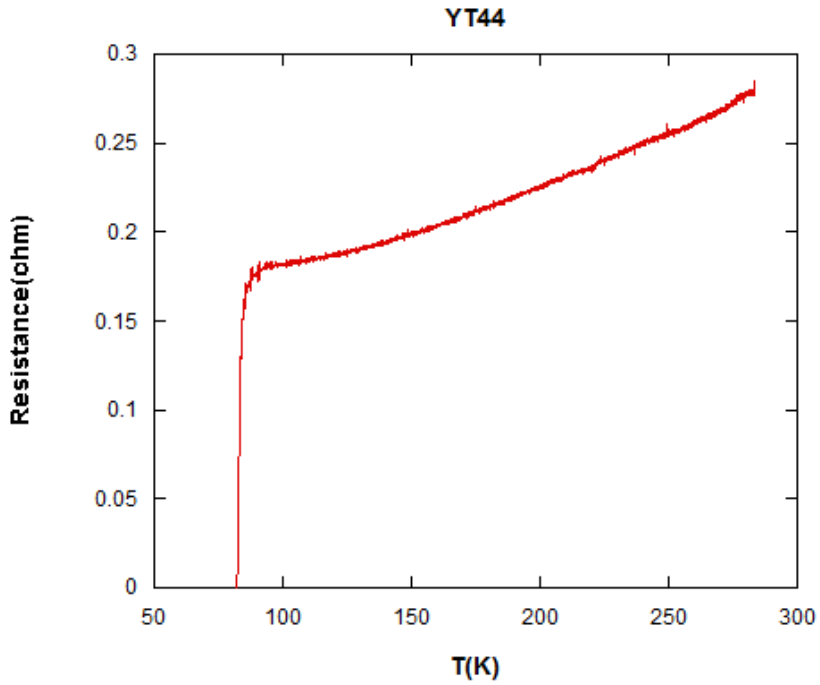

Figure 4.15 Resistance-Temperature behavior of YT44

4.3. Bolometric Results

After electrical measurement of chips, bolometric measurement was done to graph of resistance versus time to calculate the response time.

4.3.1. Bolometric Detection and Response Time

Electrical measurement is important to determine the right temperature in superconducting transition region to hold it stable. In this selected temperature, bolometric measurement was done with Stefan-Boltzmann Lamp which send signal through THz window by focusing wave collector onto the chip's center. This signal comprise the change of resistance by depend on intensity of the signal. We took into consideration resistance change versus time to detect the sensitivity of the detector which response time calculation explain in detail previous section.

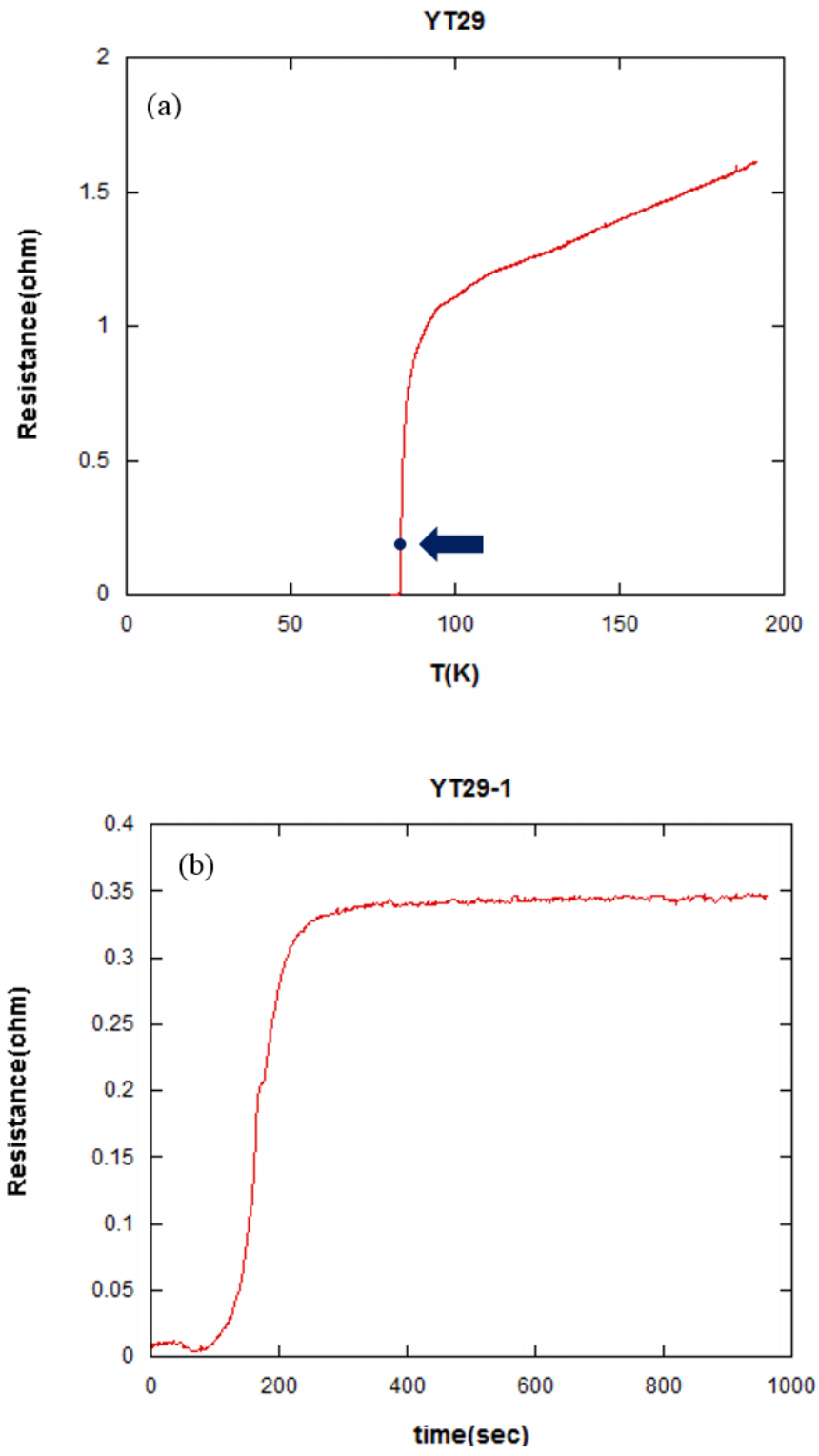

Figure 4.16. (a) The selected temperature for bolometric measurement (b) Increase of resistance to reach the selected temperature (c) (d) (e) change of resistance by under the influence of signal

(cont. on next page)

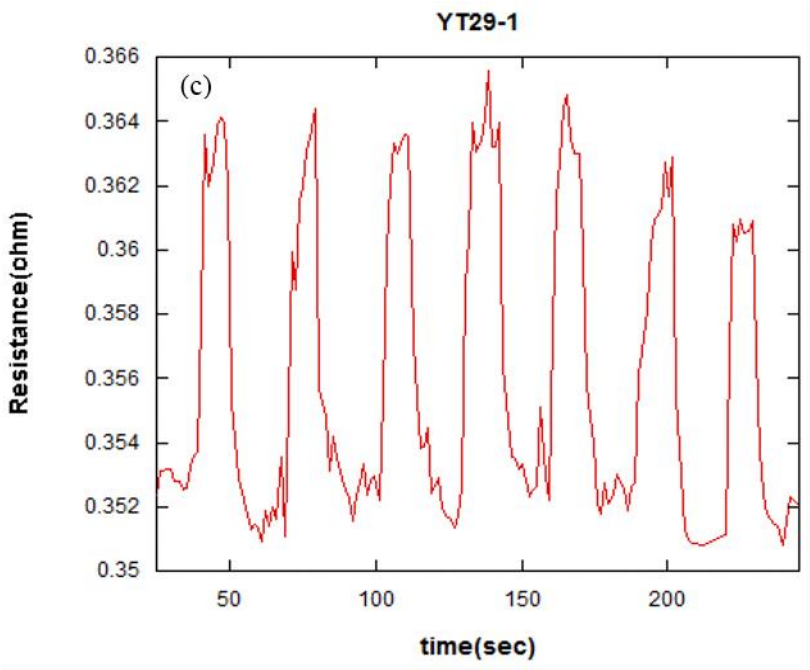

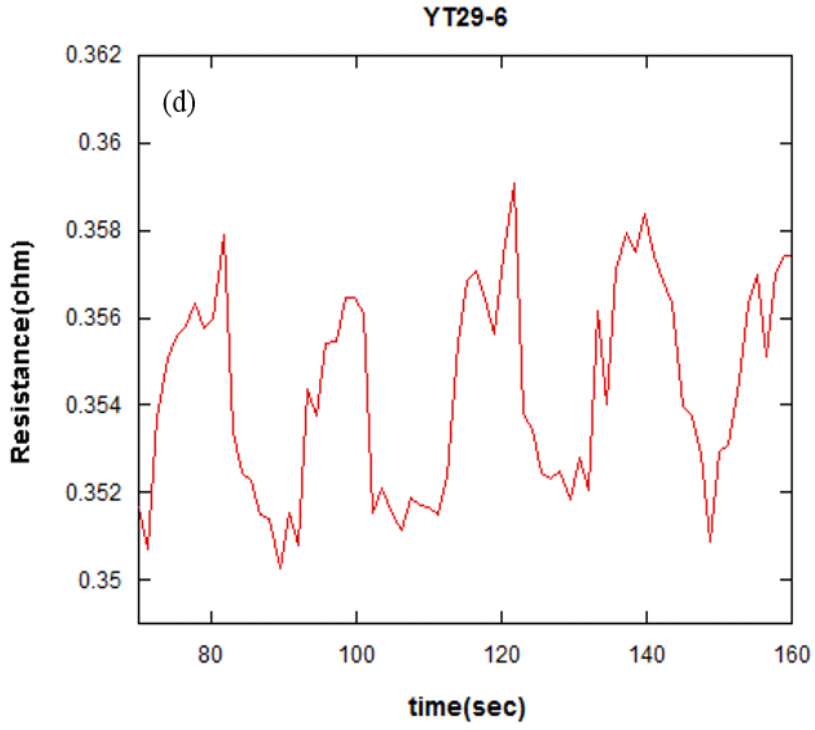

Figure 4.16. (cont.)

(cont. on next page)

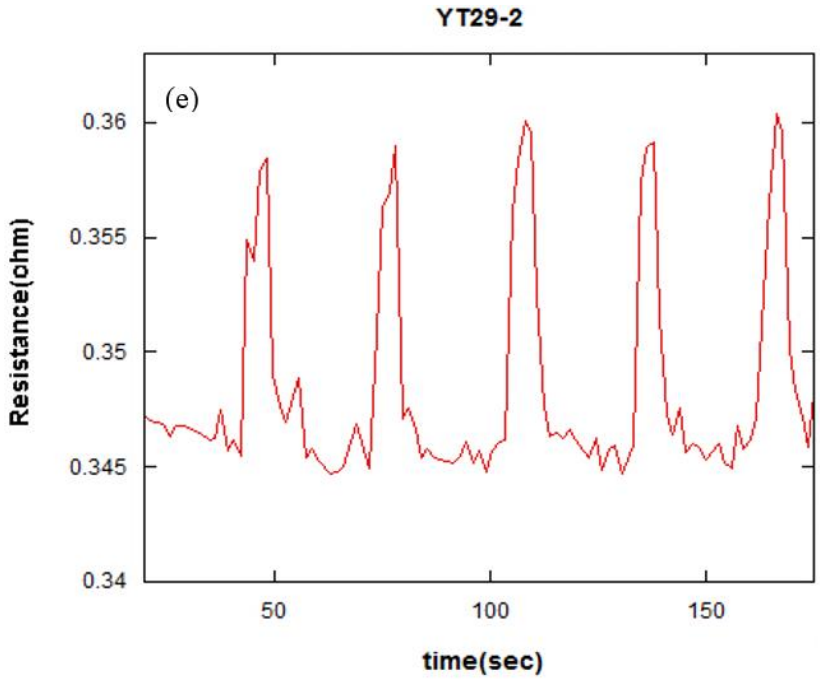

Figure 4.16. (cont.)

To observe the change of resistance, selected temperature is 84 K and it refers to 0.35 Ω shown in Figure 4.16 (a). We can see of the increase of resistance to reach from 78 K to 84 K and when it reach the selected temperature 84 K or resistance 0.35 Ω it stay stable which is shown in Figure 4.16 (b). Figure 4.16 (c) shows the result of resistance during sending signal in each 10 second and paused each 20 second. By this effect, resistance was changed increasing by 0.012 Ω. We can change the increasing ratio of the resistance by changing the intensity of the signal. Figure 4.16 (d) shows that if we decrease the intensity of the signal, our change of resistance is decreased from 0.012 Ω to 0.005 Ω. Additionally, signal was send in each 10 second and paused each 15 second in Figure 4.16 (d).We changed the selected resistance as 0.346 Ω and signal was send in each 5 second and paused each 20 second then 0.011 Ω change of resistance was observed in Figure 4.16 (e). Response time was calculated 1.9111 second for YT29 chip in Figure 4.16 This response time value was improved in the next chip's measurement.

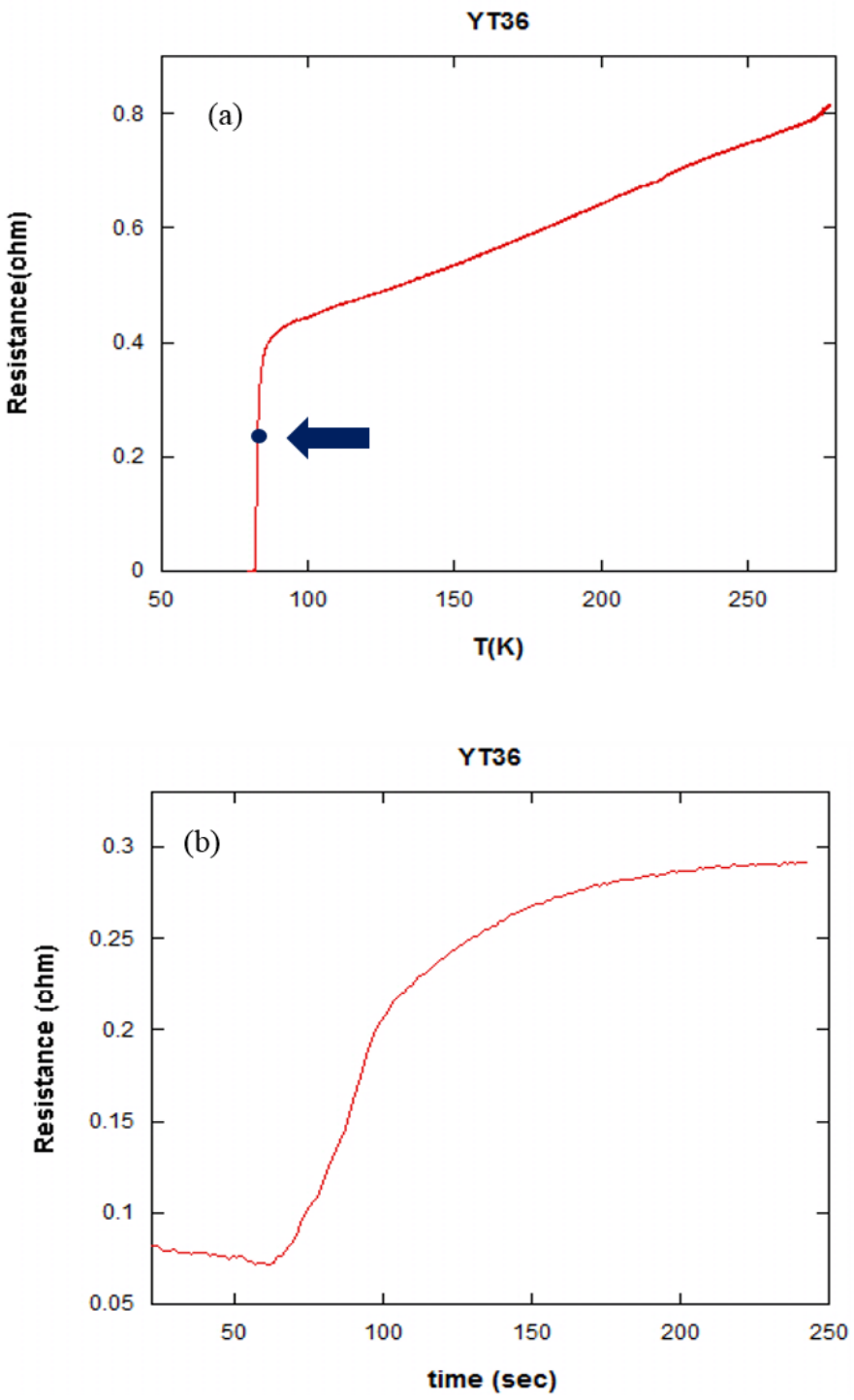

Figure 4.17. (a) The selected temperature for bolometric measurement (b) Increase of resistance to reach the selected temperature (c) Change of resistance by under the influence of signal (d) Decreasing of resistance when shut down heater

(cont. on next page)

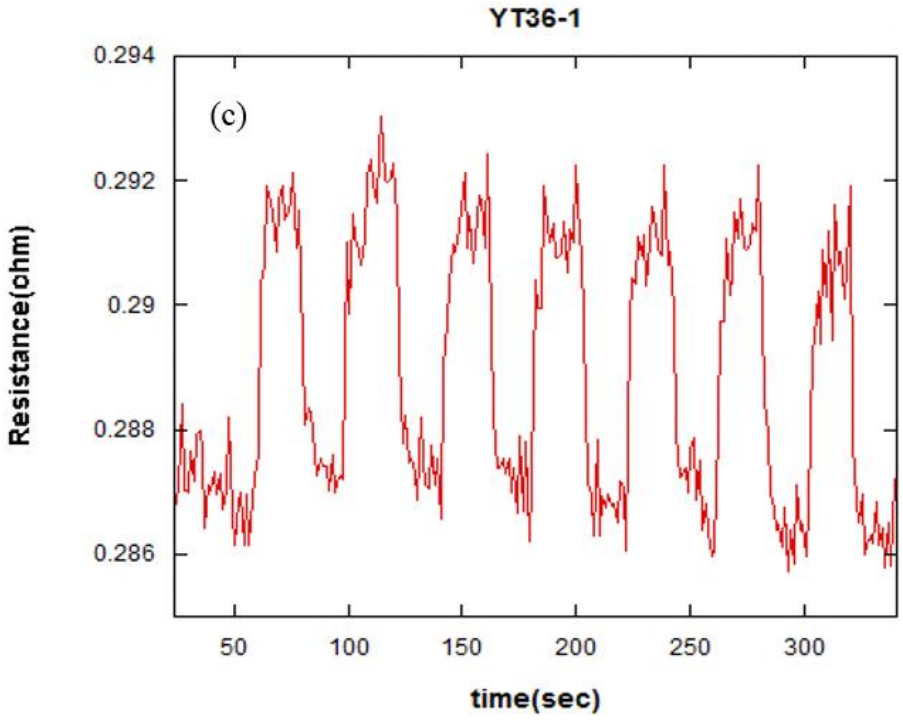

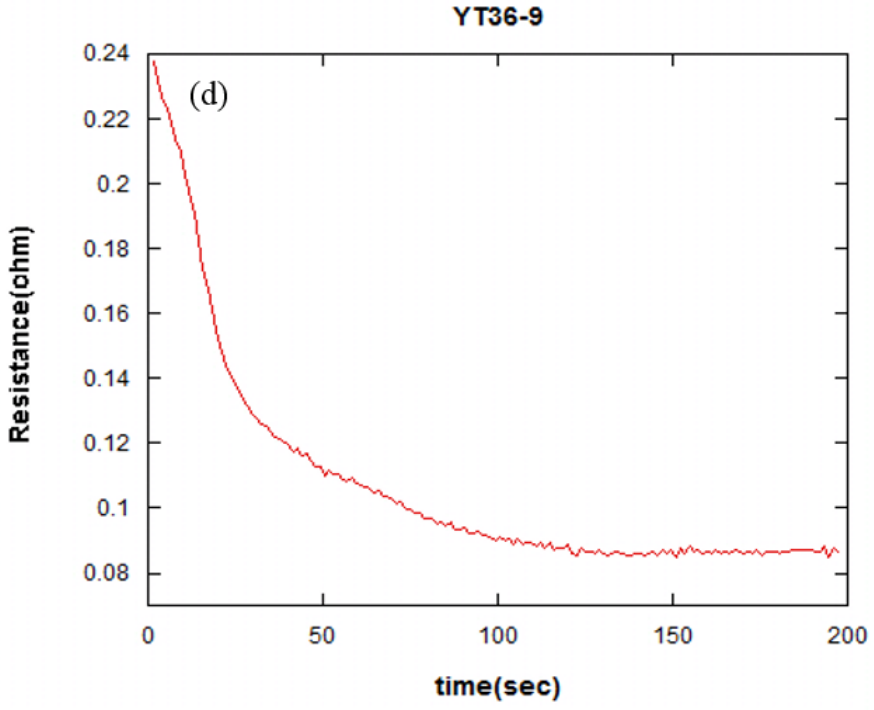

Figure 4.17. (cont.)

In Figure 4.17 (a), our selected temperature in the superconducting transition region is 83 K and it refers resistance to 0.287 Ω. It can be seen increasing of the resistance from increasing of the temperature from 78 K to 83 K and it stay the stabile when it reached the selected resistance 0.287 Ω in Figure 4.17 (b). Signal was sent in each 20 second and paused each 20 second and resistance of chip was changed 0.04 Ω in Figure 4.17 (c). After paused the signal, resistance of chip was reached the selected resistance. Response time of this chip was calculated 1.1555 second. During resistance versus temperature measurement, there was not any contact resistance in Figure 4.17 (a), however Figure 4.17 (b)-(d) shows that there exists 0.08 Ω contact resistance during bolometric measurement.

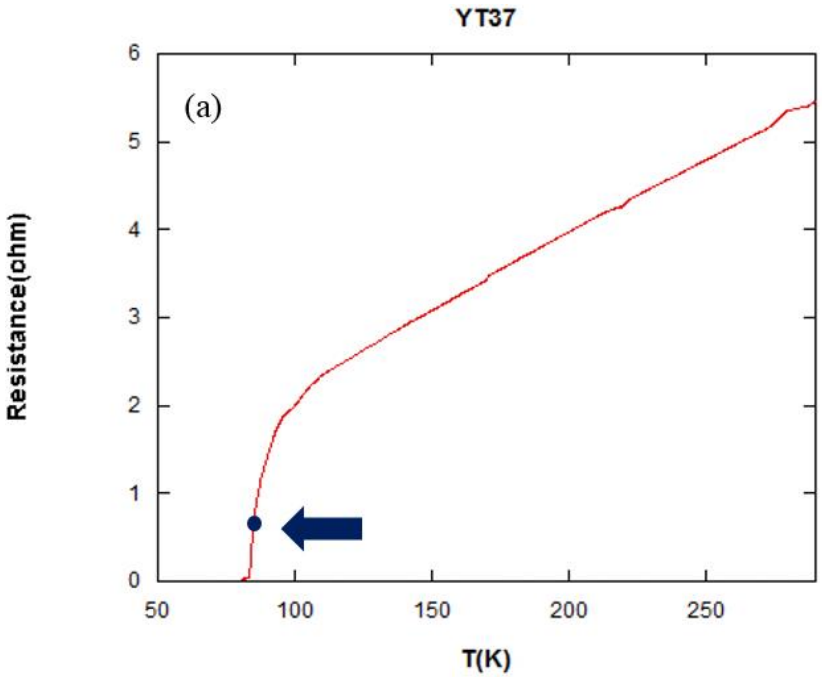

Figure 4.18. (a) The selected temperature for bolometric measurement (b) Increase of resistance to reach the selected temperature (c) (d) (e) (f) (g) Change of resistance by under the influence of signal

(cont. on next page)

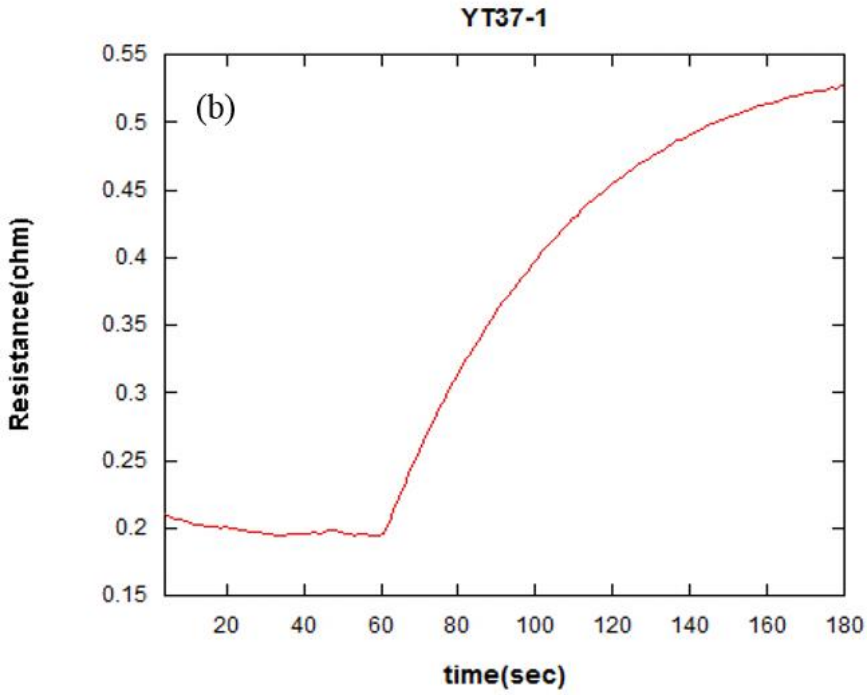

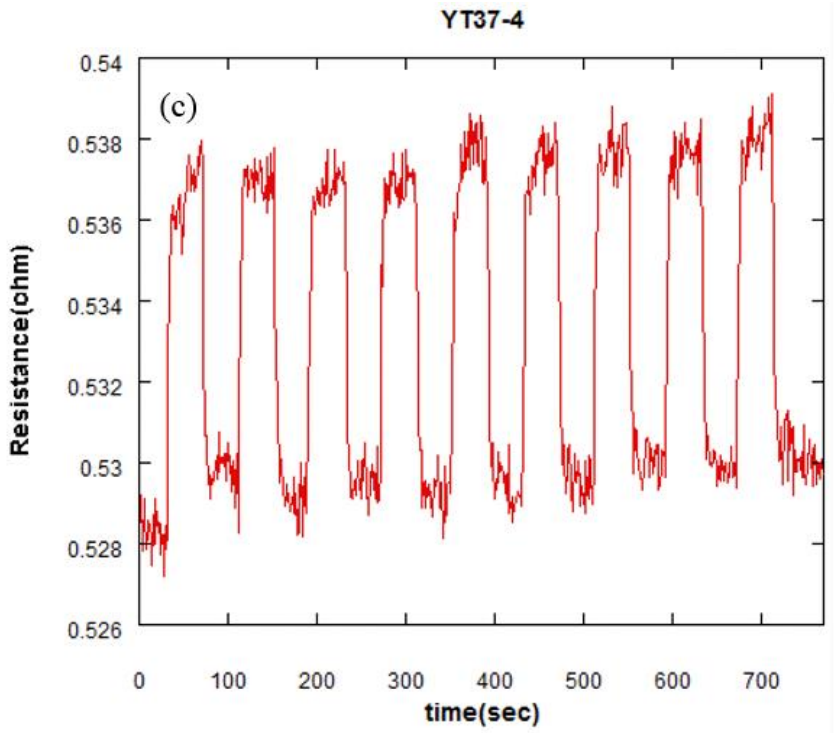

Figure 4.18. (cont.)

(cont. on next page)

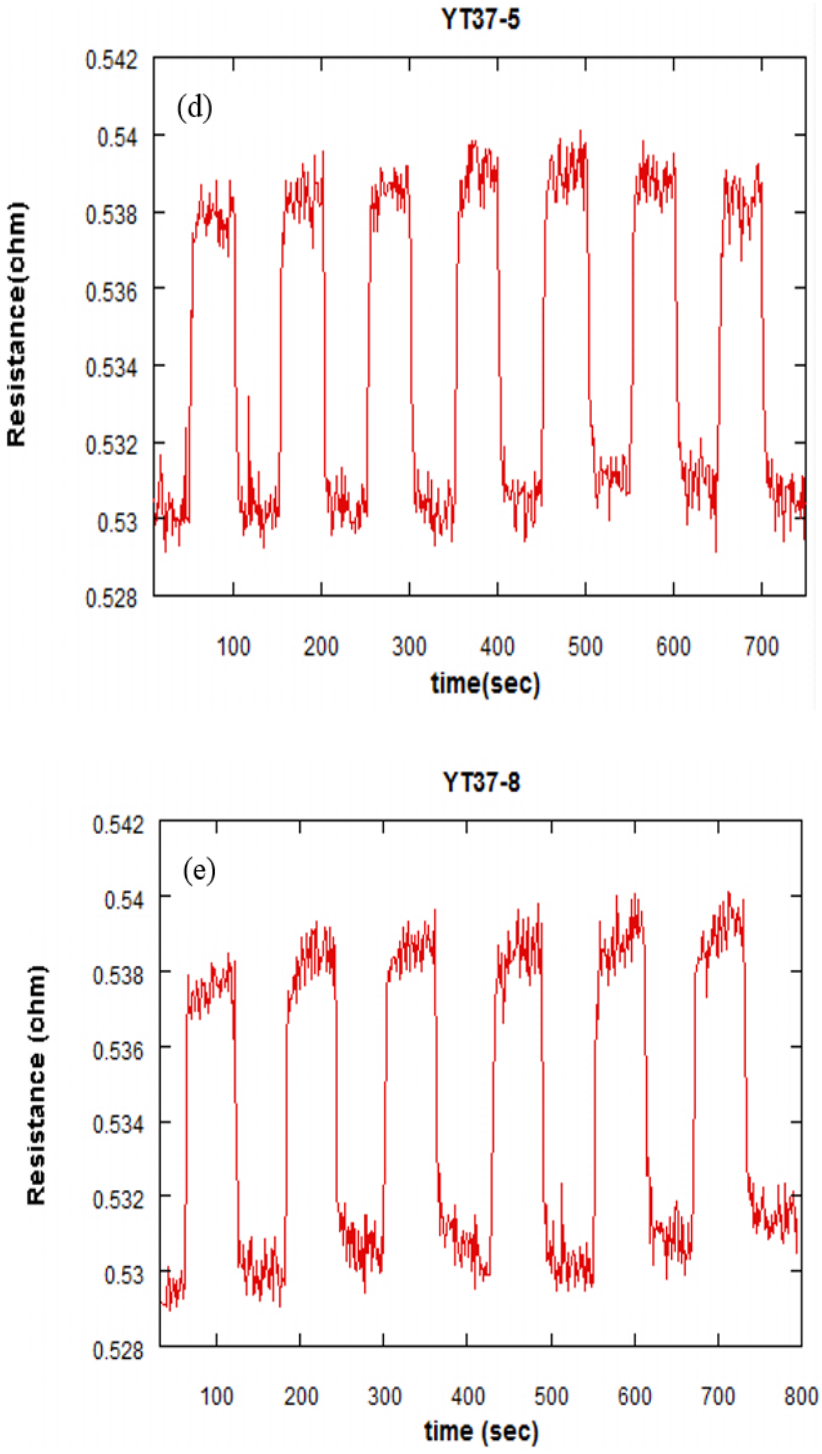

Figure 4.18. (cont.)

(cont. on next page)

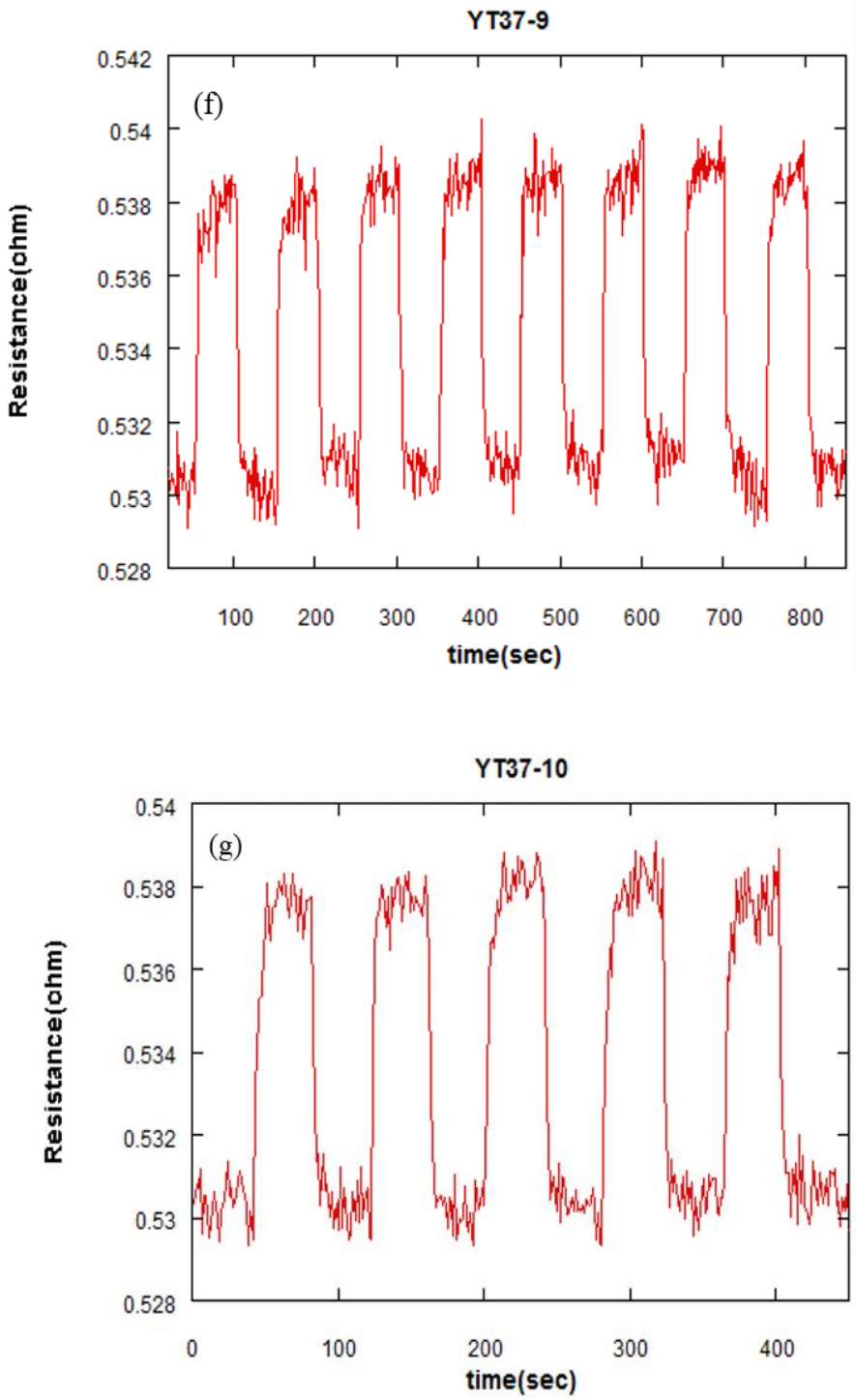

Figure 4.18. (cont.)

The selected temperature in the superconducting transition region is 84 K and it refers to 0.53 Ω in Figure 4.18 (a). It can be seen to reach chip's resistance to the selected resistance 0.53 Ω in Figure 4.18 (b). Signal was sent in each 30 second and paused each 40 second in Figure 4.18 (c). Signal was sent and paused in each 40 second

for Figure 4.18 (g), 50 second for Figure 4.18 (d) (f) and 60 second for Figure 4.18 (e) to observe the change of resistance. Same intensity was sent to chip, as can be understand the initial resistance of each measurement has the same resistance almost 0. 530 Ω from Figure 4.18 (c) to (g). Change of resistance was observed 0.008 Ω. Response time was calculated for this chip 825 ms.

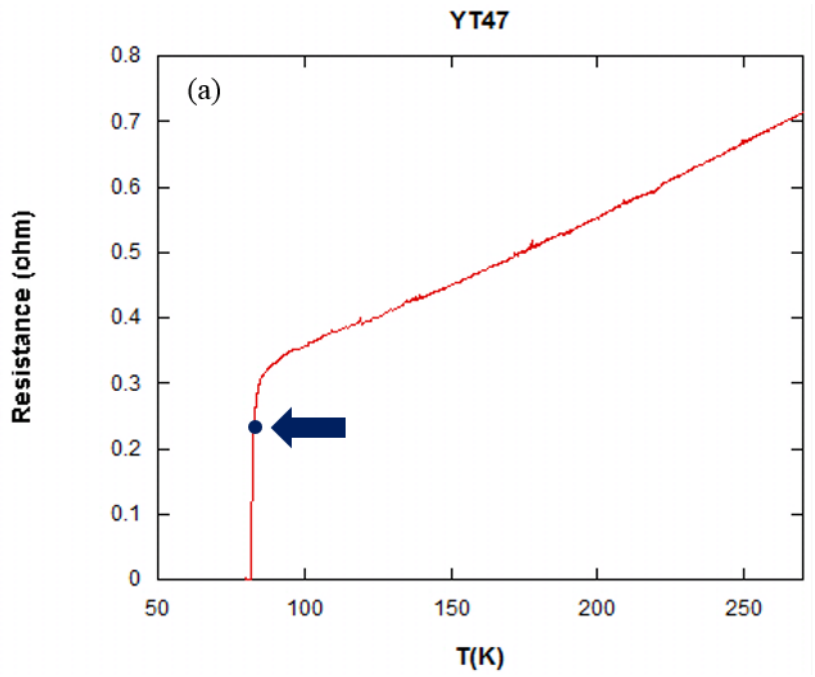

Figure 4.19. (a) The selected temperature for bolometric measurement (b) (c) (d) (e) (f) (g) Change of resistance by under the influence of signal

(cont. on next page)

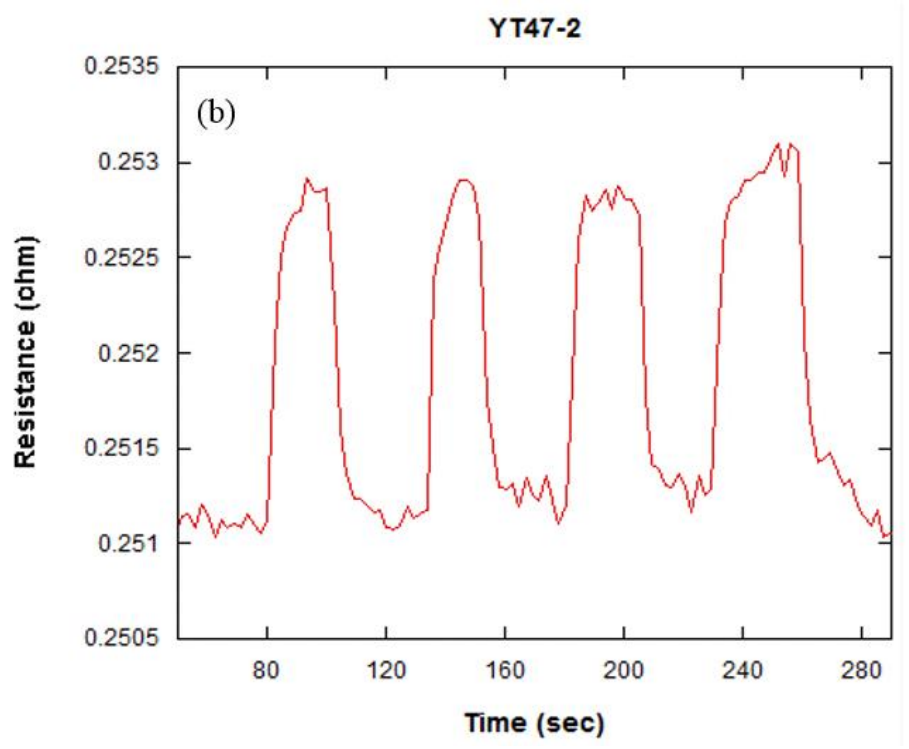

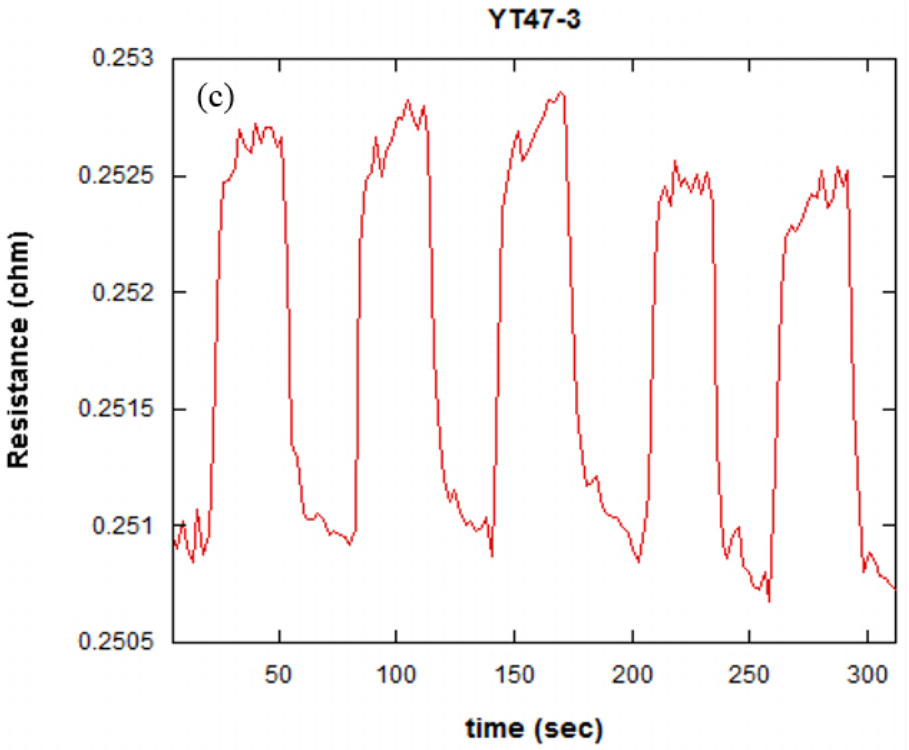

Figure 4.19. (cont.)

(cont. on next page)

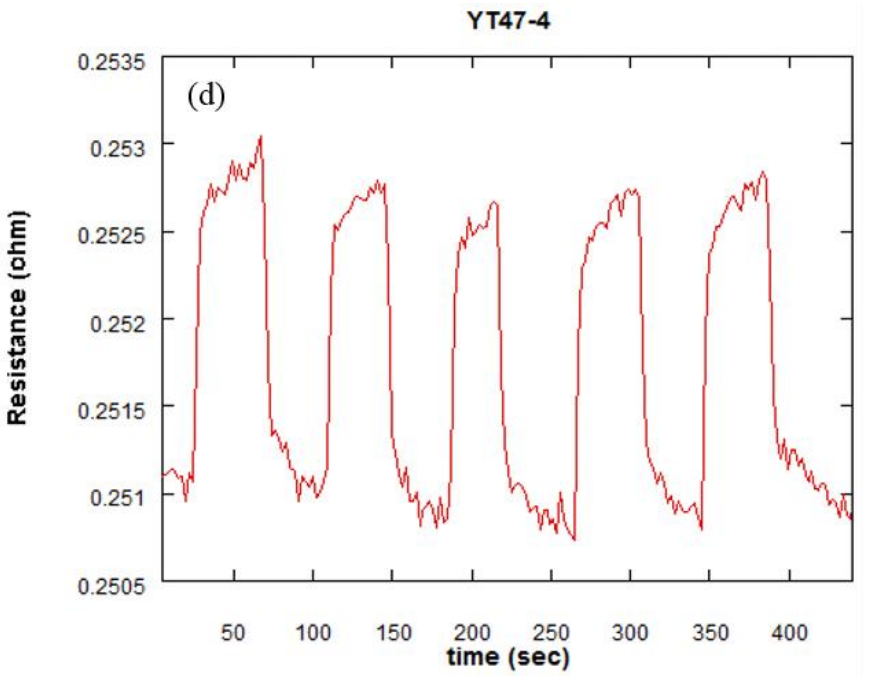

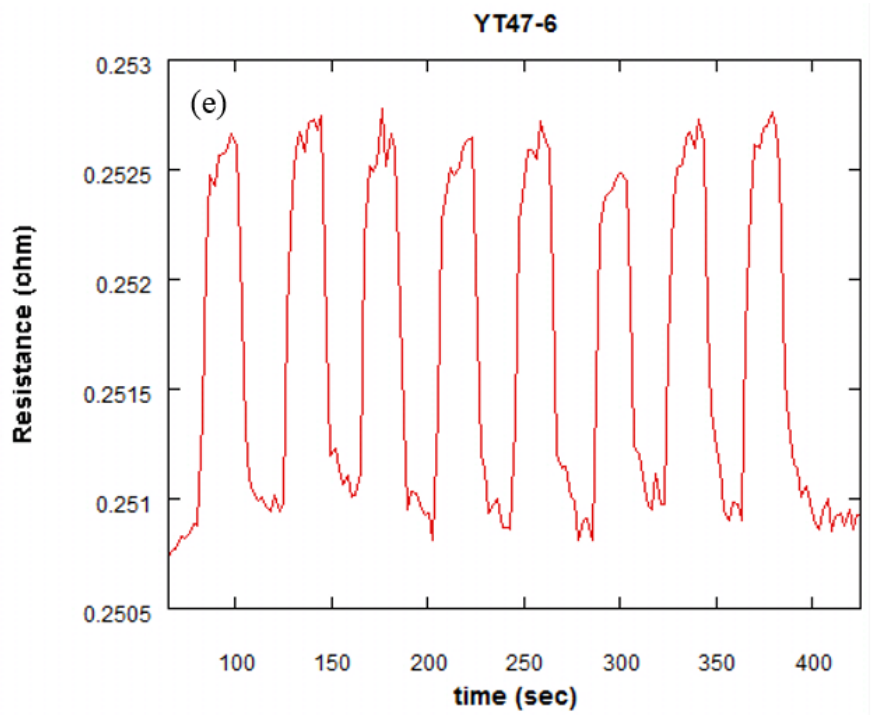

Figure 4.19. (cont.)

(cont. on next page)

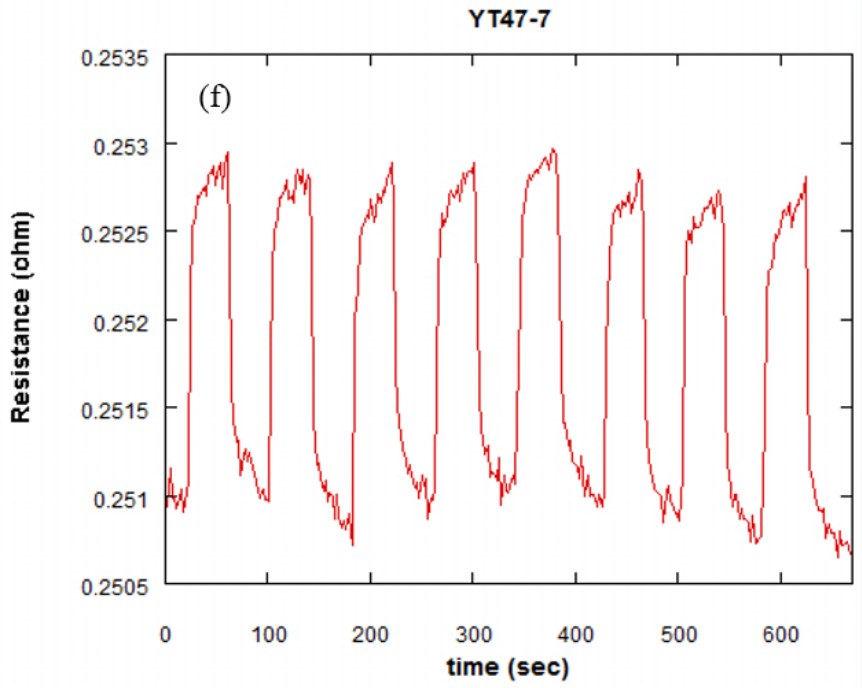

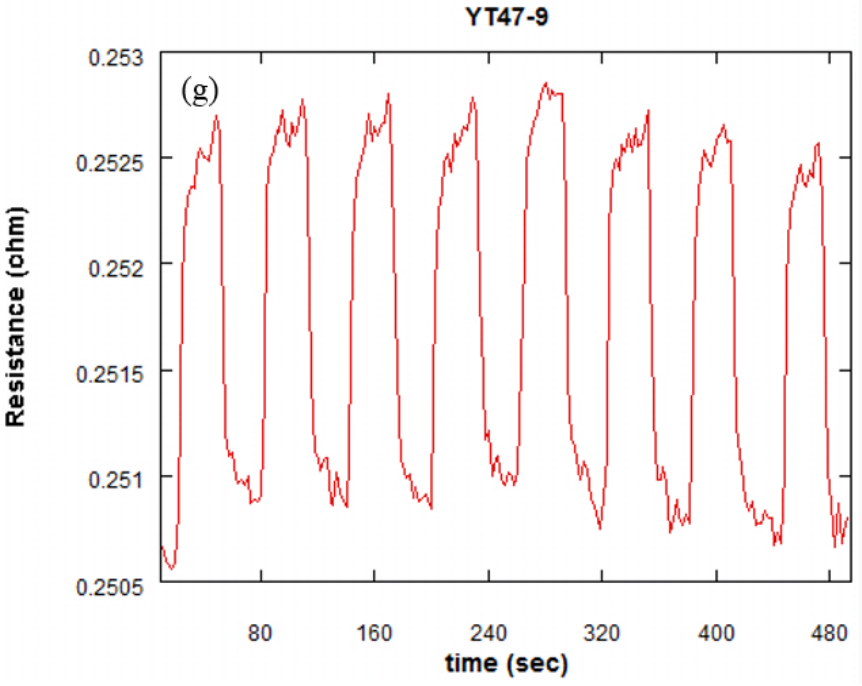

Figure 4.19. (cont.)

We assumed the optimum temperature as 84 K and it refers to 0.251 Ω in Figure 4.19 (a). Signal was sent in each 20 second and paused each 30 second in in Figure 4.19 (b). In other measurement signal was sent and paused in each 50 second for in Figure 4.19 (e), 30 second for in Figure 4.19 (c) (g) and 40 second for in Figure 4.19 (d)-(f).

Same intensity was sent and 0.0017 Ω was observed as change of resistance during applying the signal onto the chip. Response time was calculated as 972 ms.

Table 4.1. Electrical properties of some selected our samples

	R_{Tc} (onset) (ohm)	$R_{300\ K}$ (ohm)	$R_{Tc}/R_{300\ K}$	T_c (onset) (K)	ΔT_c (K)
YT29	1.10	1.60	0.69	90	6.11
YT32	0.26	0.54	0.48	89	7.20
YT36	0.44	0.81	0.54	87	4.20
YT37	2.10	5.40	0.38	90	8.32
YT38	0.57	1.12	0.51	89	4.91
YT44	0.18	0.27	0.67	88	3.51

Table 4.2. Response times of some selected our samples

	YT29	**YT36**	**YT37**	**YT47**
Response Times (s)	1.91	1.15	0.825	0.972

Resistance is changed depend on intensity of the signal. It is possible to observe this by Stefan-Boltzmann lamb's power. Figure 4.20 shows the bolometric measurement that signal was sent and paused in each 30 second. Power of the signal is adjusted 20, 30, 40 and 50 Watt and resistance of the chip is increased by increasing power of the signal. Initial resistance of the chip is not change only response resistance changed by increasing of the power. When we decreased the power below 5 Watt, we can say that chip is not sensitive like former because response resistance is so tiny to measure.

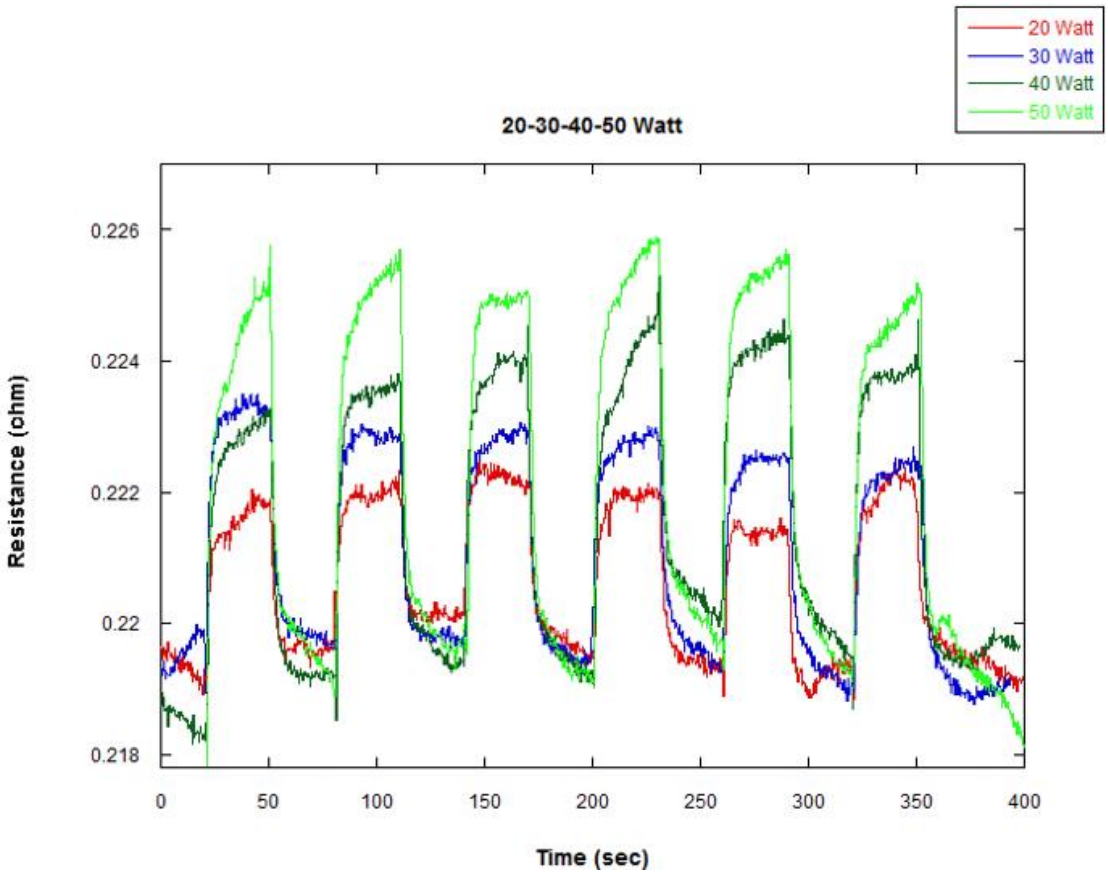

Figure 4.20. Change of resistance with different signal power

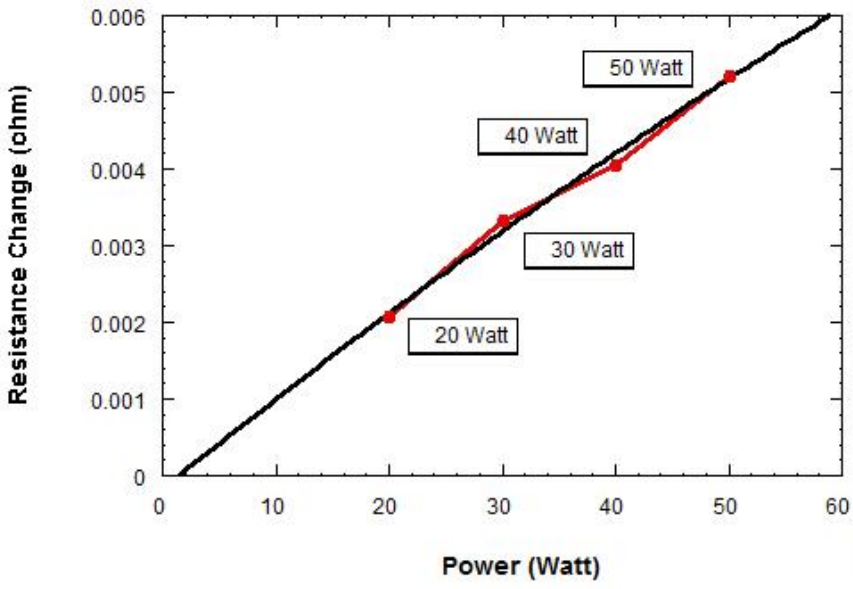

Figure 4.21. Curve fit graph of resistance-power measurement

After result of bolometric measurement with changing different power, it should be determined the power that what value of power at the nearly zero resistance. If we curve fit our Figure 4.20 graph, we reach 1.95 Watt value to zero resistance. It means that our bolometric detector has sensitivity until 1.95 Watt power from source.

CHAPTER 5

CONCLUSION

Terahertz (THz) wave is the part of electromagnetic spectrum which has different properties than other part of electromagnetic spectrum. THz waves utilize defense industry in especially security purpose to detect the explosive materials, poison gas, weapon, virus and bacteria. It is possible to pass through leather, fabric and paper in spite of metal and water and THz radiation is in the range of suitable for vibration mostly chemical and biological materials. THz radiation does not have enough energy to ionize the atoms that's why, THz radiation is not harmful for living tissue to expose people like radio waves or visible lights. Many detectors are needed to utilize of advantages of THz waves. Superconducting detectors are useful in spite of other detectors due to necessity of hard and cryogenic expensive.

In our study, superconducting bolometer was aimed to use detector as bolometric detector. Additionally, Transition Edge Bolometer's principle based on resistance modulation by during the selected temperature in the superconducting transition region.

In this study, $Bi_2Sr_2CaCu_2O_{8+\delta}$ (Bi2212) single crystal is used in literature first time as chip in bolometric detector for THz waves. It is crucial to transfer Bi222 single crystal to sapphire substrate. For this method, we used epoxy to transfer crystal. To begin with, enough epoxy was putted on the sapphire, then crystal was placed after that wait until them dry. Edges of the crystals were cut pyramid shapes to provide each layer to contact with gold layer. After that, crystals are cleaved by Scotch tape until get thickness 200-300 nm. Crystals which has 0.5 mm^2 or 1 mm^2 area masked with aluminum foil to deposit 150-200 nm gold layer with thermal evaporation system. To placed antenna structure by electron beam lithography, clean room process was performed. Samples coated with photoresist (PR) with 3000 rpm 88 sec. as thickness 2 μm. PR was made stronger with soft bake 90℃ 30 minutes. After all, antenna structure was placed on the crystal onto the crystal with log-periodic, four point contact structure by electron beam lithography. Crystals was hold in 7 second to UV light and developed with NaOH (sodium hydroxide), ion beam etching was performed to lift off layer which

electrons was not collide. Finally, contacts were taken for the electrical and bolometric measurement.

Moreover, cryostat was designed and fabricated for the electrical and bolometric measurement. Liquid nitrogen chamber in cryostat has 3 liters was coated with 15 μm metalize film as four times to reduce the vaporization speed until 0.085 liter/hour. Liquid nitrogen exist in cryostat for 30 hours at 77 K. This value is important to work hours of the bolometric detector. Labview program was written for electrical and bolometric measurements of chips to detect in our designed cryostat.

Electrical measurement in a-b axis of our chips were taken in cryostat as critical temperature values between 88 and 90 K. These critical values were enough for our measurements and thickness of crystals were changed from 200 nm to 1 μm. All samples showed sharp drop during passing from room temperature to superconducting transition region. Additionally, graphs showed the exponentially decreased until the value of critical temperature onset. According to the result of a-b axis electrical measurement, R_{Tc}/ R_{300K} value is between 0.38 and 0.69. We held the temperature of chips in the selected temperature around the superconducting transition region for bolometric measurement according to the result of the electrical measurements. Signal was sent by Stefan-Boltzmann lamp which is distance 5 cm from THz window, was focused to the chips surface by wave collector in cryostat. These parameters were taken by sending and pausing at specific second. Resistance of the chips were increased as of depending intensity of the signal. When intensity of the signal is increased, change of resistance is increased too in despite of unchanging initial resistance. Finally, response times of chips were calculated as 1.91, 1.15 s., 825, 972 ms, respectively from result of the bolometric measurement. Our measurement set-up has limitation to read right data. Lock-in-amplifier may use to more accurate result.

REFERENCES

Arnone, D. D., Ciesla, C. M., Corchia, A., Egusa, S., Pepper, M., Chamberlain, J. M., Khammo, N. (1999). Applications of Terahertz (THz) technology to medical imaging. *Terahertz Spectroscopy and Applications 11, 3828*, 209-219. doi: Doi 10.1117/12.361037.

Bednorz, J.G., K.A. Müller. (1986). Possible high Tc superconductivity in the Ba− La− Cu− O system. *Zeitschrift für Physik B Condensed Matter*. *64*:189-193.

Blain, A.W., Smail, I., Ivison, R.J., Kneib, J.-P., Frayer, D.T., Submillimeter Galaxies (2002). *Phys. Rep*. 369 111–176.

Benford, D., Transition Edge Sensor Bolometers for CMB Polarimetry (http://cmbpol.uchicago.edu/workshops/technology2008/depot/cmbpol_technologies_benford_jcps_4.pdf)

Boswell, A. (1970). Log-Periodic Dipole Arrays. *Marconi Review, 33*(178), 225.

Cibella, S., Carelli, P., Castellano, M. G., Foglietti, V., Leoni, R., Ortolani, M., & Torrioli, G. (2009). A Superconducting Bolometer Antenna-Coupled to Terahertz Waves. *Journal of Low Temperature Physics, 154*(5-6), 142-149. doi: DOI 10.1007/s10909-009-9860-8.

Codreanu, I., Fumeaux, C., Spencer, D. F., & Boreman, G. D. (1999). Microstrip antenna-coupled infrared detector. *Electronics Letters, 35*(25), 2166-2167. doi: Doi 10.1049/El:19991486.

Conwell, E.M., (1967). High field transport in semiconductors. *Solid State Physics, 9, Academic Press, New York*.

Chu, C., P. Hor, R. Meng, L. Gao, Z. Huang, Wang, YQ. (1987). Evidence for superconductivity above 40 K in the La-Ba-Cu-O compound system. *Physical Review Letters*. 58:405-407.

Danilchenko, B. A., Jasiukiewicz, C., Paszkiewicz, T., & Wolski, S. (2004). Nonlinear response of superconductor bolometer to phonon fluxes. *European Physical Journal-Applied Physics, 26*(3), 151-159. doi: DOI 10.1051/epjap:2004027.

Dattoma T., et al., (2011). Resonance wavelength dependence and mode formation in gold nano rod optical antennas with finite thickness, *Progress In Electromagnetics Research B*, Vol. 30, 337-353.

DuHamel R. H., Isbell D. E., (1957). Broadband Logarithmically Preiodic Antenna Structures, I*RE National Convention Record*, 1, 119.

El Fatimy, A., Dyakonova, N., Meziani, Y., Otsuji, T., Knap, W., Vandenbrouk, S., Madjour, K., Theron, D., Gaquiere, C., Poisson, M.A., Delage, S., Prystawko, P., Skierbiszewski, C. (2010). AlGaN/GaN high electron mobility transistors as a voltage-tunable room temperature terahertz sources. *J. Appl. Phys. 107*, 024504.

Faist, J., Capasso, F., Sivco, D. L., Sirtori, C., Hutchinson, A. L., Cho, A. Y. (1994). Quantum Cascade Laser. Science, 264, 5158, 553-556 doi: DOI: 10.1126/science.264.5158.553.

Ferguson, B., & Zhang, X. C. (2002). Materials for terahertz science and technology. *Nature Materials, 1*(1), 26-33. doi: Doi 10.1038/Nmat708.

Fischer B., Hoffmann, Helm H, Modjesch G, Jepsen P. U, 2005. Chemical recognition in terahertz time-domain spectroscopy and imagining. *Semiconductor Science and Technology* 20:S246-S253.

Fitzgerald, A. J., Cole, B. E., & Taday, P. F. (2005). Nondestructive analysis of tablet coating thicknesses usign terahertz pulsed imaging. *Journal of Pharmaceutical Sciences, 94*(1), 177-183. doi: Doi 10.1002/Jps.20225.

Fox, M., and G.F. Bertsch. (2002). Optical properties of solids. *American Journal of Physics*. 70:1269-1270.

Fumeaux, C., Gritz, M. A., Codreanu, I., Schaich, W. L., Gonzalez, F. J., & Boreman, G. D. (2000). Measurement of the resonant lengths of infrared dipole antennas. *Infrared Physics & Technology, 41*(5), 271-281. doi: Doi 10.1016/S1350-4495(00)00047-5.

Gao, L., Xue, Y.Y., Chen, F., Xiong, Q., Meng, R.L. , Ramirez, D., Chu, C.W., Eggert, J.H., Mao, H.K. (1994). Superconductivity up to 164-K in HgBa2Cam-1CumO2m+2+δ (m=1,2, and 3) under Quasi-Hydrostatic Pressures. *Physical Review B.* 50:4260-4263.

Gershenson, E.M. , Gershenson, M.E., Goltsman, G.N., Karasik, B.S., Lyulkin, A.M., Semenov, A.D., (1989). Ultra-fast superconducting electron bolometer. *J. Tech. Phys. Lett*. 15, 118–119.

Gershenzon, E.M., Goltsman, G.N., Gogidze, I.G., Gusev, Y.P., Elantev, A.I., Karasik, B.S., Semenov. A.D., (1990). Millimeter and submillimeter range mixer based on electronic heating of superconducting films in the resistive state. *Superconductivity, 3-10,* 1582–1597.

"Golay Cell", last modified 2010, https://en.wikipedia.org/wiki/Golay_cell/media/ File: Golay_cell.jpg)

Gonzalez, F. J., & Boreman, G. D. (2005). Comparison of dipole, bowtie, spiral and log-periodic IR antennas. *Infrared Physics & Technology*, *46*(5), 418-428. doi: DOI 10.1016/j.infrared.2004.09.002.

Hammar, A., Cherednichenko, S., Bevilacqua, S., Drakinskiy, V., & Stake, J. (2011). Terahertz Direct Detection in YBa2Cu3O7 Microbolometers. *Ieee Transactions on Terahertz Science and Technology*, *1*(2), 390-394. doi: Doi 10.1109/Tthz.2011.2161050.

Hammar, A. et al., (2011). *IEEE Trans. On Tera. Sci. and Tech*. 1, 2.

Hargreaves, S., Lewis, R.A. (2007). Terahertz imaging. Materials and methods, *J. Mater. Sci.: Mater. El. 18*, S299–S303.

Hazen, R., Finger, L., Angel, R., Prewitt, C., Ross, N., Hadidiacos, C., Heaney, P., Veblen, D., Sheng, Z., El Ali, A., (1988). 100-K superconducting phases in the Tl-Ca-Ba-Cu-O system. *Physical review letters*. 60:1657.

Hight-Walker, A. R. et. al.(1997). *Proceedings of SPIE* v. 3153:42.

Hoffman Laboratory, Harvard University, Discovery of the superconducting materials in the last century, (2010). http://hoffman.physics.harvard.edu/materials/SC intro.php.

Huang, Y. H., Hu, M., He, G. H., & Liu, W. L. (2013). Terahertz Time-domain Spectroscopy Technology and Its Application in the Field of Pesticide. *Advanced Polymer Processing Iii, 561*, 640-645. doi: DOI 10.4028.

Ilin, K.S., Lindgren, M., Currie, M., Semenov, A.D., Goltsman, G.N., Sobolewski, R., Cherednichenko, S.I., Gershenzon, E.M., (2000). Picosecond hot-electron energy relaxation in NbN superconducting photodetectors. *Appl. Phys. Lett. 76*, 2752–2754 doi: DOI 10.1063/1.126480.

Ito, H., Nakajima, F., Furuta, T., Ishibashi, T. (2005). Continuous THz-wave generation using antenna-integrated uni-travelling-carrier photodiodes. *Semiconduct. Sci. Technol. 20*, S191–S198.

Ji, M., Yuan, J., Gross, B., Rudau, F., An, D. Y., Li, M. Y., Wu, P. H. (2014). Bi2Sr2CaCu2O8 intrinsic Josephson junction stacks with improved cooling: Coherent emission above 1 THz. *Applied Physics Letters, 105*(12). doi: Artn 122602 Doi 10.1063/1.4896684.

Kakeya, I., Fukui, K., Kawamata, K., Yamamoto, T., & Kadowaki, K. (2008). Quantum oscillation of the c-axis resistivity due to entrance of pancake vortices into micro-fabricated BiSr2CaCu2O8+delta intrinsic Josephson junctions. *Physica C-Superconductivity and Its Applications, 468*(7-10), 669-673. doi: DOI 10.1016/j.physc.2007.11.064.

Kamihara, Y., Hiramatsu, H., Hirano, M., Kawamura, R., Yanagi, H., Kamiya, T., Hosono, H., (2006). Iron-based layered superconductor: LaOFeP. *Journal of the American Chemical Society*. 128:10012-10013.

Karasik, B. S., McGrath, W. R., Wyss, R. A., (1999). Optimal choice of materials for HEB superconducting mixers. *IEEE Transc. On Appl. Supercon*., 9, 4213-4216 doi:10.1109/77.783954.

Karpowicz, N., Zhong, H., Xu, J., Lin, K.I., Hwang, J.S., Zhang, X.C., (2005). Nondestructive subst. THz imaging, *Proc. SPIE* 5727, 132–142.

Kawase, K. 2004. Terahertz imaging for drug detection and large-scale integrated circuit inspection. *Optics and photonics news*. 15:34-39.

Kemp, M. C., Taday P. F, Cole b. E., Cluff J. A., Fitzgerald A. J., Tribe W. R., (2003). Security applications of terahertz technology. *Pro. SPIE*. 5070, 44–52.

Kinch, M.A., Rollin, B.V., (1963). Detection of millimeter and sub-millimeter wave radiation by free carrier absorption in a semiconductor. *Br. J. Appl. Phys. 14,* 672–676. doi:10.1088/0508-3443/14/10/317.

Kocakarin, I., & Yegin, K. (2013). Glass Superstrate Nanoantennas for Infrared Energy Harvesting Applications. *International Journal of Antennas and Propagation*. doi: Artn 245960 Doi 10.1155/2013/245960.

Köhler, R., Tredicucci, A. Beltram, F., Beere, H. E., Linfield, E. H., Davies, A. G., Ritchie D. A., Iotti, R. C., Rossi F. (2002). Terahertz Semiconductor-heterostructure laser. *Nature 417*, 156-159 doi: DOI 10.1038/417156a.

Köhler, R., Tredicucci, A., Beltram, F., Beere, H. E., Linfield, E. H., Davies, G., Rossi, F. (2003). Terahertz semiconductor heterostructure laser. *Physics of Semiconductors 2002, Proceedings, 171*, 145-152.

Koseoglu, H., Turkoglu, F., Simsek, Y., & Ozyuzer, L. (2011). The Fabrication of THz Emitting Mesas by Reactive Ion-Beam Etching of Superconducting Bi2212 with Multilayer Masks. *Journal of Superconductivity and Novel Magnetism, 24*(1-2), 1083-1086. doi: DOI 10.1007/s10948-010-0859-9.

Kumar, S., Hu, Q., Reno, J.L. (2009). 186 K operation of terahertz quantum-cascade lasers based on a diagonal design. *Appl. Phys. Lett*. 94, 131105.

Langley, S.P., (1881). The actinic balance. *American Journal of Science*: 187-198.

Langley, S.P., (1898). The bolometer. *Nature*. 57:53.

Lindberg, P. A. P., Shen, Z. X., Wells, B. O., Dessau, D. S., Mitzi, D. B., Lindau, I. Kapitulnik, A. (1989). Reaction of Rb and Oxygen Overlayers with Single-Crystalline Bi2sr2cacu2o8+Delta Superconductors. *Physical Review B, 39*(4), 2890-2893. doi: DOI 10.1103/PhysRevB.39.2890.

McGrath, W.R., (1995). Novel hot-electron bolometer mixers for submillimeter applications: An overview of recent developments. *Proceedings of the URSI International Symposium on Signals, Systems, and Electronics*, 147–152.

Maeda, H., Tanaka, Y., Fukutomi, M., Asano, T., (1988). A new high-Tc oxide superconductor without a rare earth element. *Japanese Journal of Applied Physics*. 27:L209.

Mehdi, I., Chattopadhyay, G., Schlecht, E., Ward, J., Gill, J., Maiwald, F., Maestrini A., (2006). Terahertz Multiplier Circuits, *Proceedings of the IEEE MTT-S International Microwave Symposium Digest*, 341-344.

Mei, Y., Green, S. M., Jiang, C., Luo, J H. L. (1988). *Appl. Phys.* 64, 6795.

Meissner, W., R. Ochsenfeld. (1933). Ein neuer effect bei eintritt der supraleitfahigkeit. *Naturwissenschaften* 21(44):787.

Meissner Effect of Superconductivity, (2002). http://users-phys.au.dk/philip /pictures/ physicsfigures/physicsfigures.html

Michishita, K., Y. H. Ikuhara and Y. Kubo. (1996). Bi-based superconductor fabricated by floating-zone method: Bismuth-based high-temperature Superconductors, *Edited by Hiroski Maeda and Kazumasa Togano. New York: Marcer Dekker*.

Moftakharzadeh, A., Kokabi, A., Bozbey, A., Ghods-Elahi, T., Vesaghi, M., Khorasani, S., Fardmanesh, M. (2008). Detectivity of YBCO transition edge bolometer: modulation frequency, bias current and absorber effects. *8th European Conference on Applied Superconductivity (Eucas'07), 97*. doi: Artn 012009 Doi 10.1088/1742-6596/97/1/012009.

Mueller, E. R. (2006). Terahertz radiation sources for imaging and sensing applications. *Photonics Spectra, 40*(11).

Phillips, T.G., Jefferts, K.B., (1973). Liquid helium cooled InSb hot electron bolometers are used in a balanced mixer configuration as detectors for an imageless microwave receiver. *Rev. Sci. Instrum*. 44 1009–1014.

Onnes, H. K. (1911). Disappearance of the electrical resistance of mercury of Helium temperature. *Akad. Van Wetenschappen (Amsterdam)* 14:113.

Onnes, H. K. December 30, 1911, College Physics (2012) origanally published in *KAWA.*

Ozyuzer, L., Koshelev, A. E., Kurter, C., Gopalsami, N., Li, Q., Tachiki, M., Welp, U. (2007). Emission of coherent THz radiation from superconductors. *Science, 318*(5854), 1291-1293. doi: DOI 10.1126/science.1149802.

Ozyuzer, L., Simsek, Y., Koseoglu, H., Turkoglu, F., Kurter, C., Welp, U.. Muller, P. (2009). Terahertz wave emission from intrinsic Josephson junctions in high-T-c superconductors. *Superconductor Science & Technology, 22*(11). doi: Artn 114009 Doi 10.1088/0953-2048/22/11/114009.

Pala, N., Abbas, A. N., (2012). Terahertz Technology for Nano Applications. *Encyclopedia of Nanotechnology* doi: DOI 10.1007/978-90-481-9751-4.

Pamplin, B.R. (ed.) (1980) Crystal Growth, Pergamon Press, Oxford.

Pawar A.Y, Sonawane D.D, Erande B.K, Derle D.V. (2013). Terahertz technology and its applications. *Drug Invention Today*. 5:157-163.

Pfann, W. G. (1952). Trans. AIME 194, 747.

Prober, D.E., (1993). Superconducting terahertz mixer using a transition-edge micro bolometer. *Appl. Phys. Lett. 62,* 2119–2121 doi: DOI 10.1063/1.109445.

Saijo, H., Morimoto, M., Kiwa, T., & Tonouchi, M. (2001). Terahertz emission properties from YBCO thin film log-periodic antennas. *Physica C, 362,* 319-323. doi: Doi 10.1016/S0921-4534(01)00696-7.

Scalari, G., Walther, C., Faist, J., Beere, H., Ritchie, D., (2006). Electrically switchable, two color quantum cascade laser emitting at 1.39 and 2.3 THz. *Applied Physics Letters*, 88, 141102 doi: DOI 10.1063/1.2191407.

Schilling, A., Cantoni, M., Guo, J., Ott. H., (1993). Superconductivity above 130 K in the Hg-Ba-Ca-Cu-O system. *Nature*. 363:56-58.

Semenov, A. D., Hubers, H. W., Il'in, K. S., Siegel, M., Judin, V., & Muller, A. S. (2009). Monitoring Coherent THz-Synchrotron Radiation with Superconducting NbN Hot-Electron Detector. *2009 34th International Conference on Infrared, Millimeter, and Terahertz Waves, Vols 1 and 2*, 275-276.

Sizov, F., Rogalski, A., (2010). THz Detectors-Review, *Progress in Quantum Electronics* 34,278-347.

Takahashi, H., Igawa, K., Arii, K., Kamihara, Y., Hirano, M., Hosono, H., (2008). Superconductivity at 43 K in an iron-based layered compound LaO1-xFxFeAs. *Nature*. 453:376-378.

Takekawa, S., Nozaki, H., Umezono, A., Kosuda, K., & Kobayashi, M. (1988). Single-Crystal Growth of the Superconductor Bi2.0(Bi0.2sr1.8ca1.0)Cu2.0o8. *Journal of Crystal Growth, 92*(3-4), 687-690. doi: Doi 10.1016/0022-0248(88)90057-7.

Tanaka, M., Takahashi, T., Katayamayoshida, H., Yamazaki, S., Fujinami, M., Okabe, Y., Kajimura, K. (1989). Evidence for Non-Metallic Nature of the Bio Plane in Bi2casr2cu2o8 from Scanning Tunnelling Spectroscopy. *Nature, 339*(6227), 691-693. doi: Doi 10.1038/339691.

Thoma, P., Scheuring, A., Hofherr, M., Wunsch, S., Il'in, K., Smale, N., Siegel, M. (2012). Real-time measurement of picosecond THz pulses by an ultra-fast YBa2Cu3O7-d detection system. *Applied Physics Letters, 101*(14). doi: Artn 142601 Doi 10.1063/1.4756905.

Tonouchi, M., & Saijo, H. (2003). Terahertz radiation from YBCO thin film log-periodic antennas. *Journal of Superconductivity, 16*(5), 867-871. doi: Doi 10.1023/A:1026211103543.

Tonouchi, M. (2007). Cutting-edge terahertz technology. *Nature Photonics* 1(2):97-105.

Turkoglu, F., Koseoglu, H., Demirhan, Y., Ozyuzer, L., Preu, S., Malzer, S., Kadowaki, K. (2012). Interferometer measurements of terahertz waves from Bi2Sr2CaCu2O8+d mesas. *Superconductor Science & Technology, 25*(12). doi: Artn 125004 Doi 10.1088/0953-2048/25/12/125004.

Turkoglu, F., Ozyuzer, L., Koseoglu, H., Demirhan, Y., Preu, S., Malzer, S., Muller, P. (2013). Emission of the THz waves from large area mesas of superconducting Bi2Sr2CaCu2O8+delta by the injection of spin polarized current. *Physica C-Superconductivity and Its Applications, 491*, 7-10. doi: DOI 10.1016/j.physc.2013.01.014.

Wang, H. B., Wu, P. H., & Yamashita, T. (2001). Stacks of intrinsic Josephson junctions singled out from inside Bi2Sr2CaCu2O8+x single crystals. *Applied Physics Letters, 78*(25), 4010-4012. doi: Doi 10.1063/1.1379065.

Wang, X., You, L. X., Liu, D. K., Lin, C. T., Xie, X. M., & Jiang, M. H. (2012). Thin-film-like BSCCO single crystals made by mechanical exfoliation. *Physica C-Superconductivity and Its Applications, 474*, 13-17. doi: DOI 10.1016/j.physc.2011.12.006.

Wang, X., You, L. X., Yang, X. Y., Xie, X. M., Lin, C. T., & Jiang, M. H. (2012). Exfoliated Thin Bi2Sr2CaCu2O8+delta Single Crystal and Its Intrinsic Josephson Junctions. *Ieee Transactions on Applied Superconductivity, 22*(2). doi: Artn 1100104 Doi 10.1109/Tasc.2012.2188028.

Warren L. Stutzman, Gary A. Thiele, (1981). Antenna Theory and Design, Wiley & Sons

Watanabe, T., Fujii, T., & Matsuda, A. (1997). Anisotropic resistivities of precisely oxygen controlled single-crystal Bi2Sr2CaCu2O8+delta: Systematic study on "spin gap" effect. *Physical Review Letters, 79*(11), 2113-2116. doi: DOI 10.1103/PhysRevLett.79.2113.

Wu, M.K., Ashburn, J., Torng, C., Hor, P.H., Meng, R., Gao, L., Huang, Z., Wang, Y., Chu, C., (1987). Superconductivity at 93 K in a new mixed-phase Y-Ba-Cu-O compound system at ambient pressure. *Physical Review Letters*. 58:908-910.

Yamada, Y., Watanabe, T., & Suzuki, M. (2007). Fabrication and transport properties for cleaved thin film BSCCO single crystals. *Ieee Transactions on Applied Superconductivity, 17*(2), 3533-3536. doi: Doi 10.1109/Tasc.2007.899574.

Yamaki, K., Tsujimoto, M., Yamamoto, T., Furukawa, A., Kashiwagi, T., Minami, H., & Kadowaki, K. (2011). High-power terahertz electromagnetic wave emission from high-T-c superconducting Bi2Sr2CaCu2O8+delta mesa structures. *Optics Express, 19*(4), 3193-3201. doi: Doi 10.1364/Oe.19.003193.

You, L. X., Yurgens, A., Winkler, D., Lin, C. T., & Liang, B. (2005). Superconducting properties of ultrathin Bi2Sr2CaCu2O8+x single crystals. *Journal of Applied Physics, 98*(3). doi: Artn 033913 Doi 10.1063/1.2006992.

You, L. X., Yurgens, A., Winkler, D., Lin, C. T., & Liang, B. (2006). Thickness dependence of the superconducting properties of ultra-thin Bi2Sr2CaCu2O8+x single crystals. *Superconductor Science & Technology, 19*(5), S205-S208. doi: Doi 10.1088/0953-2048/19/5/S08.

Young, D.T., Irvin, J.C., (1965). Millimeter frequency conversion using Au-n-type GaAs Schottky barrier epitaxial diodes with a novel contacting technique, *Proc. IEEE 53*, 2130–2132.

Yurgens, A., Winkler, D., Zavaritski N. V., Claeson, T., (1996a). Strong temperature dependence of the c-axis gap parameter of Bi2Sr2CaCu2O8+x intrinsic Josephson junctions. *Physical Review B* 53:R8887.

Yurgens, A. (2000). Intrinsic Josephson junctions: recent developments. *Superconductor Science and Technology*. 13:R85-R100.